THE UNIVERSITY OF MICHIGAN

COLLEGE OF ENGINEERING
Department of Aerospace Engineering
Aircraft Propulsion Laboratory

TWO PHASE DETONATIONS AND DROP SHATTERING STUDIES

Second Annual Progress Report
(February 1, 1965 to January 31, 1966)

by

E. K. Dabora
K. W. Ragland
A. A. Ranger

J. A. Nicholls
Principal Faculty Investigator

ORA Project 06324

under contract with:

National Aeronautics and Space Administration
Contract No. NASr-54(07)
Washington, D. C.

administered through:

FICE OF RESEARCH ADMINISTRATION ANN ARBOR

April 1966

FOREWORD

This report covers the progress made from February 1, 1965 to January 31, 1966 on a continuing study of the relation of two phase detonations with liquid rocket motor instability under NASA contract NASr-54(07) which started in February 1, 1964. The study is made under the direction of Professor J. A. Nicholls, Department of Aerospace Engineering. The contribution of the authors are as follows:

Sections I, II	Dabora
Section III	Dabora and Ragland
Section IV	Ragland
Section V	Ranger
Sections VI-VII	Joint contribution

ACKNOWLEDGMENTS

The authors wish to thank D. F. Giere for his active participation in conducting the spray detonation experiments, S. A. Crist for his assistance in the design and initial operation of the shock tube for the drop shattering experiments and Professor M. Sichel for the helpful discussions throughout this work. They would like also to express their thanks to C. J. Iott, Technician, for his able assistance in the experimental aspects of this work and to R. C. Stitt and W. V. Whitman for their general help.

TABLE OF CONTENTS

		Page
FOREWORD		ii
ACKNOWLEDGMENT		iii
ABSTRACT		v
LIST OF FIGURES		vii
LIST OF TABLES		x
NOMENCLATURE		xi
I.	INTRODUCTION	1
II.	SPRAY DETONATIONS—THEORY	4
	A. Properties of a Two Phase System	4
	B. Comparison of Spray and Gaseous Detonations	8
	C. Detonation Properties of DECH-O_2 Mixtures	12
III.	SPRAY DETONATIONS—EXPERIMENT	15
	A. Production of Monodisperse Sprays	15
	B. Combustion of a Single Droplet Stream	26
	C. Detonation in Monodisperse Sprays	29
IV.	DETONATION OF A LIQUID FILM	54
	A. Experimental Studies	54
	B. Other Observations of Film Detonations	68
	C. Physical Explanation of Film Detonations	69
	D. Theoretical Analysis of Film Detonations	70
V.	DROP SHATTERING STUDIES	87
	A. Review of Drop Breakup Studies	88
	B. Experimental Arrangement and Procedure	124
	C. Discussion of Results	140
VI.	CONCLUSIONS	150
VII.	FUTURE PLANS	152
APPENDIX		153
REFERENCES		156

ABSTRACT

The theoretical properties of C-J detonations in two phase mixtures of liquid diethylcyclohexane and gaseous oxygen are presented for an equivalence ratio range of .1-3. Experiments on detonations in monodisperse sprays with drop sizes of 290, 750, and 940μ are described. Detonations are initiated by transmitted shocks from either $2H_2$-O_2 detonations or high pressure helium as drivers. For the 940μ spray at equivalence ratio of .5, the detonation velocity is 5600 ft/sec or 15% below the theoretical. In general, pressures behind the front are compatible with shocks travelling at the experimental detonation speed. Among other photographs of the phenomenon presented, streak photographs reveal a structure reminiscent of spinning detonations.

Experiments in which the fuel is in the form of a thin film on the walls of the tube are also described. Like the spray case, self-supporting waves are observed. At a first step in the analytical treatment of the phenomenon, a formulation of a boundary layer problem with mass and heat addition, consistent with the physical interpretation is presented. Some analog computer results of the latter problem are obtained.

Studies of drop shattering under conditions similar to those of detonations are initiated. A review of the theoretical and experimental studies found in the literature is presented and the results on water drops of

750 and 1090μ in diameter subjected to M = 1.5, 2.7, and 3.25 shocks are described. Preliminary results on the velocity of the drops and their deformation after the passage of the wave are included. A 1080μ drop is found to be completely shattered in 135 μsec when shock M = 3.25. The Weber number in all the experiments is very much larger than the critical and hence shear type breakup is observed throughout.

LIST OF FIGURES

		Page
2.1	Properties of DECH-O_2 Detonations	13
3.1	Monodisperse Sprays of DECH in Air	17
3.2	Drop Generator with Provision for Co-flow	19
3.3	290μ Spray without Co-flow	20
3.4	Needle Plate Configurations	21
3.5	290μ Spray with Co-flow Showing Reduced Coalescence	22
3.6	Distance vs. Velocity of Drops under Free-Fall	25
3.7	Detonation Tubes used for Spray and Film Detonations	27
3.8	Schematic of a Single Stream Injector Arrangement	28
3.9	Single Stream Combustion	30
3.10	Detonation Tube for Visual and Photographic Observation	32
3.11	Detonation and Helium Driven Shock Tubes	33
3.12	Photographic Sequence of 750μ Spray Detonation	35
3.13	Generator Housing	39
3.14	Typical 940μ Spray Photograph at Observation Section	40
3.15	Typical Pressure Traces of 940μ Spray Detonation	41
3.16	Pressure Switch	43
3.17	Circuit for Raster Signals	44
3.18	Typical Raster Record	45
3.19	Variation of Detonation Velocity with Distance from Spray Generator	46

3. 20	Schematic of Schlieren Arrangement	47
3. 21	Typical Schlieren Photographs of 940μ Spray Detonation	48
3. 22	Typical Shadow and Direct Light Photographs of Spray Detonations	50
3. 23	Schematic Streak Photography Setup	51
3. 24	Streak Photograph of the Self-Luminous Detonation	52
3. 25	Combined Luminous and Shadow Streak Photograph of the Detonation	53
4. 1	Self-Luminous Photographs and Pressure Traces of Detonation of DECH Film	55
4. 2	Test Setup for Observing a Liquid Layer Behind a Normal Shock	58
4. 3	Photographs of Liquid Layer on Flat Plate Behind Shock in Nitrogen	59
4. 4	Traces from Thin Film Heat Transfer Gauge and Pressure Transducers.	63
4. 5	Thin Film Heat Transfer Gauge Trace of a Stoichiometric Hydrogen-Oxygen Detonation at 1 Atmosphere Initial Pressure	66
4. 6	Normal Shock Moving Across a Flat Plate with Boundary Layer Combustion	72
4. 7	Network for Analog Computer used to Solve the General Blasius Equation	82
4. 8	Analog Computer Solution of the Blasius Equation for M_s = 1. 57, and B = 31. 1	83
5. 1	Schematic Diagram of Shock Tube	125
5. 2	Shock Mach Number vs. Testing Time	127
5. 3	Output Trace of Pressure Transducer and Heat Transfer Gauge	128
5. 4	Shock Mach Number vs. Driver Pressure	129
5. 5	Convective Mach Number, Reynolds Number, and Weber Number vs. Shock Mach Number	131

5.6	Ruptured Steel Diaphragm	133
5.7	Photograph of Shock Tube Test Section	135
5.8	Schematic of Drop Generating System	136
5.9	Trigger and Time Delay Circuit	138
5.10	Photographing Sequence of the Shattering of 780μ Drops by M_s = 1.54 Shock	141
5.11	Photographing Sequence of the Shattering of 750μ Drops by M_s = 2.7 Shock	142
5.12	Photographing Sequence of the Shattering of 1090μ Drops by M_s = 3.25 Shock	143
5.13	Waterdrop Flattening vs. Time After Collision	144
5.14	Waterdrop Displacement vs. Time After Collision	145
5.15	Comparison of Experimental Breakup Time Results	146

LIST OF TABLES

		Page
I.	Comparison Between Spray and Gaseous Systems	9
II.	Products of Combustion at C-J Condition of DECH-O_2 Mixtures	14
III.	Mach Number of Transmitted Shock into Air at Atmospheric Conditions	36
IV.	Apparent Liquid Layer Thickness Behind M = 2. 2 Shock	61
V.	Summary of Heat Transfer Results	67
VI.	Summary of Initial Conditions Satisfying the Blasius Equation for Various Values of M_s and B	85
VII.	Summary of Shock Wave-Drop Interaction Studies	102

NOMENCLATURE*

A	constant defined by Eq. (4.7) (IV); = $16\mu_\ell / \rho_\ell D$ (V)
a	speed of sound (II, III); acceleration, radius of sphere (V)
$\bar{a}$	vector acceleration (V)
B	constant defined by Eq. (4.29)(IV); = $F/\beta^{2/3}$, $2/\rho_\ell$ (V)
B'	constant defined by Eq. (4.26) (IV)
b	function of time (V)
C	constant (V)
C_D	drag coefficient
C_p	specific heat of the mixture at constant pressure (IV)
c	specific heat of liquid (II, III)
c_p	specific heat at constant pressure
c_v	specific heat at constant volume
D	drop diameter; binary diffusion coefficient (IV)
$\bar{D}$	average drop size
d_j	diameter of jet
ΔE	voltage change
e	specific energy
F	crest configuration parameter
f	frequency (II, III); Blasius function, the solution of Eq. (4.22) (IV); convective acceleration, forcing parameter (V)
g	acceleration due to gravity
g_1	convective acceleration

*Note: for symbols denoting more than one item, the roman numeral appearing after the notation refers to the section where the particular notation is used.

ΔH	heat of combustion per unit mass
h	specific enthalpy
h_i^o	standard heat of formation per unit mass for species i at temperature T^o
h_L	latent heat of vaporization per unit mass
I_o	current
K	$= 2\pi / \lambda$, curvature constant (V)
k	coefficient of thermal conductivity
M	Mach number
M_i	symbol for chemical species i
m	molecular weight
N	total number of chemical species present
n	stoichiometric fuel-oxidizer mole ratio
P	$= 1/2\ \rho_g V^2 C_D - K\sigma / D$ (V)
p	pressure
p_D	diaphragm pressure
p_h	pressure head
p_θ	pressure at angle θ
p_4	driver pressure
Q	heat release per unit mass of mixture
q	heat flux vector (IV); dynamic pressure (V)
R	universal gas constant
Re	Reynolds number
R_o	resistance (IV); jet radius (V)
S	distance
s	entropy
T	temperature
T^o	standard reference temperature
t	time
t_b	breakup time

u	mass average velocity in x direction
$\bar{u}$	non-dimensional velocity
u_j	jet velocity
u_{min}	minimum jet velocity
V	velocity (II, III); convective flow velocity, volume (V)
v	mass average velocity in the y direction (IV)
We	Weber number = $\rho_g V^2 D/\sigma$
W_i	molecular weight of species i
w	defined by Eq. (4.15) (IV), velocity (V)
$\bar{w}$	vector velocity
x, y, z	cartesian coordinates (V)
x	distance from shock along wall (IV)
Y_i	mass fraction of species i
y	distance normal to wall at the shock (IV)
z	defined by Eq. (4.14) (IV)
α	thermal resistivity (IV), wave amplitude (V)
β	density ratio, liquid to gas sheltering parameter (V)
β_i	defined by Eq. (4.6)
β_T	defined by Eq. (4.5)
γ	ratio of specific heats
δ	ratio of specific heat of fuel to that of the oxidizer (II, III); boundary layer thickness (V)
ϵ	liquid volume fraction (II, III); relative displacement (V)
η	fuel oxidizer mass ratio (II, III); similarity parameter defined by Eq. (4.19) (IV); wave amplitude (V)
η_o	initial wave amplitude
θ_m	angle defining edge of drop
λ	wavelength, (II, III, V); dummy variable (IV)

μ	viscosity, micron = 10^{-4} cm
ν_i'	stoichiometric coefficient for species i appearing as a reactant
ν_i''	stoichiometric coefficient for species i appearing as a product
ρ	density
σ	mass fraction (II, III); surface tension (V)
τ	time (II, III); shearing stress, time modulus (V)
ϕ	equivalence ratio (II, III); fuel to oxidizer ratio (IV)
ψ	stream function defined by Eq. (4.18)

Subscripts

e	edge of boundary layer or free stream behind shock
F	fuel
f	gaseous fuel, or final
G	"all gaseous" case
g	gaseous oxidizer
i	chemical species
ℓ	liquid
o	oxidizer
S	spray
s	shock
w	wall
1	upstream of wave
2	downstream of wave
∞	free stream

I. INTRODUCTION

The work described in this progress report represents a continuation of our study of two phase detonations and their possible relation to rocket motor instability. In our previous progress report (Ref. 1) we showed that it is relatively easy to establish experimentally a self-supporting high pressure wave in a two phase system consisting specifically of liquid diethylcyclohexane (DECH) as fuel and gaseous oxygen. Our experiments then were conducted mostly in polydisperse sprays which lacked quantitative repeatability. Since the mechanism of two phase detonation would involve shattering and/or evaporation of the liquid phase, both of which depend to a large extent on the drop sizes involved, it was felt that any drop size effect would be camouflaged in polydisperse sprays. Accordingly we have concentrated our efforts on the production and the study of monodisperse sprays. For drops of 500 μ in diameter and larger, such sprays are easy to produce, as will be seen later, whereas sprays with lower size drops are somewhat difficult to obtain. In fact only "nearly monodisperse" sprays have been obtained so far for the lower size drops.

To assess our experimental results, the properties of DECH-O_2 Chapman-Jouguet detonations have been computed. The computation is performed after first treating the DECH-O_2 mixture as an hypothetical

ideal gaseous mixture and then, on the basis of an analytical treatment, the properties of the spray detonations are deduced. It is shown that for all practical purposes, a dilute spray can be treated as an ideal gas with modified equation of state, molecular weight and ratio of specific heats.

Our work has been directed towards the establishment and detailed study of steady detonation. Initiation is established by Mach 2.3-4.5 transmitted shocks. Although the transient process from initiation to the establishment of a detonation is an important subject, it has not been studied here. However, it may be mentioned that a theoretical study on the amplification of pressure waves in a two phase system which is related to the initiation mechanism has been advanced by Busch, Laderman, and Oppenheim[2]. The study shows that amplification does take place and that under certain conditions pressure overshoots beyond a steady-state is possible. It appears then that a two phase system like a gaseous combustible mixture can develop into detonations. Furthermore from studies of mixtures under highly turbulent regimes[3], the induction distances can be very small. Since such conditions are certainly prevalent in a rocket motor the relevance of our study to rocket motor instability becomes obvious.

Our previous report showed that it is not necessary to have the fuel drops highly dispersed in the gaseous oxidizer, but a thin film of fuel on the wall of a 2 in. diameter tube can in fact be sufficient to support a

steep fronted high pressure wave. The connection of such a phenomenon with rocket motor instability can be inferred from the observation by Harrje and Sirignano[4] that impingement of fuel on the baffles in rocket motor rendered the motor more susceptible to instability. A highly simplified treatment of detonation in a system consisting of a fuel film whereby only half the effective heat release is considered supporting the wave has been presented by Cherepanov[5]. An analysis which treats this problem more realistically as a boundary layer problem with heat and mass addition is formulated and presented here. However no numerical results have been obtained as yet.

Our experimental results on spray detonations indicate that drop shattering plays a significant role in the mechanism of two phase detonations. Therefore a separate facility for the study of drop shattering was built. This facility which was described briefly in our last report is described in greater detail here. In addition, a review of the theoretical and experimental studies found in the literature is presented and our experimental data are compared to these studies.

II. SPRAY DETONATIONS — THEORY

The similarity between the jump relations of dilute spray detonation and those of gaseous detonations has been pointed out before[1, 6, 7]. This similarity stems from the fact that the equation of state of a dilute spray is analogous to that of a perfect gas. Hence if the detonation properties of an all gaseous system are known, one can readily derive the properties of a dilute spray with the same heat release per unit mass.

In view of some recent advances in the evaluation of the properties of two phase systems[8], it is worth while to show in some detail how the two corresponding detonative systems (gaseous and spray) compare and to calculate in particular the properties of the DECH-O_2 spray system. This work has been presented, without details, in the paper by Dabora, Ragland and Nicholls[7].

A. Properties of a Two Phase System

Consider a system consisting of a gas with suspended liquid drops. The properties of such a system can be derived from the work of Rudinger[8] who makes the following assumptions:

1. The gaseous phase behaves like an ideal, calorically perfect gas.
2. The liquid phase has constant specific heat and density.
3. The liquid phase droplets random motion does not contribute to the pressure. (Rudinger shows that drops larger than a few hundredths of a micron affects the pressure by less than 1%.)

4. No mass transfer takes place between phases (i. e. , evaporation and chemical reactions are excluded).

5. The system is considered as continuum; i. e. , the droplet size and their average separation are considered small enough compared to the dimensions of the container or to the wavelength of sound waves.

If the mass ratio of the liquid phase to the gaseous phase is η and the fraction of volume occupied by the liquid phase is ϵ then the density of the system can be written as

$$\rho_s = \rho_g (1 - \epsilon)(1 + \eta) \tag{2.1}$$

Under equilibrium conditions η does not change but ϵ is variable; also the temperatures of the two phases remain equal. In view of assumption 3, the pressure is the same as that due to the gas so that

$$p_g = \rho_g \frac{R}{m_g} T \tag{2.2}$$

or

$$p_s = \frac{\rho_s RT}{m_g (1 + \eta)(1 - \epsilon)} \tag{2.3}$$

The specific internal energy of the system, e_s, is

$$e_s = \frac{1}{1 + \eta} c_{vg} T + \frac{\eta}{1 + \eta} cT \tag{2.4}$$

and the enthalpy is

$$h_s = e_s + \frac{p_s}{\rho_s} \tag{2.5a}$$

$$= e_s + \frac{RT}{m_g (1+\eta)(1-\epsilon)} \tag{2.5b}$$

$$= e_s + \frac{RT}{m_g (1+\eta)} \left(1 + \frac{\epsilon}{1-\epsilon}\right) \tag{2.5c}$$

$$= \frac{1}{1+\eta} T \left(c_{vg} + \frac{R}{m_g}\right) + \frac{\eta}{1+\eta} cT + \frac{RT\epsilon}{m_g (1+\eta)(1-\epsilon)} \tag{2.5d}$$

$$= \frac{1}{1+\eta} c_{pg} T + \frac{\eta}{1+\eta} cT + \frac{p_s}{\rho_s} \epsilon \tag{2.5e}$$

The last term in Eq. (2.5e) can be written as

$$\frac{p_s}{\rho_s} \epsilon = \frac{\eta}{1+\eta} \frac{p_s}{\rho_\ell} \tag{2.6}$$

so that

$$h_s = \frac{1}{1+\eta} c_{pg} T + \frac{\eta}{1+\eta} cT + \frac{p_s}{\rho_\ell} \tag{2.5f}$$

The specific heat at constant pressure can be found by evaluating

$$\left(\frac{\partial h_s}{\partial T}\right)_p$$

from Eq. (2.5f). Thus:

$$c_{ps} = \frac{c_{pg}(1 + \eta\delta_s)}{1 + \eta} \tag{2.7}$$

and since $c_{vs} = (\partial e_s/\partial T)_v$, one finds that

$$\gamma_s = \frac{c_{pg} + \eta c}{c_{vg} + \eta c} = \gamma_g \frac{(1 + \eta\delta_s)}{(1 + \eta\gamma_g\delta_s)} \tag{2.8}$$

The isentropic relations can be determined from the first law of thermodynamics:

$$Tds = de_s - p_s \frac{d\rho_s}{\rho_s^2} \tag{2.9}$$

Setting ds = 0 and using Eq. (2.3, 2.4), we obtain

$$\frac{m_g (c_{vg} + \eta c)}{R} \frac{dT}{T} = \frac{d\rho_s}{(1 - \epsilon)\rho_s} \tag{2.10}$$

After noting that the coefficient on the left-hand side is equivalent to $1/(\gamma_s - 1)$ and substituting ϵ from Eq. (2.6), we can integrate Eq. (2.10) and obtain

$$T \left(\frac{\rho_s}{1 - \epsilon}\right)^{-(\gamma_s - 1)} = \text{const} \tag{2.11}$$

or after eliminating T by Eq. (2.3)

$$p_s \left(\frac{\rho_s}{1 - \epsilon} \right)^{-\gamma_s} = \text{const} \tag{2.12}$$

The equilibrium speed of sound is obtained by evaluating $(\partial p_s / \partial \rho_s)_{eq}$ from this equation, after ϵ is eliminated by Eq. (2.6). Thus

$$a_s^2 = \gamma_s \frac{p_s}{\rho_s (1 - \epsilon)} \tag{2.13}$$

or

$$a_s^2 = \frac{\gamma_s RT}{m_g (1 + \eta)(- \epsilon)^2} \tag{2.14}$$

The above properties have been derived without the restriction that the spray is dilute, i.e., $\epsilon \ll 1$.

B. Comparison of Spray and Gaseous Detonations

Consider two systems, one of which consists of a spray of liquid fuel in a gaseous oxidizer and the other a uniform mixture of the same fuel in a gaseous form and the same gaseous oxidizer. Further, let the mass ratio, η, of fuel to oxidizer be the same in both systems. The properties of the spray system have just been evaluated. These properties are compared to those of the all gaseous system in Table I. It can be seen from this table that a dilute spray, i.e., $\epsilon \ll 1$, can effectively be treated as an ideal gas. The condition that $\epsilon \ll 1$ is well satisfied in our case since $\epsilon \cong 10^{-3}$ for the richest mixture that will be considered.

TABLE I. COMPARISON BETWEEN SPRAY AND GASEOUS SYSTEMS

Property	Spray		Gaseous Mixture
	Exact	Approx. (dilute spray, $\epsilon \ll 1$)	
Density	$\rho_s = \rho_g (1 + \eta)(1 - \epsilon)$	$\rho_g (1 + \eta)$	$\rho_G = \rho_g (1 + \eta)$
Equation of state	$p_s = \dfrac{\rho_s RT}{m_g (1 + \eta)(1 - \epsilon)}$	$\dfrac{\rho_s RT}{m_g (1 + \eta)}$	$P_G = \dfrac{\rho_G RT \left(1 + \eta \dfrac{m_g}{m_f}\right)}{m_g (1 + \eta)}$
Specific heat at constant pressure	$C_{p_s} = \dfrac{C_{p_g} (1 + \eta\delta_s)}{1 + \eta}$	Same	$C_{p_G} = \dfrac{C_{p_g} (1 + \eta\delta_G)}{1 + \eta}$
Ratio of specific heats	$\gamma_s = \dfrac{\gamma_g (1 + \eta\delta_s)}{1 + \eta\gamma_g\delta_s}$	Same	$\gamma_G = \dfrac{\gamma_g (1 + \eta\delta_G)}{1 + \eta \dfrac{\gamma_g}{\gamma_f} \delta_G}$
Enthalpy	$h_s = \dfrac{C_{p_g} T (1 + \eta\delta_s)}{1 + \eta} + \dfrac{\epsilon p_s}{\rho_s}$	$C_{p_s} T$	$h_G = \dfrac{C_{p_g} (1 + \eta\delta_G)}{1 + \eta}$
Speed of sound	$a_s^2 = \dfrac{\gamma_s RT}{m_g (1 + \eta)(1 - \epsilon)^2}$	$\dfrac{\gamma_s RT}{m_g (1 + \eta)}$	$a_G^2 = \dfrac{\gamma_G RT \left(1 + \eta \dfrac{m_g}{m_f}\right)}{m_g (1 + \eta)}$
Effective molecular weight	m_s = (not defined)	$m_g (1 + \eta)$	$m_G = \dfrac{m_g (1 + \eta)}{1 + \eta \dfrac{m_g}{m_f}}$

The jump relations for C-J gaseous detonations, wherein the gases before and after the wave are considered as two distinct ideal gases with their appropriate γ's and molecular weights, are known[9] and rewritten below:

$$\frac{\left(M_1^2 - \frac{\gamma_2}{\gamma_1}\right)^2}{M_1^2} = 2\left[\frac{Q}{C_{p1} T_1} - \frac{\gamma_1 - \gamma_2}{\gamma_1 (\gamma_2 - 1)}\right]\frac{\gamma_2^2 - 1}{\gamma_1 - 1} \tag{2.15}$$

$$\frac{P_2}{P_1} = 1 + \frac{\gamma_1}{\gamma_2 + 1}\left(M_1^2 - \frac{\gamma_2}{\gamma_1}\right) \tag{2.16}$$

$$\frac{\rho_1}{\rho_2} = 1 - \frac{1}{\gamma_2 + 1}\left(M_1^2 - \frac{\gamma_2}{\gamma_1}\right)\frac{1}{M_1^2} \tag{2.17}$$

$$\frac{T_2}{T_1} = \frac{m_2}{m_1}\left[1 - \frac{\left(M_1^2 - \frac{\gamma_2}{\gamma_1}\right)}{M_1^2(\gamma_2 + 1)}\right]\left[1 + \frac{\gamma_1}{\gamma_2 + 1}\left(M_1^2 - \frac{\gamma_2}{\gamma_1}\right)\right] \tag{2.18}$$

For $Q/C_{p1} T_1 \gg 1$, which implies $M_1^2 \gg 1$, the above equations can be greatly simplified. If the following assumptions are also made:

1. $Q_G = Q_S$; i. e., the heat release/unit mass for the spray case is the same as its gaseous counterpart. In actual systems they should differ approximately by the ratio of the heat of vaporization to the heating value of the fuel which is usually less than 1%,

2. $\delta_S = \delta_G$; i. e., the specific heat of the liquid fuel is the same as its C_p when it is in the gaseous phase,

3. γ_2 and m_2 in both cases are the same, a reasonable assumption since the initial constituents are the same,

then the ratios of the spray detonation parameters to those of its all gaseous counterpart can be shown to be, after substituting condition 1 by either the spray or the all gaseous equivalent properties of Table I,

$$\frac{M_{1S}^2}{M_{1G}^2} = (1 + \phi n) \frac{(\gamma_{f1} - 1) + \phi n \, \gamma_{f1} \, (\gamma_{g1} - 1)}{(\gamma_{f1} - 1) + \phi n \, (\gamma_{g1} - 1)} \tag{2.19}$$

$$\frac{(P_2/P_1)_S}{(P_2/P_1)_G} = 1 + \phi n \tag{2.20}$$

$$\frac{(\rho_2/\rho_1)_S}{(\rho_2/\rho_1)_G} = \frac{(T_2/T_1)_S}{(T_2/T_1)_G} = \frac{V_{1S}}{V_{1G}} = 1 \tag{2.21}$$

Equations (2. 19) and (2. 20) indicate that a spray detonation exhibits higher propagation Mach numbers and higher pressure ratios than its equivalent all-gaseous counterpart. It should be added, that the Mach number and the density ratio results are in no way contradictory to those obtained in our earlier report[1] for there, the Mach number and the initial density are based on the speed of sound and the density respectively of the gaseous component in the two phase mixture.

C. Detonation Parameters for DECH-Oxygen Mixture

The C-J detonation properties of DECH (hypothetically assumed to exist in the gaseous phase) with oxygen initially at P = 1 atm and T = 298.15^{o}K are obtained from the computer program of Zeleznik and Gordon[10]*. The heat of formation for DECH and its C_p used are - 73 (Kcal/mole) and .44 (cal/gm^{o}K) respectively, evaluated from Ref. 11, 12. The results are plotted in Fig. 2.1 wherein the properties of the spray counterpart, calculated according to Eq. (2.19-2.21) are also shown. It can be seen that like most hydrocarbons, DECH exhibits peak pressure ratio and detonation Mach number at richer than stoichiometric mixtures. The computer program gives, among other things, the composition of the products of combustion which are presented in Table II.

*The authors are grateful to Drs. Zeleznik and Gordon for making the computer program available to them.

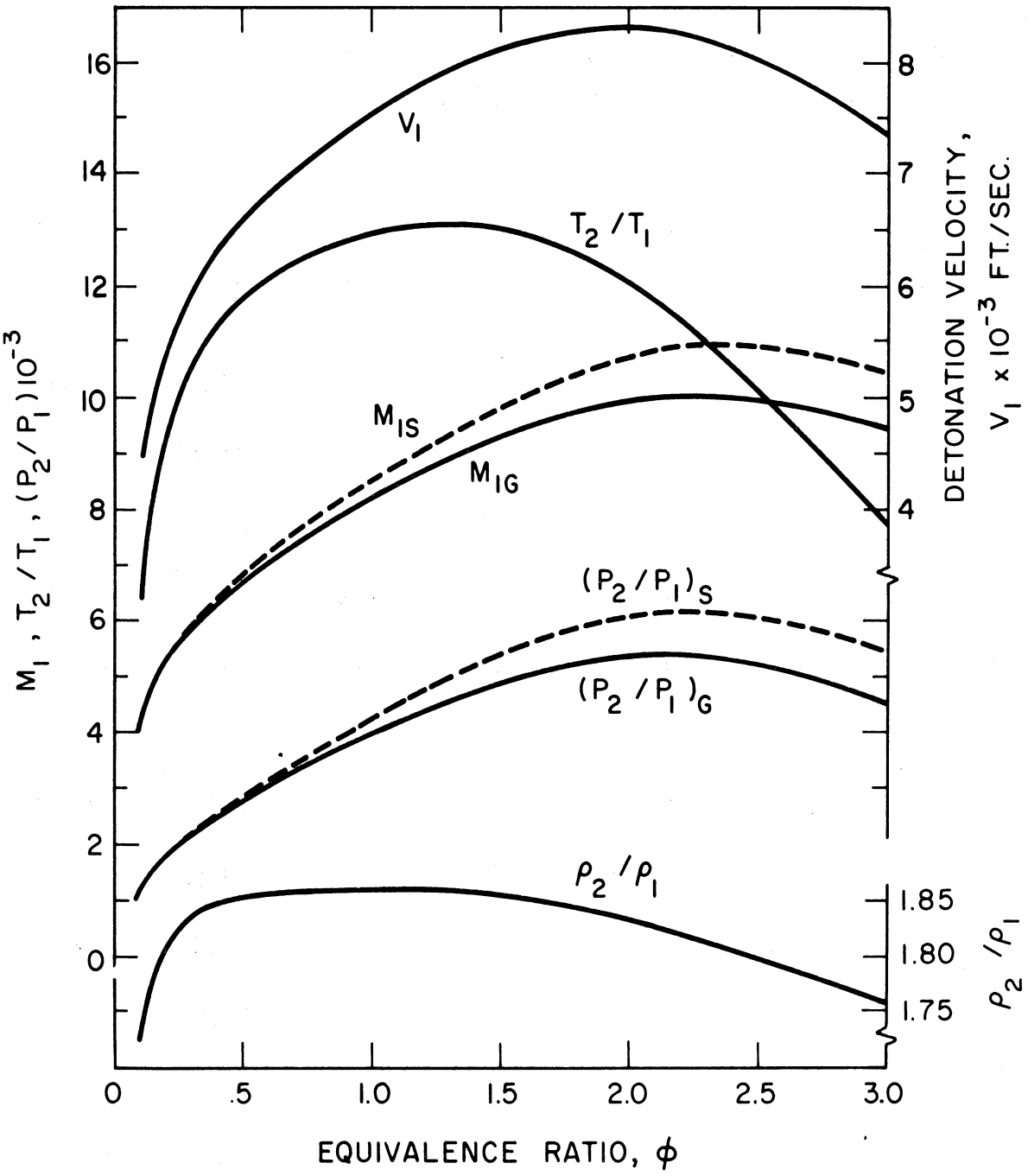

Fig. 2. 1. Properties of DECH-O_2 Detonations

TABLE II. PRODUCTS OF COMBUSTION AT THE C-J CONDITION OF DECH-O_2 MIXTURES (mole fractions)

	Equivalence ratio = ϕ					
Species	.2	.5	1.0	1.5	2.0	3.0
CO	.00453	.08549	.24565	.36764	.44430	.49910
CO_2	.11877	.16812	.13389	.07982	.03736	.00023
H	.00045	.01261	.04483	.06714	.05024	.00104
H_2	.00062	.01168	.05263	.13205	.26463	.49705
HCO	*	.00001	.00009	.00024	.00034	.00008
H_2O	.11115	.18722	.24535	.24608	.18342	.00129
O	.01005	.06014	.05672	.02049	.00188	*
O_2	.73182	.37791	.10246	.01478	.00051	*
OH	.02261	.09683	.11839	.07175	.01731	*
CH_3	*	*	*	*	*	.00005
CH_4	*	*	*	*	*	.00080
C_2H_2	*	*	*	*	*	.00320
C_2H_4	*	*	*	*	*	.00001

* $< 10^{-5}$

Other products considered whose mole fraction was less than 10^{-5} were C, C_2, C_3, C (solid), CH, and CH_2.

III. SPRAY DETONATIONS — EXPERIMENTS

A. Production of Monodisperse Sprays

In order to assess the influence of drop sizes on two phase detonations, it is desirable to obtain a spray with uniform size drops. The method which is based on the vibration of parallel liquid capillary jets described in our previous report[1] has been adopted for the production of monodisperse sprays. The characteristics of such a spray or drop generator will now be described.

The generator consists mainly of a cylindrical chamber 1.75 in. I.D. x 3/4 in. in length on one end of which is attached an injector plate having the desired number and size of capillary needles. The needles are usually 1/4 in. in length and protrude from the surface of the plate about 1/8 in. The liquid is forced through the capillary needles vertically downward and the chamber as a whole is vibrated longitudinally at a frequency in accordance with Rayleigh's[13] instability equation relating the frequency at maximum disturbance amplification with the velocity and diameter of the jet.

$$f = \frac{u_j}{4.508\, d_j} \tag{3.1}$$

Under this condition the size of the drops is

$$D = 1.89\, d_j \tag{3.2}$$

and the distance between drops

$$\lambda = 2.38\ D \tag{3.3}$$

Because of surface tension, it is found theoretically[1,14] that the initial minimum velocity with which the liquid could be ejected as a continuous jet rather than as intermittent, irregular drops varies as

$$u_{min} = \sqrt{\frac{8\sigma}{\rho_\ell\ d_j}} \tag{3.4}$$

However, it was found experimentally that for DECH and water and for needle sizes in the range of .004 in. - 020 in. I.D., the minimum velocity is about 30% lower than predicted by Eq. (3.4).

From a knowledge of the variation of a drop diameter with its terminal velocity such as was calculated in Fig. 21 of Ref. 1 and Eq. (3.2, 3.4), it is possible to find the drop diameter for which the initial velocity is equal to the terminal velocity. For DECH falling in oxygen at standard conditions this diameter is 380 μ. Thus drops of diameter larger than this diameter, tend to accelerate whereas smaller drops will decelerate. Deceleration usually results in coalescence of drops from the same stream and in practice we have found that coalescence is minimal when the initial velocity of the drops is less than 1/3 of the terminal velocity, i.e., for accelerating drops. Figure 3.1 shows nine streams of 750 μ drops in a 3 x 3 array at the shedding location and at 2 ft below the drop generator. Although all streams are not in the same plane, the drops appear in good focus because collimated light was used. Their uniformity as well as the accelerating effect are evident.

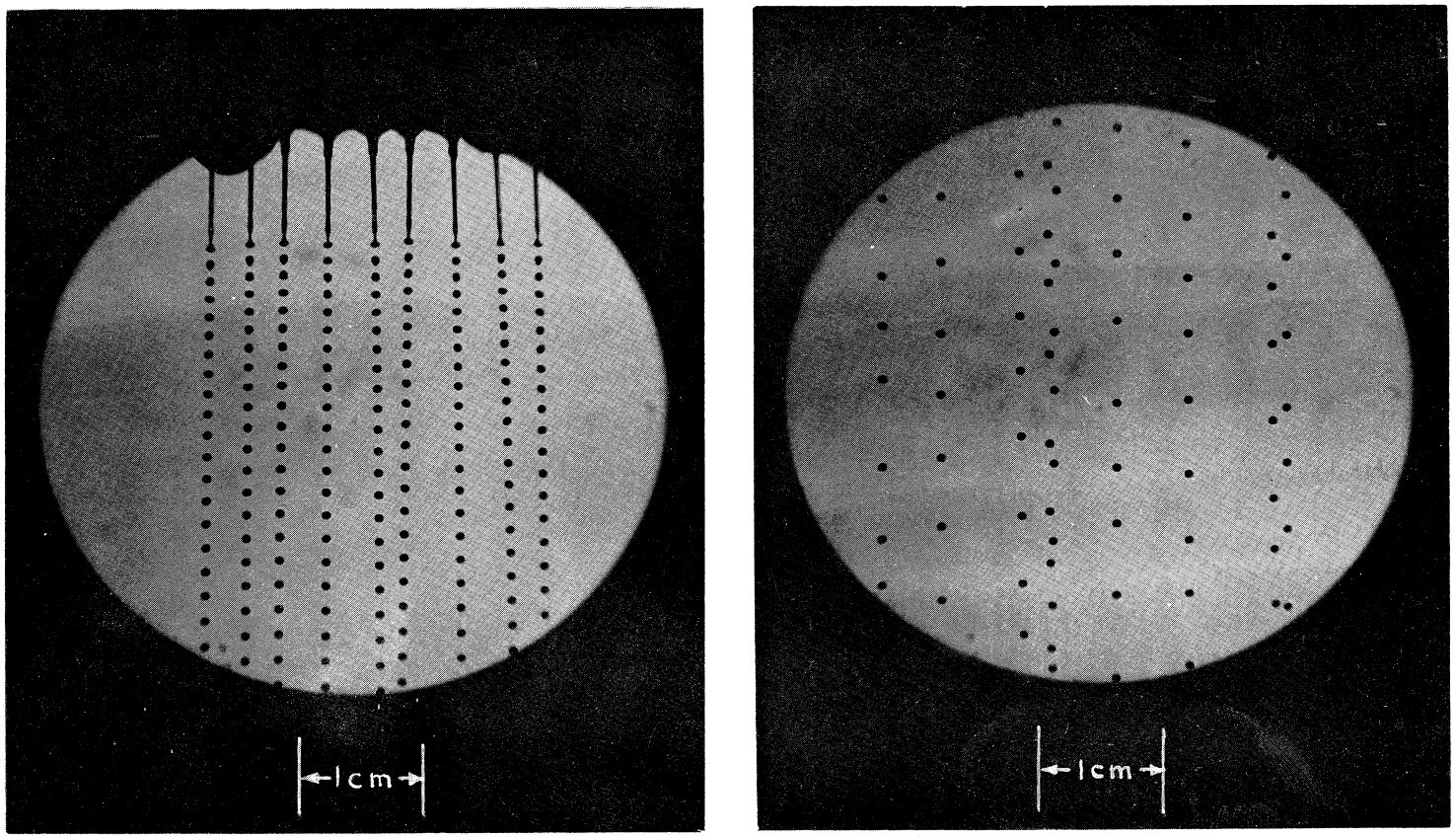

Fig. 3.1. Monodisperse Sprays of DECH in Air at 460 cps

a) At generator head
b) 2 ft below generator

For drops of diameters in the neighborhood of 380 μ and lower, we have found that a modification of the generator as shown in Fig. 3. 2 which allows a coflow of the gas (in this case O_2) is effective in minimizing coalescence. Figure 3. 3 shows 294 μ drops near the generator head and 2 ft below it when no coflow was used. The needle plate configuration is as shown in Fig. 3. 4a. It is evident that at 2 ft appreciable coalescence has taken place. When some coflow was used this coalescence decreased appreciably as could be seen from Fig. 3. 5. The main effect of the coflow is to prevent the drops of the same stream from following in the wake of their predecessors. The optimum amount of coflow is arrived at by experimentation and usually results in a very gentle stream.

Examination of the spreading of the spray show that if the needles are arranged inside a circle of 1 in. diameter or less the spreading at 8 ft below the generator does not exceed 4 in. diameter. This should be taken into consideration if wall wetting in the detonation tube is to be avoided.

From the above results it is felt that an adequate method of producing monodisperse or nearly monodisperse sprays in the size range of 200-1500 μ is now available. It should be mentioned that inasmuch as the velocity of the drops in general change as they fall, the mixture ratio of the liquid to the surrounding gas in the tube changes and it is of importance to calculate the distance at which nearly steady velocity is attained. If $\rho_g/\rho_\ell \ll 1$, an assumption well satisfied in our case, the acceleration of a single drop can be written as

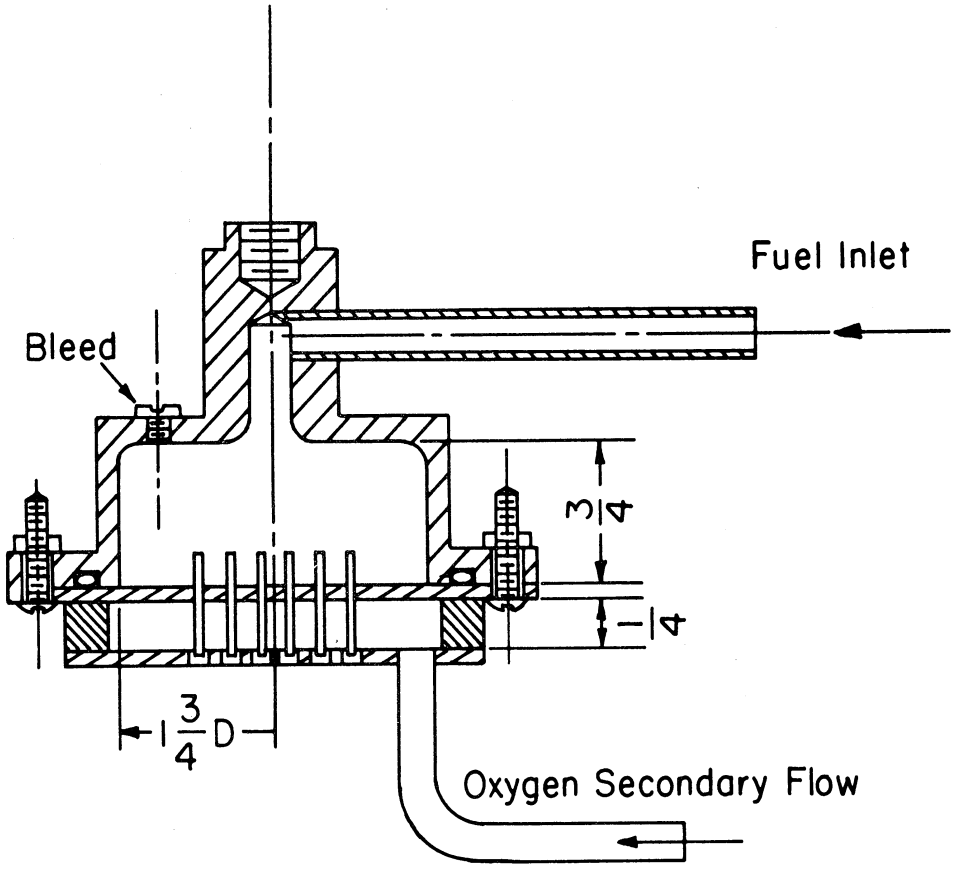

Fig. 3. 2. Drop Generator with Provision for Coflow

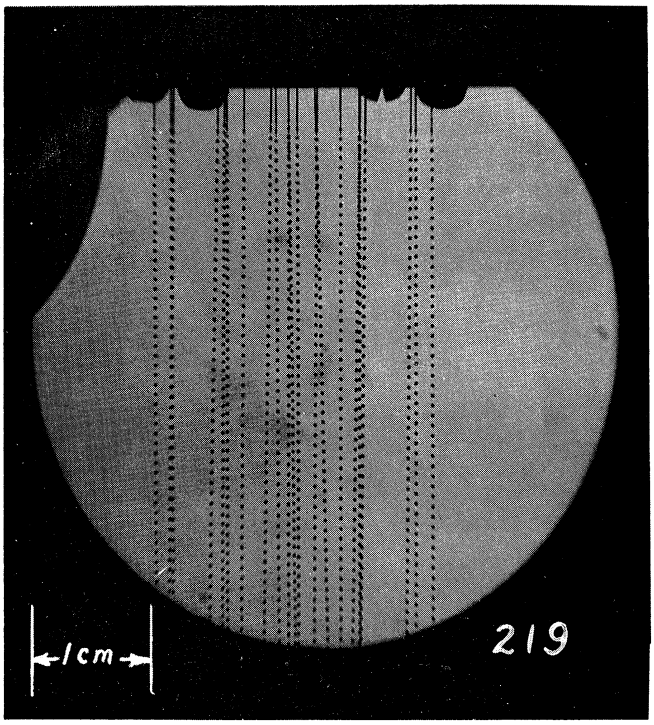

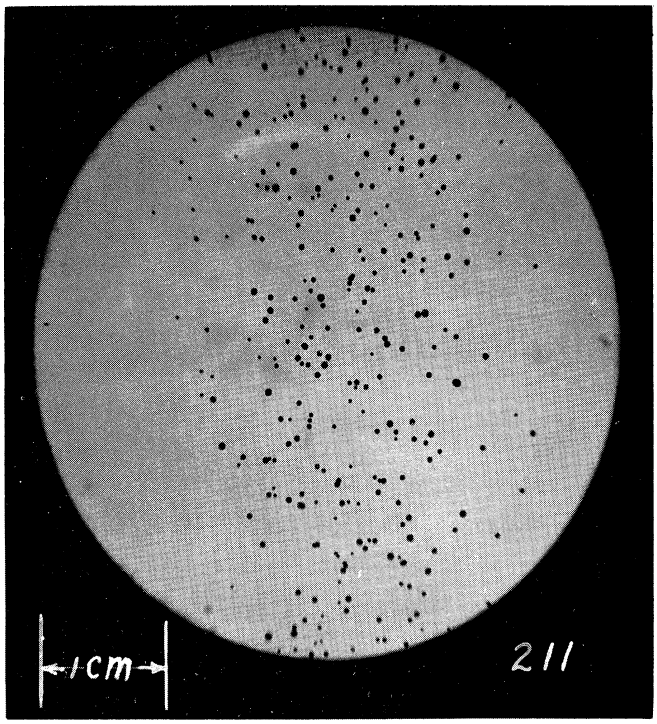

(b)

Fig. 3.3 290μ Spray without Coflow
(DECH at 2000 cps)

a) At generator head
b) 2 ft below generator

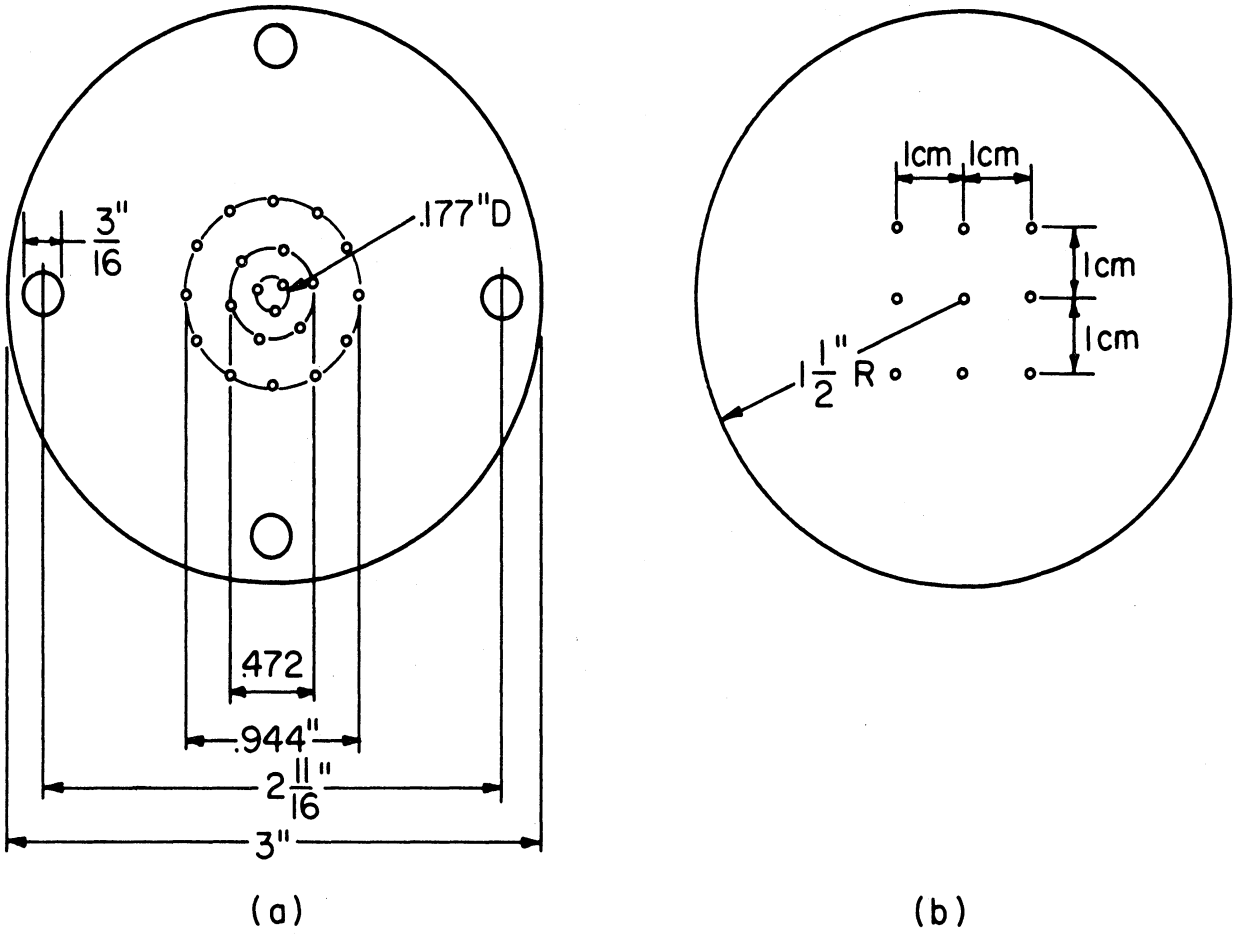

Fig. 3.4. Needle Plate Configurations

(a) No. 3: 21-.006 in. I.D. Needles
(b) No. 6: 9-.016 in. I.D. Needles

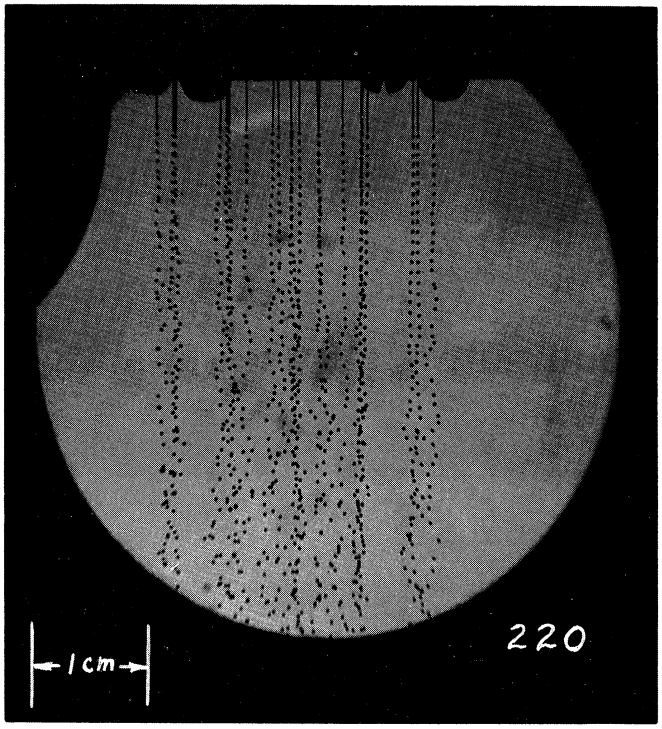

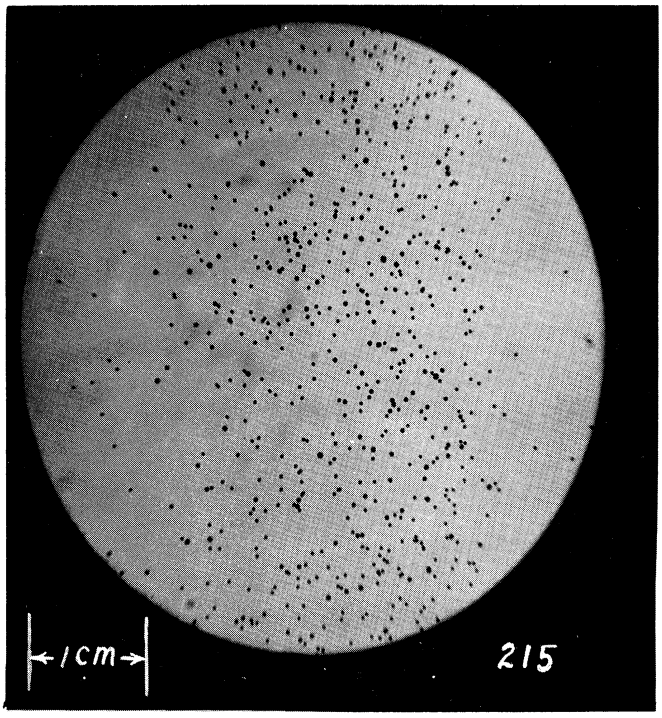

(b)

Fig. 3. 5. 290μ Spray with Coflow Showing Reduced Coalescence (DECH at 2000 cps)

a) At generator head
b) 2 ft below generator

$$\dot{u} = g - \frac{3}{4}\frac{\rho_g u^2 C_D}{\rho_\ell D} \tag{3.5}$$

After non-dimensionlizing the acceleration by g and the velocity by the terminal velocity, this equation can be written as

$$\frac{\dot{u}}{g} = 1 - \frac{u^2}{u_\ell^2} \tag{3.6}$$

where the terminal velocity is

$$u_\ell = \left(\frac{4}{3}\frac{\rho_\ell}{\rho_g}\frac{Dg}{C_{D_\ell}}\right)^{1/2} \tag{3.7}$$

For Stokes flow Re C_D = const and therefore Eq. (3.6) can be written as

$$\dot{\bar{u}} = 1 - \bar{u} \qquad \text{(Stokes)} \tag{3.8}$$

For $10 < Re < 1000$, it can be found that $Re^{1/2} C_D \cong$ const and hence Eq. (3.6) can be written as

$$\dot{\bar{u}} = 1 - \bar{u}^{3/2} \qquad (10 < Re < 1000) \tag{3.9}$$

After expressing the nondimensional time $d\tau$ in terms of $\bar{u}$, the non-dimensional distance $\bar{S}$ travelled by the drops can be expressed as

$$\bar{S} = \bar{u}_o - \bar{u}_f + \ell n \frac{(1 - \bar{u}_o)}{(1 - \bar{u}_f)} \qquad \text{(Stokes)} \tag{3.10}$$

or

$$\bar{S} = 2\left(\bar{u}_o^{1/2} - \bar{u}_f^{1/2}\right) + \frac{1}{3}\ell n \frac{\left(\bar{u}_o^{1/2} - 1\right)^2}{\left(\bar{u}_f^{1/2} - 1\right)^2} \frac{\left(1 + \bar{u}_f^{1/2} + \bar{u}_f\right)}{\left(1 + \bar{u}_o^{1/2} + \bar{u}_o\right)}$$

$$+ \frac{2}{\sqrt{3}}\left[\tan^{-1}\left(\frac{1 + 2\bar{u}_f^{1/2}}{\sqrt{3}}\right) - \tan^{-1}\left(\frac{1 + 2\bar{u}_o^{1/2}}{\sqrt{3}}\right)\right] \qquad (3.11)$$

$$(10 < Re < 1000)$$

Equations (3. 10) and (3. 11) are plotted in Fig. 3. 6 assuming the initial velocity $\bar{u}_o = 0$. It is seen that initially the non-dimensional distance is weakly dependent upon the type of flow assumed. If the drop is started at $\bar{u}_o \neq 0$ the distance travelled by it before it reaches a certain $\bar{u}_f$ can be evaluated from difference in $\bar{S}$ at the corresponding two velocities. For example starting with velocity $\bar{u}_o = .25$ the distance for the drop to reach 95% of the terminal velocity is $\bar{S} = 1.43$ for $(10 < Re < 1000)$. The actual distance is related to the non-dimensional distance as

$$S = \frac{\bar{S}\, u_\ell^2}{g} \qquad (3.12)$$

Equations (3. 10) and (3. 11) can of course be used also for cases where the initial velocity is larger than the terminal velocity.

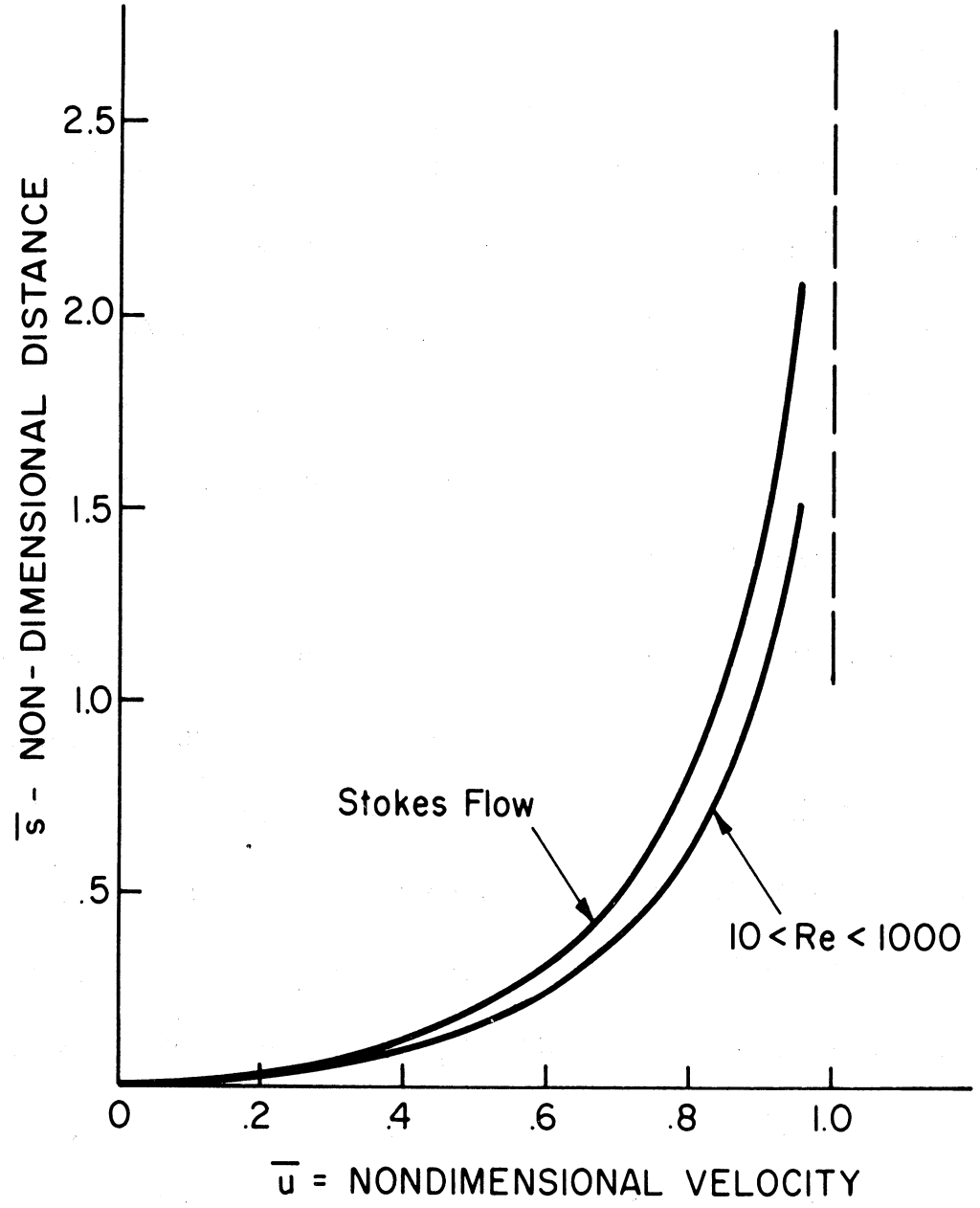

Fig. 3. 6. Distance vs. Velocity of Drops under Free-Fall

B. Combustion of a Single Droplet Stream

Experiments on polydisperse sprays have been described in detail[1, 15]. Because of the heavy wall wetting, inherent in the system for the production of the spray, it was not possible to obtain a quantitative measurement of the effect of fuel-oxygen ratio. For example, it was not possible to detect differences in propagation velocity in the stoichiometric mixture and mixtures with up to an equivalence ratio of 7.

For a systematic study, it was decided to concentrate our efforts for the present on monodisperse sprays. As a prelude to such a study, a single stream of 750 μ drops of DECH was set up along the centerline of the tube. (The tube designs used are basically the same as those described in Ref. 1. They are usually modified somewhat to suit a particular experiment. For completeness, their schematic design is reproduced in Fig. 3.7 and we shall indicate here only the modifications.) The .016 in. I.D. needle used to produce the stream of drops and its support are sketched in Fig. 3.8. The support is placed at location (4) of tube design II shown in Fig. 3.7, and is vibrated laterally as indicated. On the basis of the analysis described in the previous section the drops attain their terminal velocity in about 3 ft of fall. The mixture ratio varies from $\phi = .03$ (at the injection location) to .01 if the total tube inside area is taken into consideration. The burning drops were photographed using an image converter camera and the velocity of the wave as well as its pressure were

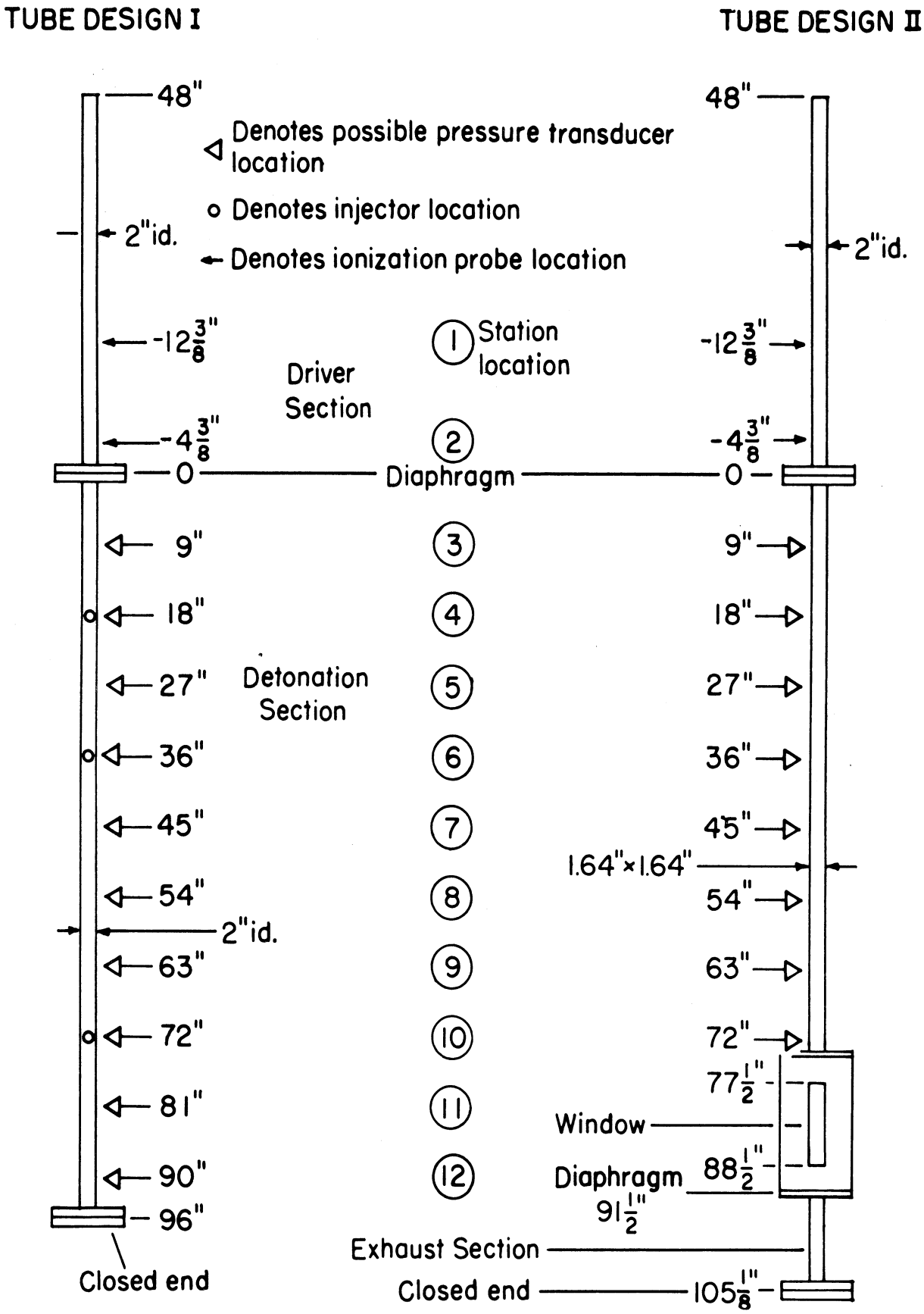

Fig. 3. 7. Detonation Tubes used for Spray and Film Detonations

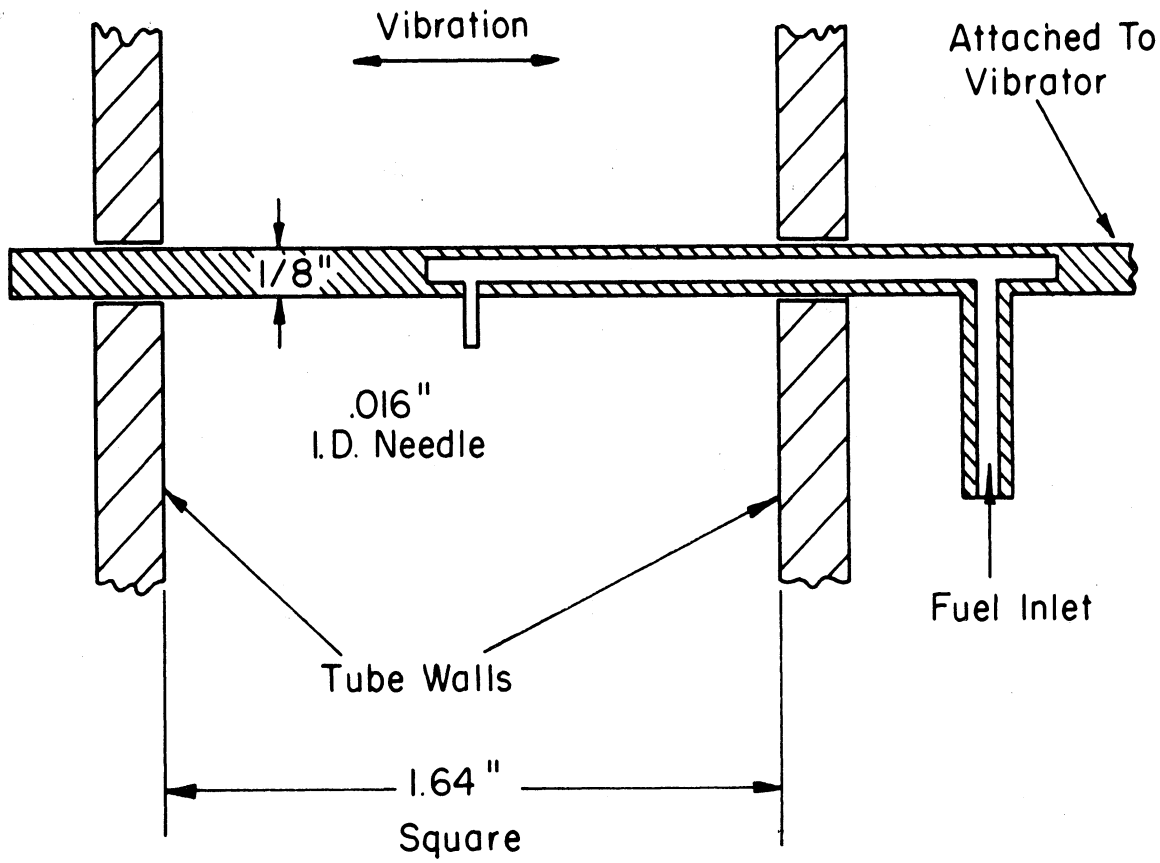

Fig. 3.8. Schematic of a Single Stream Injector Arrangement

monitored by 4 pressure transducers. The driver gas was, as usual, the detonation products of $2H_2 - O_2$ mixture. It was found that appreciable combustion could not be produced at $2H_2 - O_2$ original pressure less than 2 atmospheres. Figure 3. 9 shows some typical photographs. The wave moves downward at the test section at Mach ~ 3. 2. The luminosity appears at 70 μsec after the passage of the wave. Figure 3. 9 shows a luminous head brighter than the rest of the flame. If this head is assumed to correspond to the position of an original drop which, due to its relatively large mass, moves very slowly compared to the convective flow of the gas surrounding it, then the luminosity behind it must be due to fuel from previously processed drops. This must be so because with respect to the wave the wake of each drop is ahead of it. As might be expected, because of the very lean mixture, no acceleration of the wave or augmentation of the overpressure were observed in these experiments with fuel as compared to identical experiments without fuel.

C. Detonation in Monodisperse Sprays

Having ascertained from the previously described experiment that combustion of relatively large drops can take place within a reasonable time, experiments with monodisperse sprays with drop sizes of 750, 290 and 940 μ were conducted. Experiments with the first two types might be considered exploratory, whereas the most extensive data so far has been obtained for the 940 μ spray.

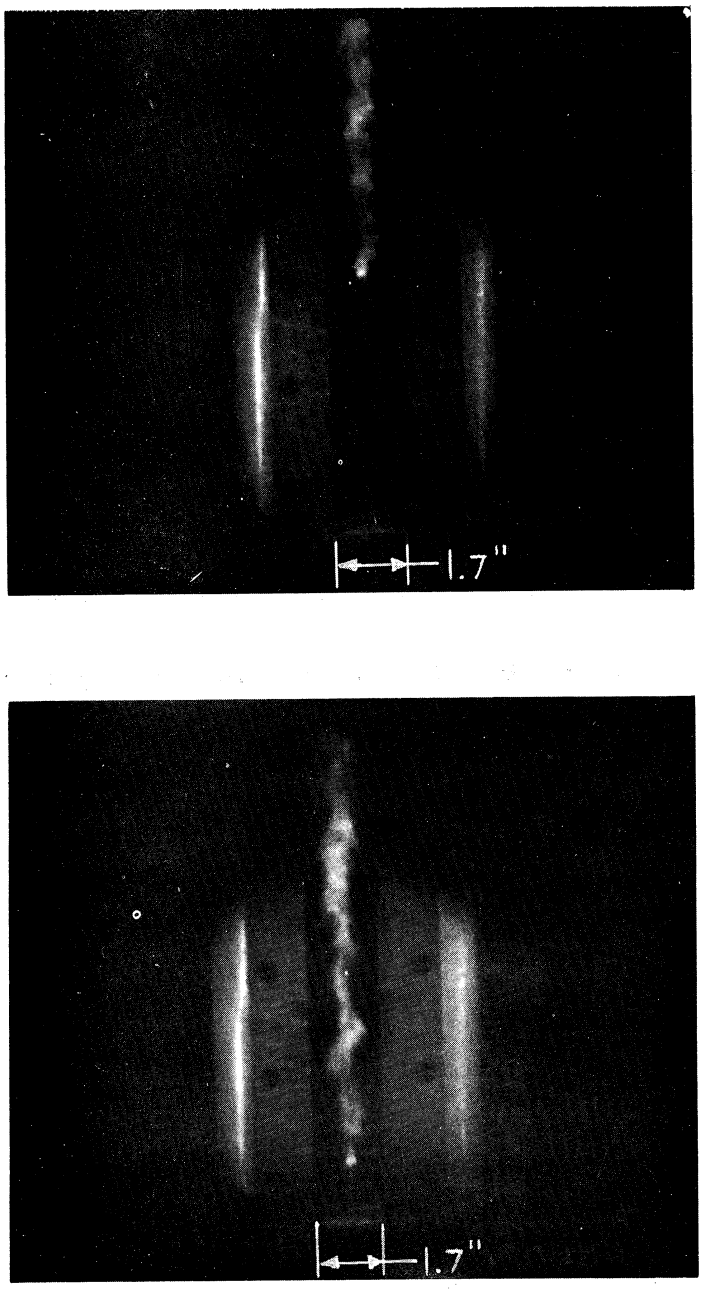

Fig. 3.9. Single Stream Combustion

750 μ Spray. Experiments with the 750 μ sprays were conducted in 3 in. I.D. plexiglass tube for visual and photographic observation. The drop generator arrangement inside the tube is shown in Fig. 3.10. To prevent any damage to the vibrator that might be caused by the pressure acting on the drop generator when detonation takes place, fixed constraints were incorporated to limit the drop generator travel. Because of the location of the drop generator, it was necessary to introduce the transmitted shock at an angle as shown. Schematic details of the two driver shock tubes used are shown in Fig. 3.11. The tube with an area ratio 1:1 was used with $2H_2 + O_2$ or He at high pressure as driver, and the tube with the area ratio of 9:1 was used exclusively with He to obtain higher transmitted shock strengths. The drop generator used is similar to the one shown in Fig. 3.2 without the coflow chamber and the needle configuration is an array of 3 x 3 x .016 in. I.D. as shown in Fig. 3.4b. With this arrangement the variation in equivalence ratio is from .49 at the generator to about .16 at distances of 3 ft and over from the generator. The plexiglass tube of 1/2 in. wall thickness held for about 5 or 6 runs before shattering. In addition its optical quality deteriorated with each run.

It was found that when $2H_2 + O_2$ mixture was used as driver, the detonation was marginal when the original pressure was 20-25 in. Hg. With the driver originally at 1 atmosphere detonation occurred consistently with the pressure ratio increasing as the wave moves down the tube. The highest

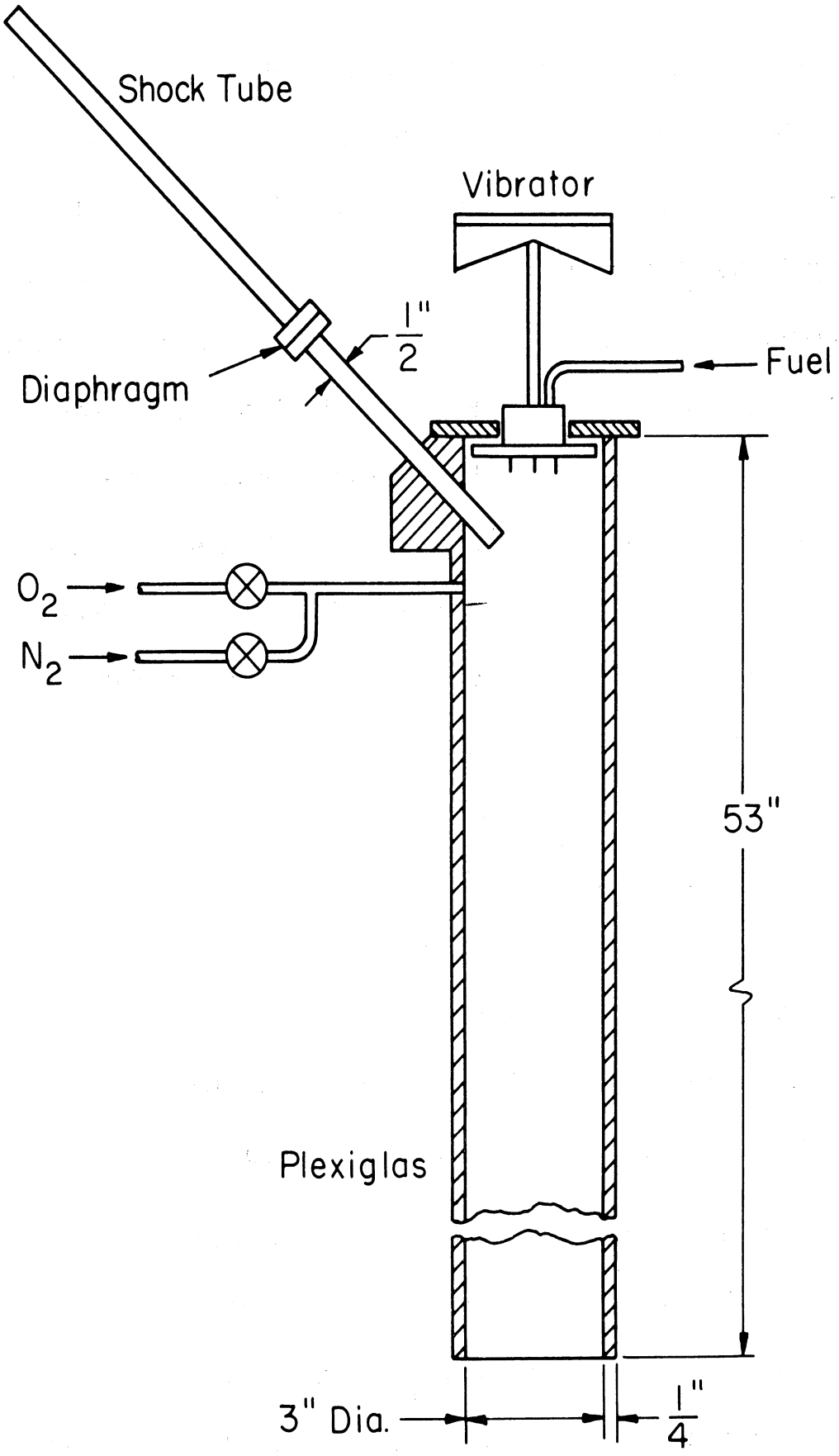

Fig. 3. 10. Detonation Tube for Visual and Photographic Observation

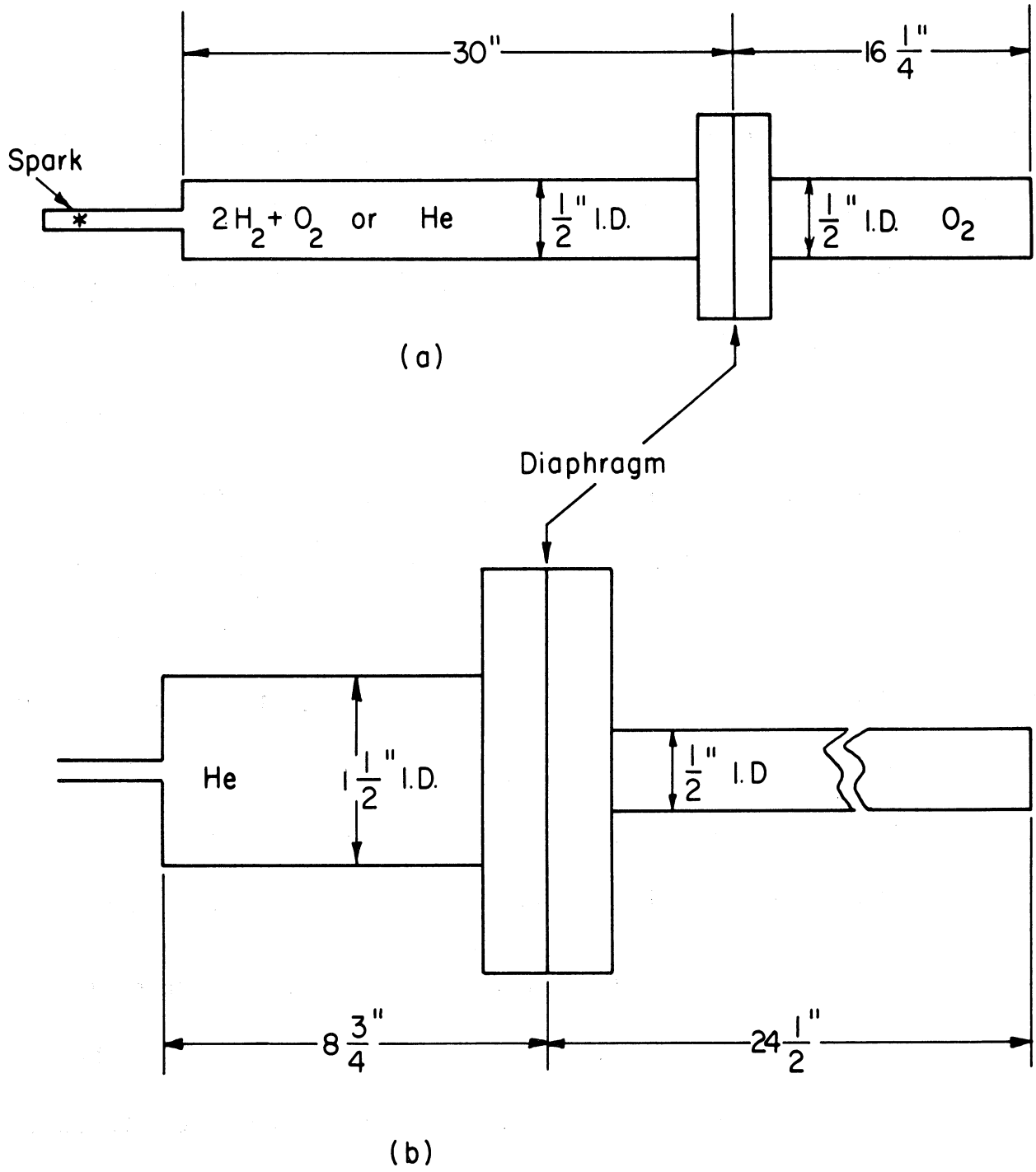

Fig. 3.11. Detonation and Helium Driven Shock Tubes

pressure ratio recorded was 11.3 which is below the theoretical value of 15 from Fig. 2.1. Similarly velocities between 2500-2700 ft/sec which are lower than theoretical were measured. Figure 3.12 shows three consecutive frames of the combustion field taken with a Fastax camera at 6100 frames/sec. The three prongs visible at the front of the combustion zone correspond to the three rows of drop streams with each row consisting of three streams viewed in line.

The helium driver was used to ascertain that combustion is not initiated by the hot gaseous products of the H_2-O_2 detonations. The theoretical and experimental Mach numbers of the transmitted shock for the helium driver are presented in Table III, and for comparison, the Mach number of the transmitted shock due to detonation of $2H_2$-O_2 are also shown. In both cases the transmitted shocks hit the combustible mixture at distances beyond the measurement point and therefore they could be somewhat weaker than shown.

Our results on shock initiation by the He shock tube indicate that a Mach number of about 3.8 is needed before detonation could be started in the heterogeneous mixture, whereas somewhat lower strength shocks were adequate for ignition when $2H_2$-O_2 driver was used. The fact that ignition in the latter case can be initiated only when the original pressure is above 25 in.Hg indicates that the phenomenon is more likely controlled by conditions behind the transmitted shock rather than by the temperature of the hot gases of the $2H_2$-O_2 products following it which would be approximately the same at all pressures

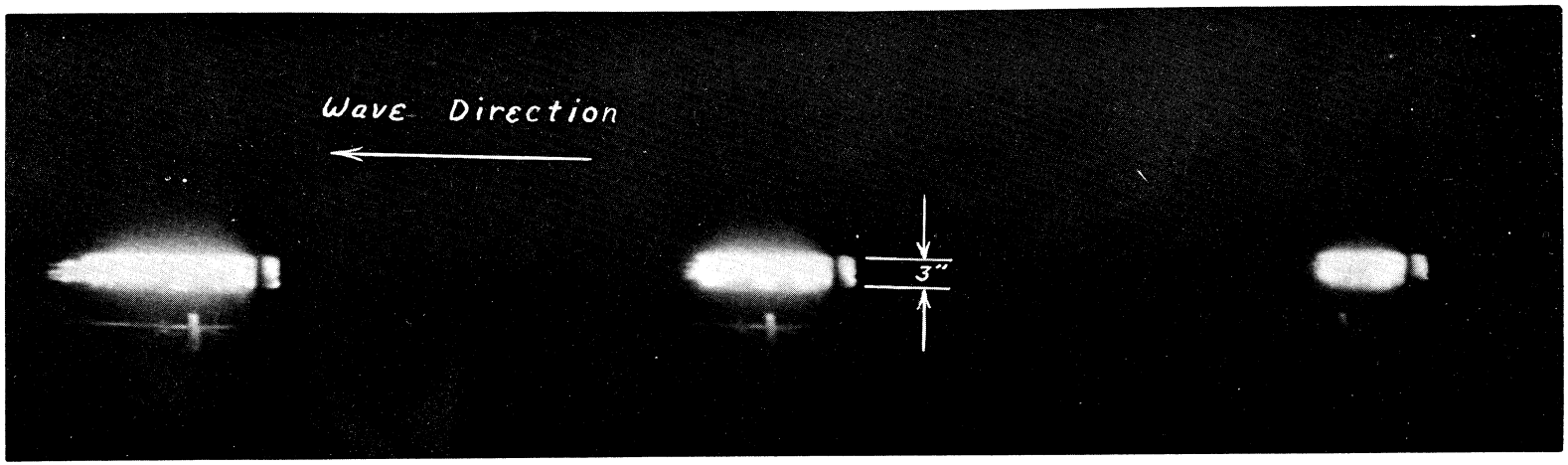

Fig. 3.12. Photographic Sequence of 750μ Spray Detonation.

TABLE III. MACH NUMBERS OF TRANSMITTED SHOCK INTO AIR AT ATMOSPHERIC CONDITIONS

Reservoir Gas	Res. Pressure	Area Ratio	M_s (theo)	M_s (exp)
He	2075 psi	1	3.88 (Ref. 10)	3.73*
	2160	9	4.85 (Ref. 11)	
	1980	9		4.46
	1725	9	4.53 (Ref. 11)	
	1400	9		4.10
	1250	9		3.72
	1200	9		4.12
	1000	9		3.87
$2H_2 + O_2$ (deton)	30 in. Hg	1	4.5 (Ref. 12)	3.8**
	25	1		2.3
	20	1		2.0
	15	1		1.7

*Measured at 15.125 in. from diaphragm.
**Measured at 9.18 in. from diaphragm.

used. This, of course, is further confirmed by the fact that initiation can be accomplished by the He shock tube. On the other hand, the discrepancy between the strength of the transmitted shocks necessary to produce combustion by the two methods could perhaps be explained by the possibility that in the case of H_2-O_2 detonation, both shock heating and hot gas ignition play a role. That is, some heating is effected by the relatively weak shock and later on combustion takes place by contact with the hot products of H_2-O_2 detonation. When helium is used however, the environment condition created by the transmitted shock must by itself be conducive to combustion since the helium itself would be cold.

2. 290 μ Spray. Some experiments with 290 μ sprays were conducted in a setup similar to that of 750 μ spray. The spray generator was similar to that of Fig. 3.2 (i.e., with coflow) and the needle configuration was as shown in Fig. 3.4a. A similar needle configuration with only 9 needles was also used. The variation in equivalence ratio along the tube is estimated to be from .18 to .27 in the former case and .08 to .12 in the latter, with the higher values attained within a foot from the injection point. For the leaner mixtures no quantitative data was obtained but judging by the noise level high pressure waves must have taken place. For the richer mixtures detonation did develop in 3 out of 9 runs. In one run a pressure ratio of 33.5 and a velocity of 4450 ft/sec were measured. The velocity is lower than the theoretical of Fig. 3.1 but the pressure is much higher. Further experiments on the 290 μ sprays will be conducted before any conclusions are made.

3. 940 μ Spray. The detonation tube for this size spray is the same as design II shown in Fig. 3.7 except that the large round driver tube is removed and replaced by a smaller tube which enters at angle through the side of the spray generator housing as shown in Fig. 3.13. The spray generator assembly is placed on top of the square tube. The plexiglass housing allows observation of the spray to check that it is properly set up. The needle configuration is similar to that shown in Fig. 3.4b except the .016 in. needles are replaced by .020 in. needles. The mixture ratio obtainable by this setup varies from ϕ = 2.1 at the generator location to ϕ = .49 at 4 ft and over. A typical photograph of the spray at the optical section, 6 1/2 ft from the generator is shown in Fig. 3.14. The uniformity of the drop sizes is apparent. The spacings, however, are random and some drops do hit the wall, but no extensive wall wetting is observed. In every run of the over fifty runs made detonation was observed. In all these runs the driver was $2H_2 + O_2$ detonations. Pressure and velocity measurements were made with Kistler pickups types 603 and 601A. Typical pressure traces from two pickups are shown in Fig. 3.15. The pressure ratio range measured from similar traces was 16-32 and the detonation velocity (usually on the basis of 4 pickups) varied between 3940-5090 ft/sec. This velocity is about 30% lower than the theoretical and the pressure ratio corresponds in general to that of a shock wave travelling at the experimental speed.

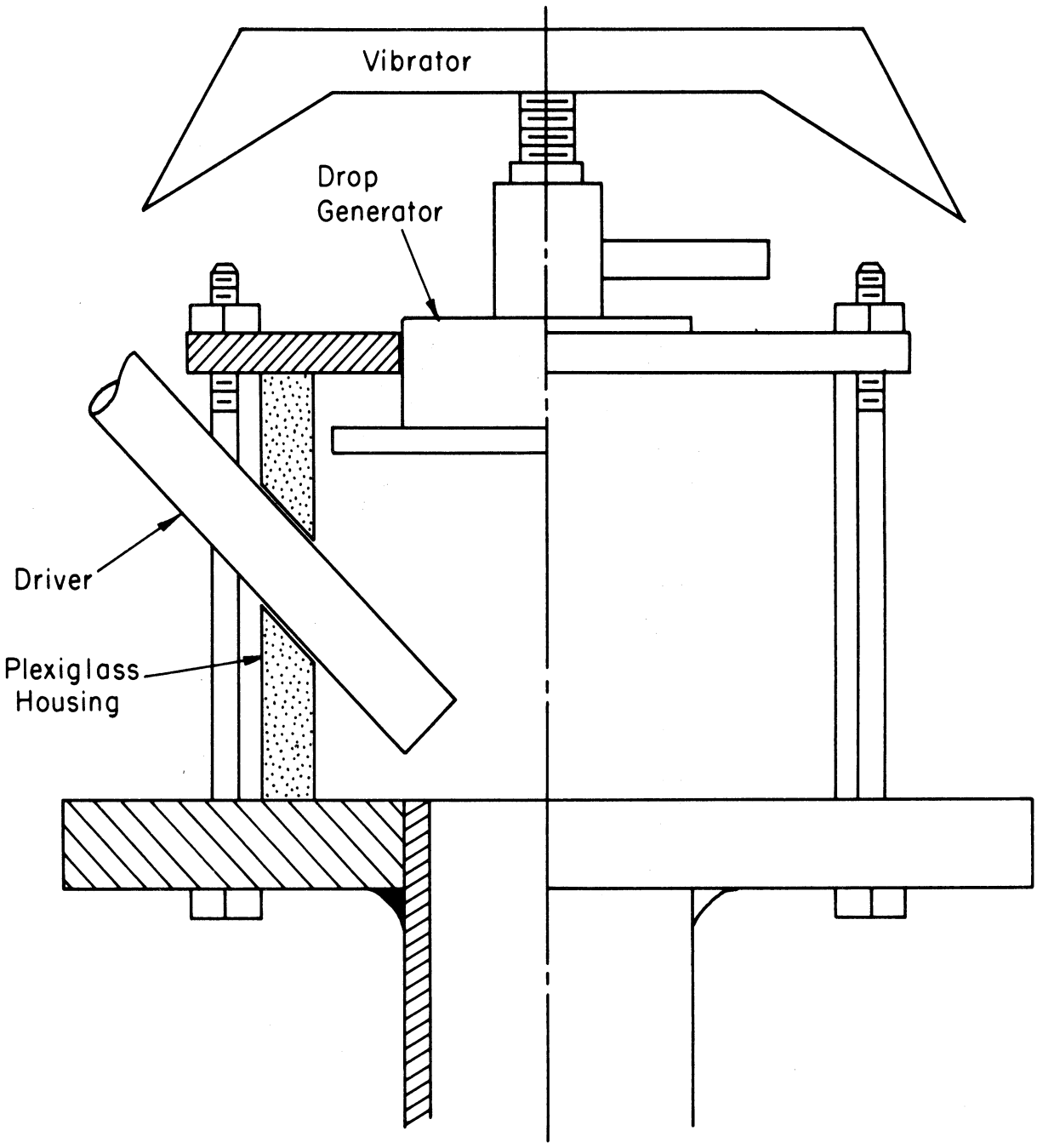

Fig. 3.13. Generator Housing

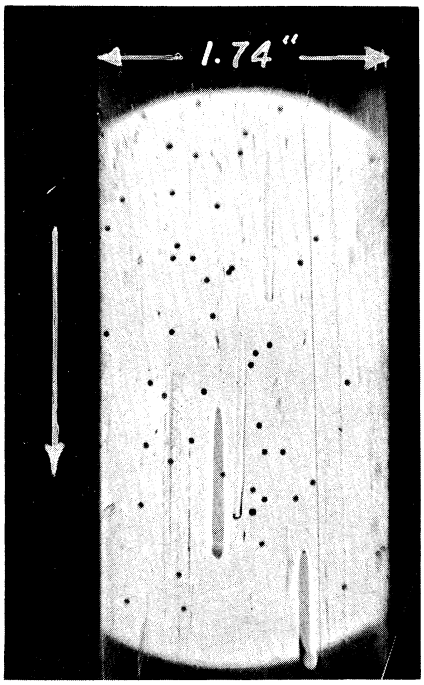

Fig. 3.14. Typical 940μ Spray Photograph at Observation Section.

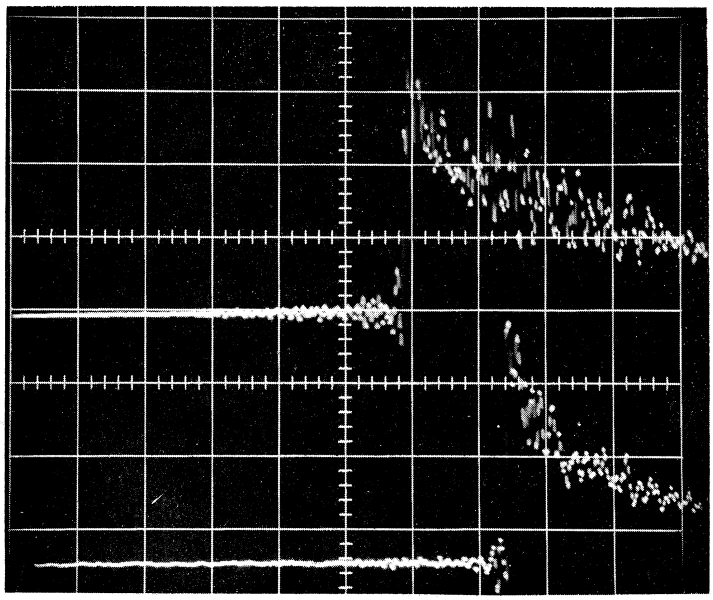

Station 6

93 psi/div.

143 psi/div.

Station 8

200 μsec/div.

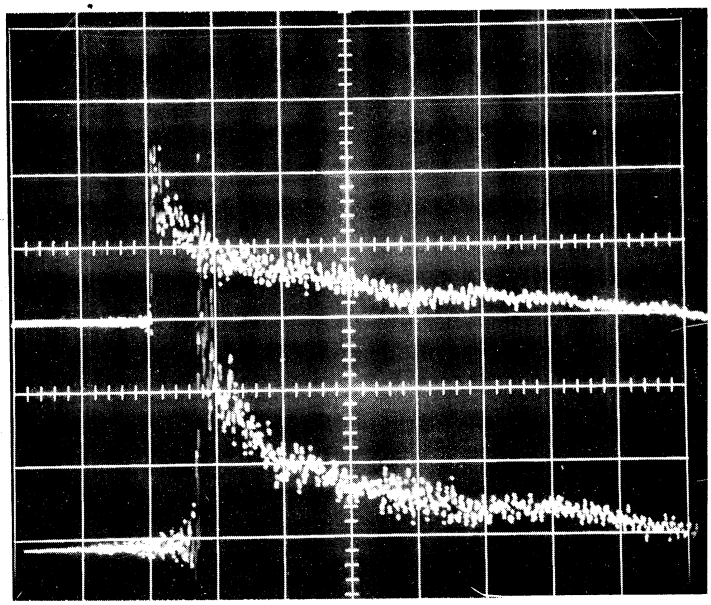

143 psi/div.

Station 6

93 psi/div.

Station 8

500 μsec/div.

Fig. 3.15. Typical Pressure Traces of 940μ Spray Detonation.

To ascertain whether the detonation reached a steady velocity, a 4 ft extension was added to the tube and the velocity was measured by the use of pressure switches designed by Willmarth[16], and developed for our application here. The switch has ~ 1 μsec response. Its design is shown in Fig. 3. 16. Ten such switches were flush mounted along the walls of the tube and the closing signals from the capcitor circuit[17] shown in Fig. 3.17 were displayed on the oscilloscope operated in a modified raster-sweep. A typical raster display is shown in Fig. 3. 18. The results of velocity measurements are shown in Fig. 3. 19. They indicate that a steady velocity is reached at about 8 ft from the injector. The average steady velocity is 5600 ft/sec or about 1000 ft/sec below the theoretical of Fig. 2. 1.

The detonation phenomenon was also observed photographically using schlieren, a combination of shadow and direct light, and streak techniques. The schlieren setup is shown in Fig. 3. 20. An image converter camera (Beckman and Whitley type 501A) is used for photography which effectively provided a fast shutter. Some typical photographs are shown in Fig. 3. 21 which show a complicated structure behind the front of the wave. In many cases the front is surprisingly planar and in some cases one can observe bow shocks around individual drops due to the convective flow. With a schlieren system it was not possible to determine the onset of combustion and therefore a combined shadow and direct light photography was used with the same

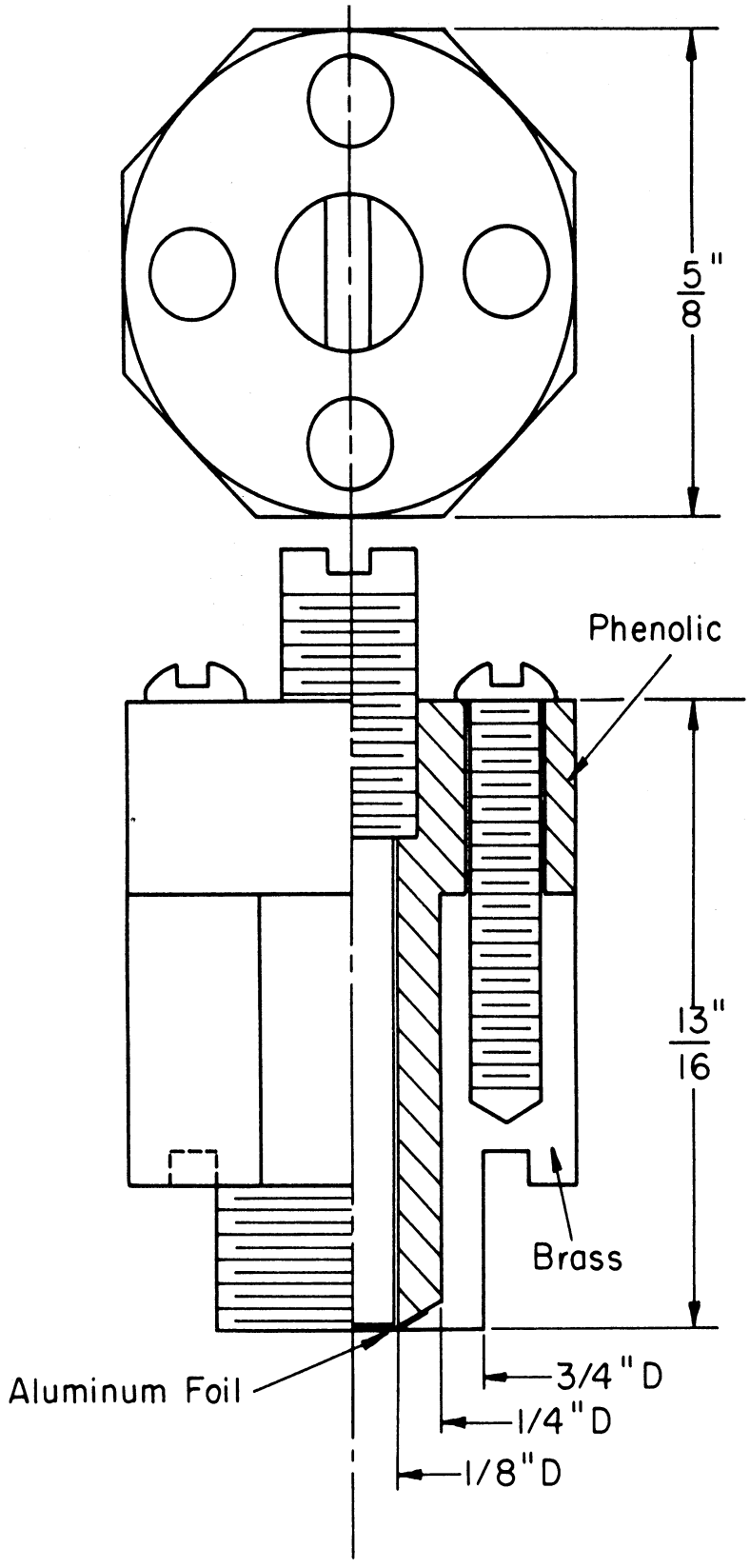

Fig. 3.16. Pressure Switch

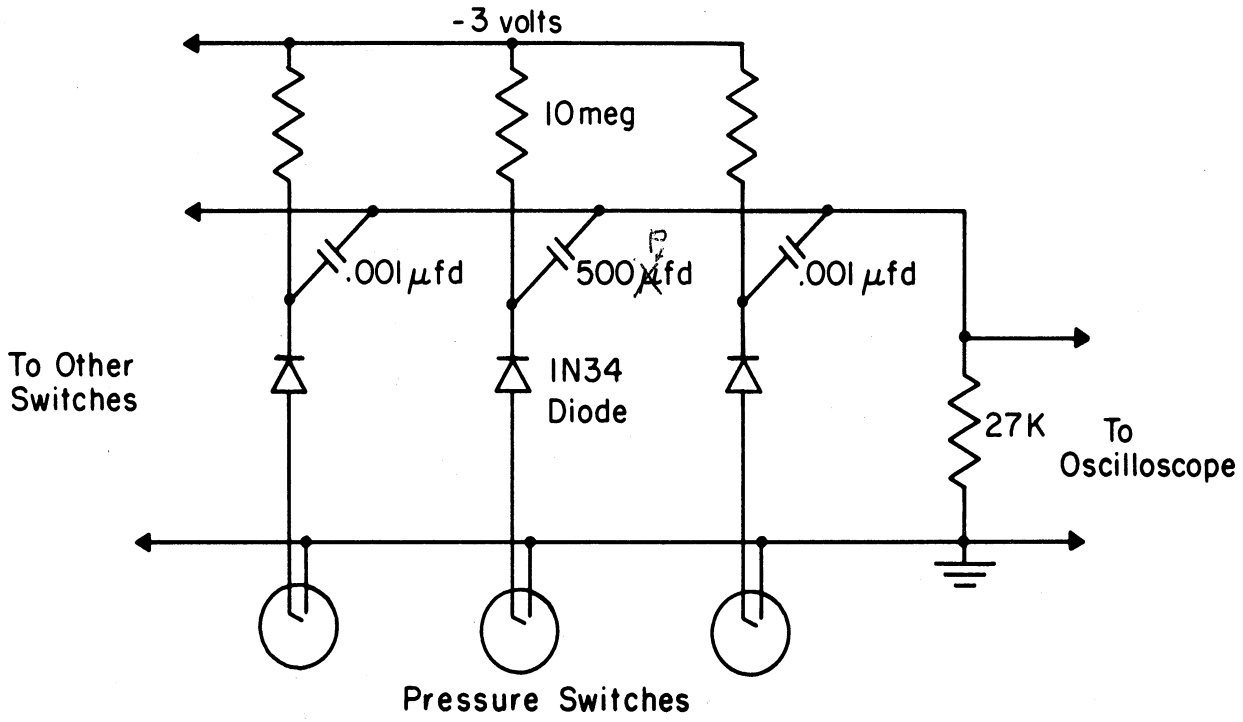

Fig. 3.17. Circuit for Raster Signals

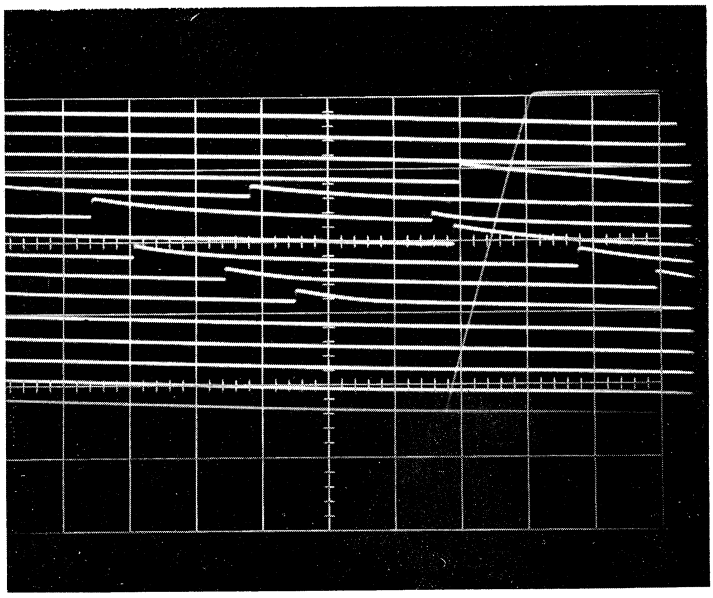

Horizontal Sweep Rate: 20 μsec/div.

Total Time per Line (including dead time): 244.7 μsec

Fig. 3.18. Typical Raster Record.

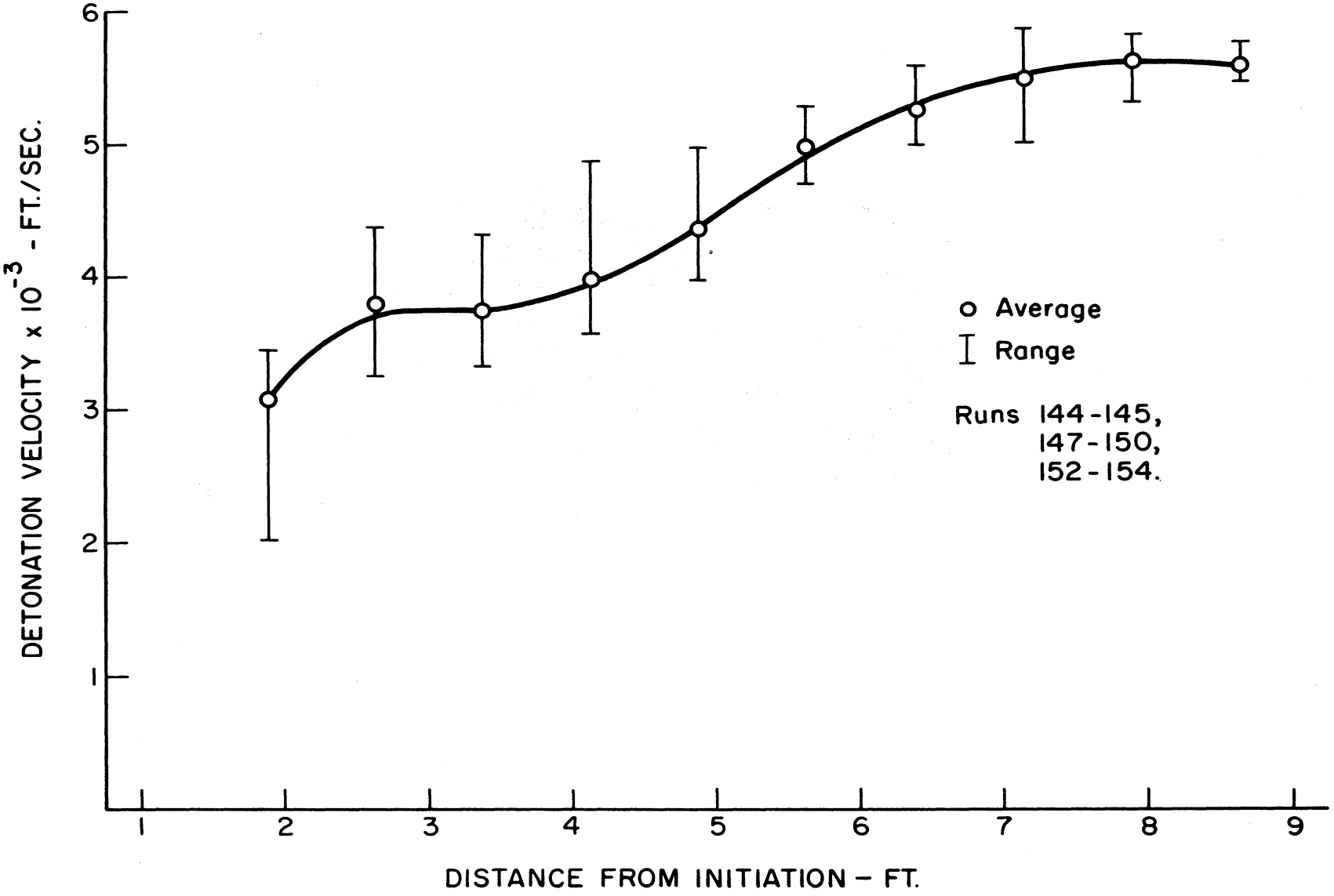

Fig. 3.19. Variation of Detonation Velocity with Distance from Spray Generator

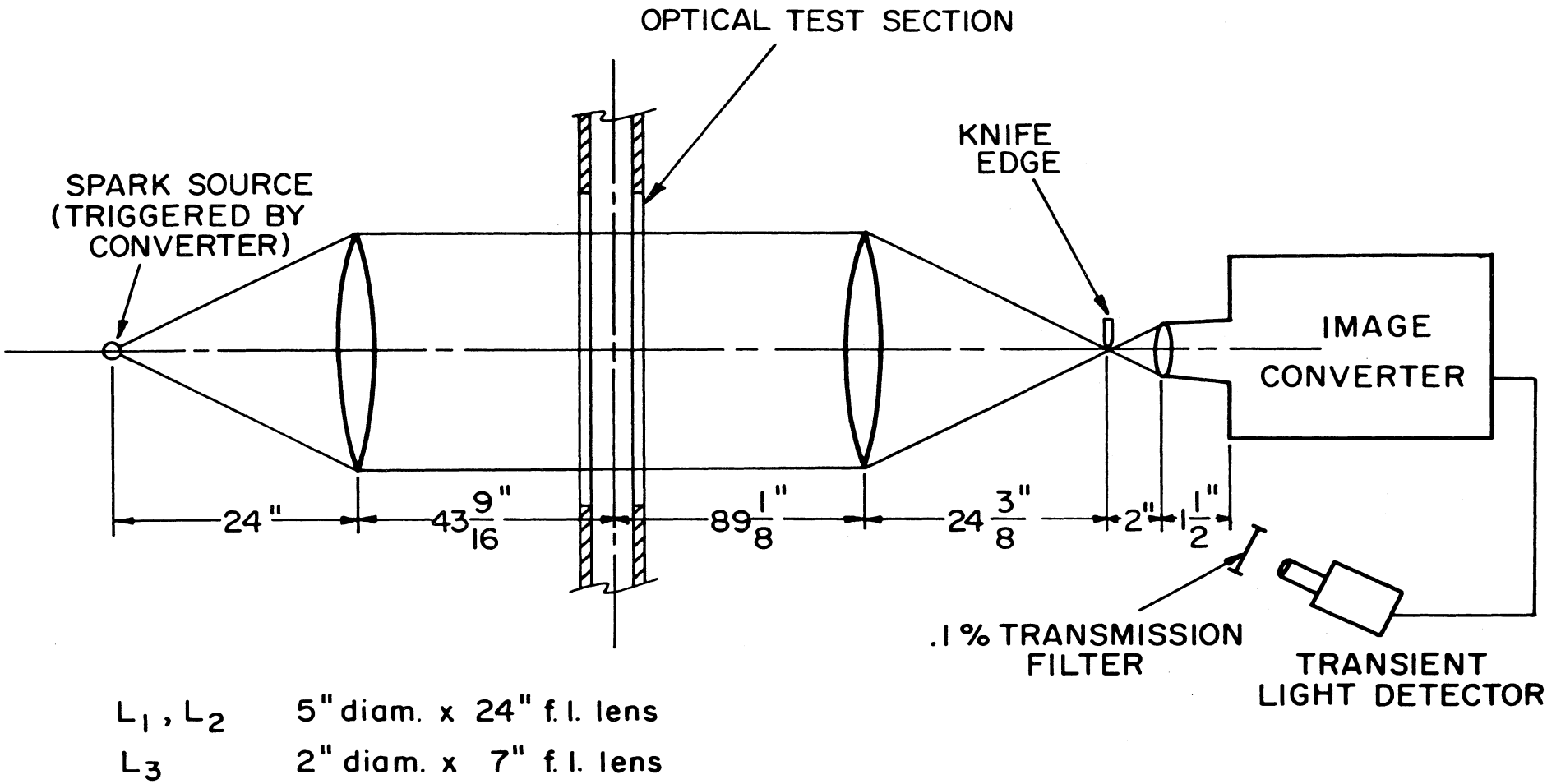

Fig. 3. 20. Schematic of Schlieren Arrangement

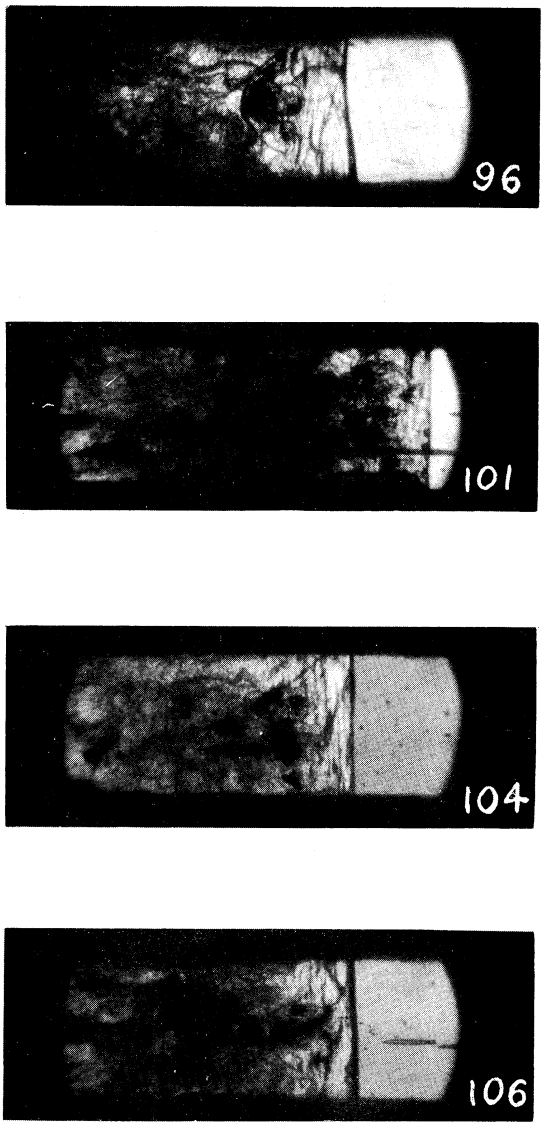

Fig. 3. 21. Typical Schlieren Photographs of 940 μ Spray Detonation.

setup as the schlieren, except that the knife-edge was removed. Some typical photographs obtained this way are shown in Fig. 3. 22. They reveal that combustion starts approximately . 6 in. (~ 11 μsec) behind the front. Such a time delay corresponds very closely to drop breakup times based on extrapolation of the data of Wolfe and Andersen[18] and, from our data in Section V, it corresponds to the time at which the beginning of breakup is manifested. It appears then, that the mechanism of heterogeneous detonation is controlled by the mechanical breakup of the drops.

The setup for streak photography is shown in Fig. 3. 23. This setup was used in two ways. In one, only direct light of the luminous event was photographed and in the other a shadow technique was incorporated in part of the field of view. Typical photographs are shown in Fig. 3. 24 and 3. 25. The traces of some drops revealing their fate are apparent in both photographs. Evidently some combustion does take place before complete breakup of the drop which is inferred from the shadow portion to be the end of the dark zone following the initial trajectory of the drop.

In some cases a structure behind the front similar to that of spinning detonations is observed, but this should not be too surprising since spin is usually associated with extended reaction lengths and certainly the reaction length in heterogeneous systems is long.

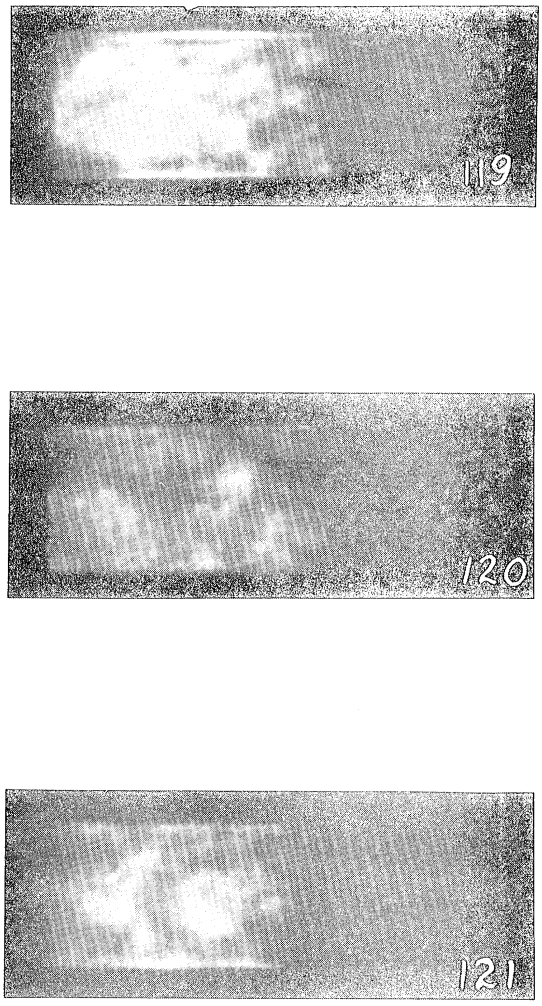

Fig. 3. 22. Typical Shadow and Direct Light Photographs of Spray Detonations.

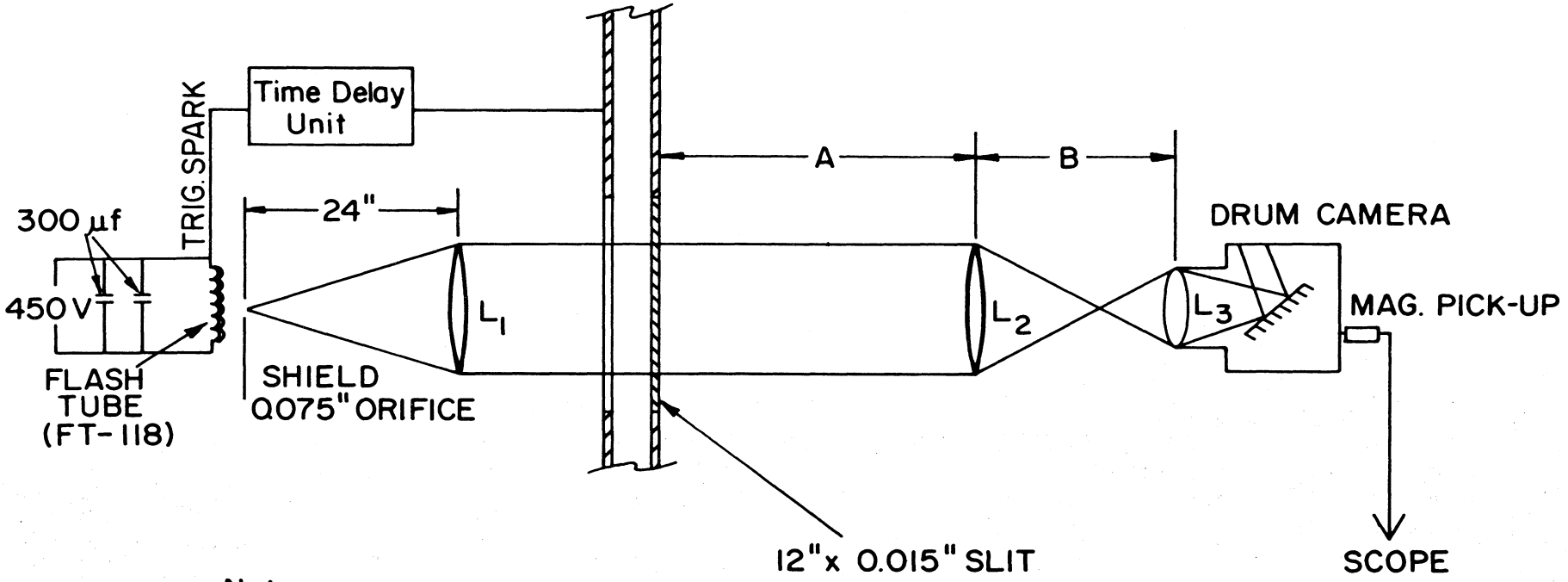

Note:

Direct Photography: Flash Tube & L_2 Not Used, A + B = 73"

Shadow + Direct Photography: A = 90", B = 26"

L_1, L_2 5" diam. x 24" f.l. lens

L_3 $1\frac{3}{16}$" diam. x 7" f.l. lens

Fig. 3. 23. Schematic Streak Photography Setup

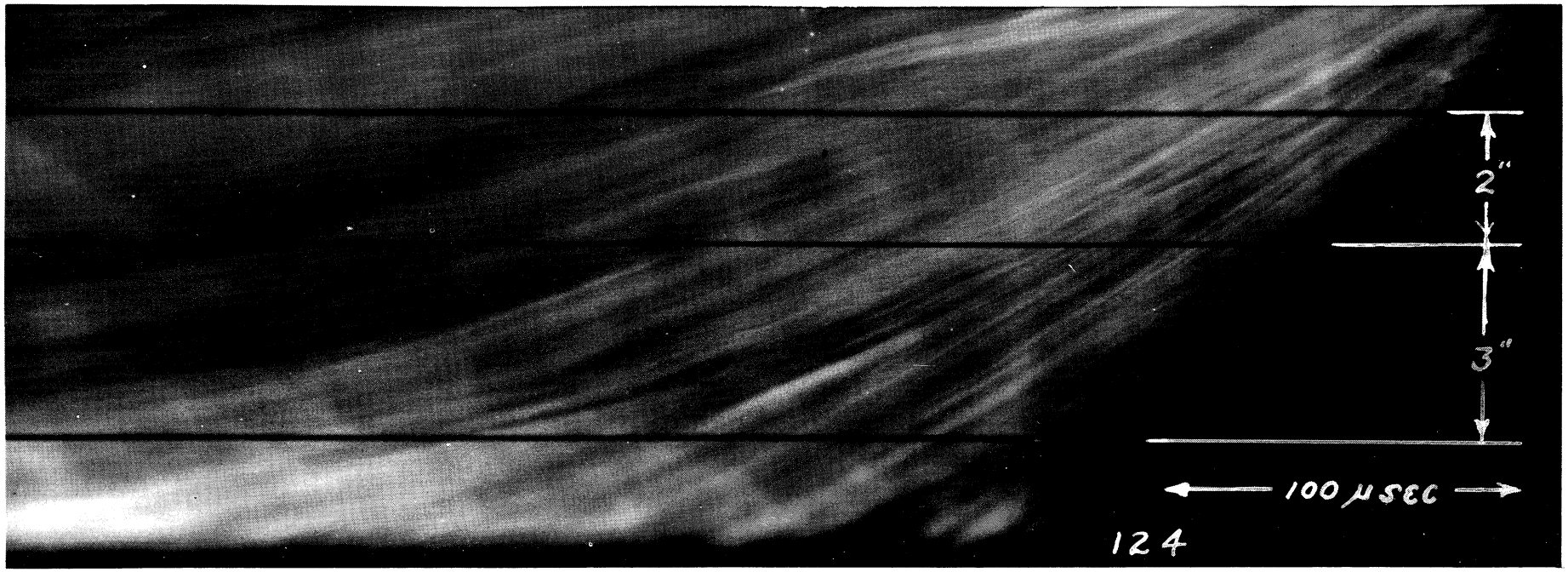

Fig. 3. 24. Streak Photograph of the Self Luminous Detonation.

Fig. 3. 25. Combined Luminous and Shadow Streak Photograph of the Detonation.

IV. DETONATION OF A LIQUID FILM

In Ref. 1 experiments were reported which demonstrated that a detonation wave can propagate in a tube in which the walls are coated with a thin film of liquid fuel; the tube is filled with gaseous oxygen such that the fuel and oxidizer are completely unmixed. Results from pressure transducers, self-luminous framing camera photographs and spark schlieren photographs showed the detonation-like characteristics of this phenomena. This work was continued experimentally and theoretically during the past year.

A. Experimental Studies

Using the same test setup as described for the burning of a single stream of drops (Fig. 3.7, tube II) but with the drop generator removed, self-luminous photographs of the film detonation were taken with the image converter camera. DECH was applied by means of a felt swab which was wetted with fuel and run up the tube wall to the 1.5 ft mark. The procedure was as follows: fill the test section with one atm. oxygen, remove the exit diaphragm and apply the DECH to the walls with the oxygen flowing in the test section, replace the exit diaphragm, fill the driver with 1 atm. stoichiometric hydrogen-oxygen, and finally fire the spark plug in the driver. The results, which are shown in Fig. 4.1a and 4.1b, give further confirmation of the results shown in Fig. 11 and 12 of Ref. 1. The combustion is confined to a narrow region along the walls. The pressure traces which are also shown were made with a Kistler

3000 ASA at f 2.0, 1.9

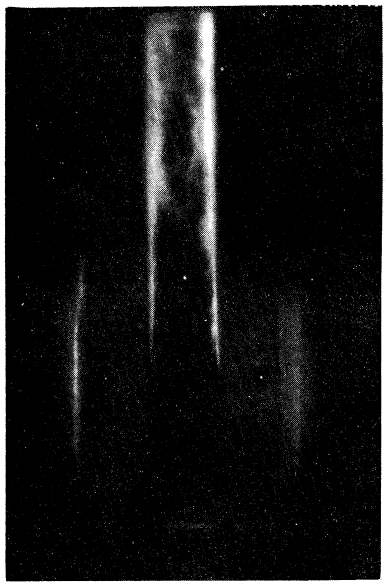

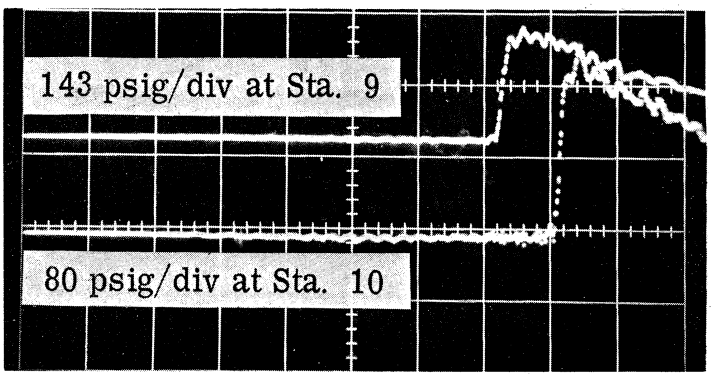

200 μsec/div triggered at Sta. 2

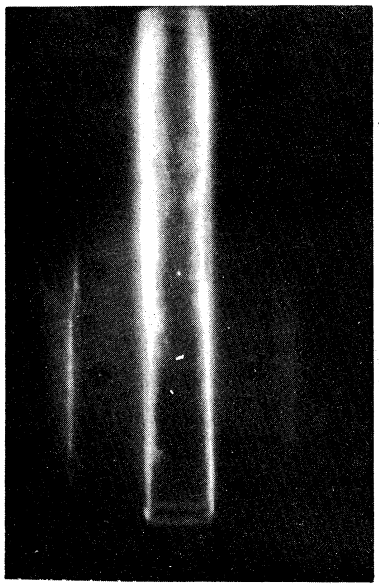

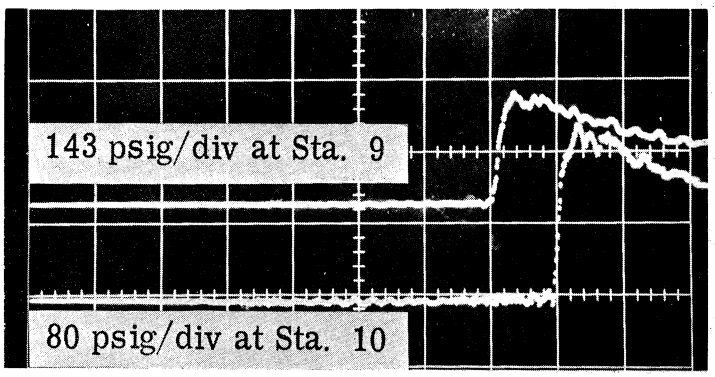

200 μsec/div triggered at Sta. 2

3000 ASA at f 1.4, 1.9

Fig. 4.1. Self-Luminous Photographs and Pressure Traces of Detonation of DECH Film Placed (a) on Two Walls.

3000 ASA at f 1. 4, 1. 9

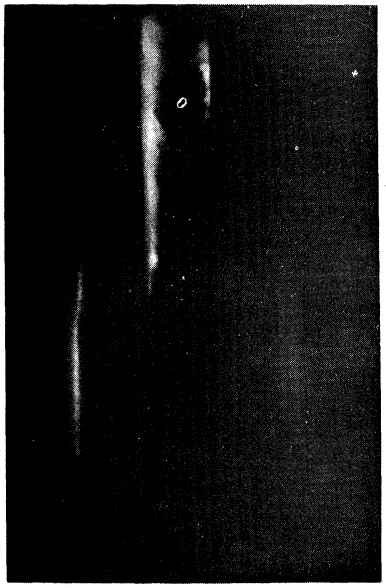

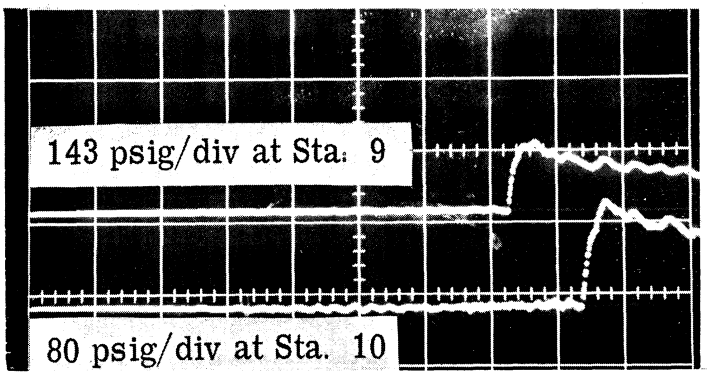

200 μsec/div triggered at Sta. 2.

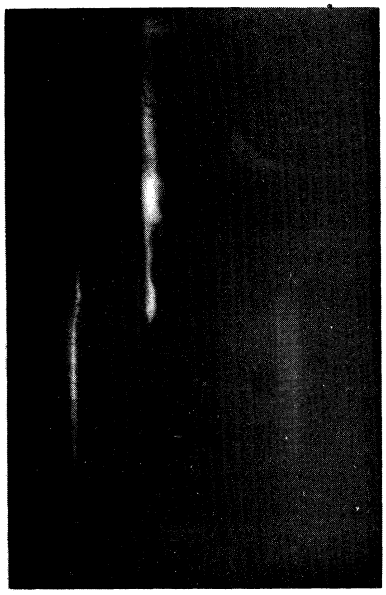

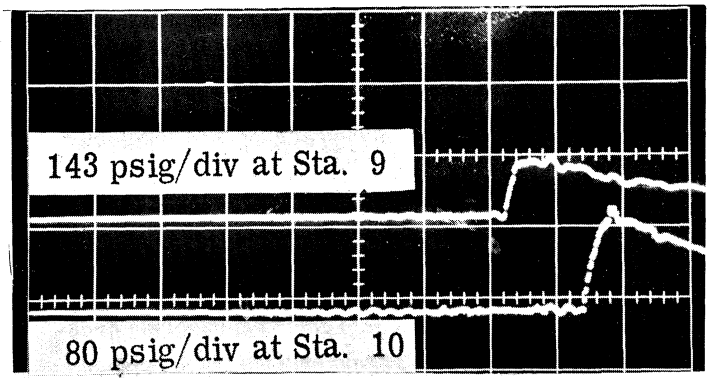

200 μsec/div triggered at Sta. 2

3000 ASA at f 1. 4, 1. 9

Fig. 4. 1. (b). On One Wall.

603 and 601A respectively which were filtered by means of a 27,000 Ω input resistance in conjunction with the capacitance of 25 ft of lead cable. As mentioned before, for the case when DECH was swabbed on two walls the measured velocity was 3750 ft/sec and the pressure ratio was about 17 to 1. When DECH was swabbed on one wall only the measured velocity was 3160 ft/sec and the pressure ratio was about 10 to 1.

Another series of experiments was made in the shock tube shown in Fig. 5.1 to examine the nature of the removal of the fuel from the wall in an inert environment. A flat plate was mounted in the test section of the shock tube as shown in Fig. 4.2 and a thin layer of DECH was placed on top of the flat plate. Spark schlieren photographs were taken with an image converter camera (as shown in Fig. 3.20) at 1 μsec exposure, at various times after passage of the shock. All the tests were made with a Mach 2.2 shock into a 1 atm. nitrogen. The results, which are shown in Fig. 4.3, indicate that the layer of liquid remains near the wall although the apparent thickness of the layer grows and the surface becomes rougher until the fuel is "used up." The thickness of the liquid layer as a function of time after passage of the shock (as determined from Fig. 4.3) is shown in Table IV. Also shown is the approximate boundary layer thickness with mass addition for a Mach 2.2 shock (the method for obtaining this is given below and results are available for this Mach number only at this date). It is evident that the liquid fuel remains within the boundary layer.

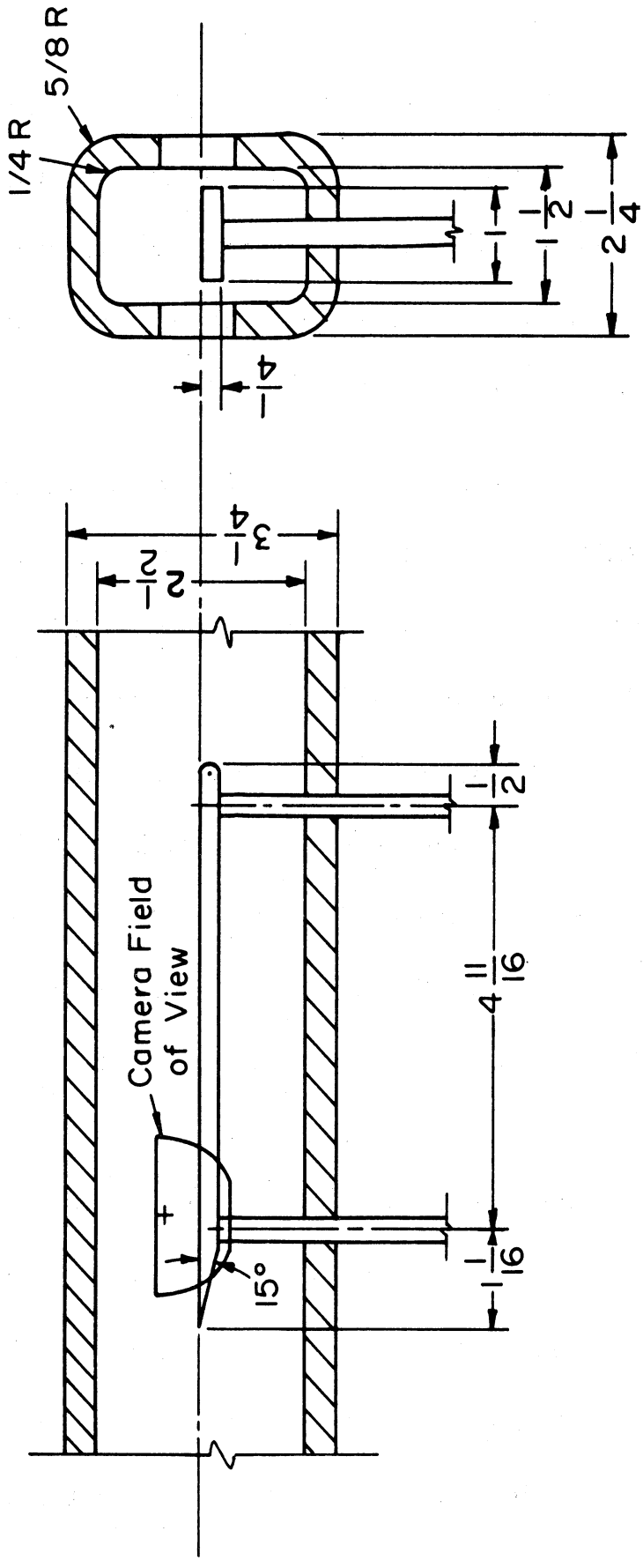

Fig. 4. 2. Test Setup for Observing a Liquid Layer Behind a Normal Shock

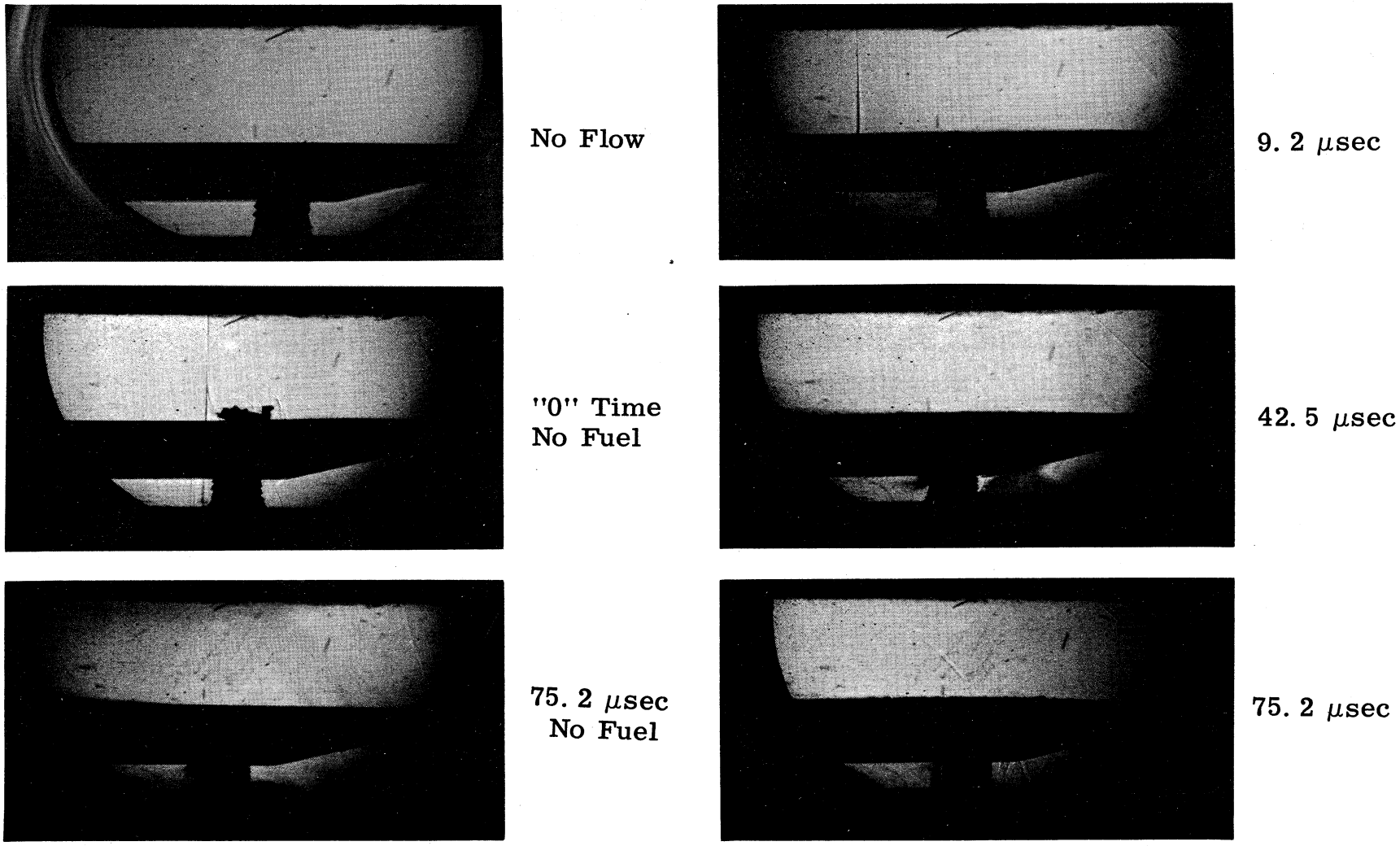

Fig. 4. 3. Photographs of Liquid Layer on Flat Plate Behind Shock in Nitrogen.

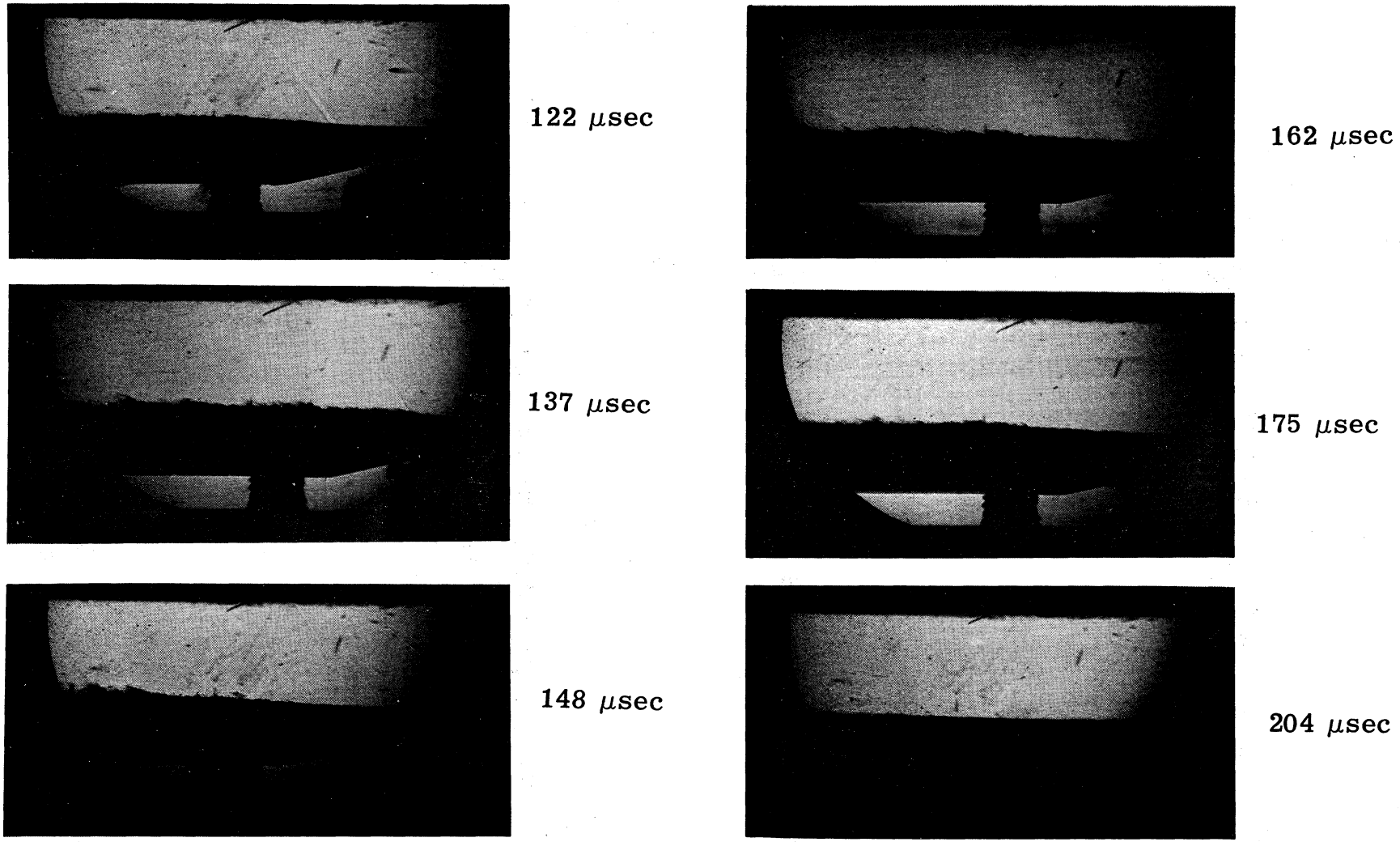

Fig. 4. 3. continued.

TABLE IV. APPARENT LIQUID LAYER THICKNESS AND APPROXIMATE BOUNDARY LAYER THICKNESS BEHIND M = 2. 2 SHOCK

Time after Shock (μsec)	Distance Shock Moved (in.)	Thickness of Liquid Layer (in.)	Approx. Boundary Layer Thickness (in.)
0	0	0	0
9. 2	. 28	. 010	. 06
42. 5	1. 28	. 023	. 13
75. 2	2. 26	. 033	. 17
122	3. 68	. 043	. 22
137	4. 13	. 057	. 23
148	4. 46	. 050	. 24
167	4. 88	. 050	. 25
175	5. 27	. 050	. 26
204	6. 15	. 020	. 28

As a further instrumentation technique for studying heterogeneous detonations, several thin film heat transfer gauges were constructed and calibrated according to the techniques of Ref. 19 and 20. The gauges consist of a narrow strip of Hanovia bright platinum which was fused to the end of a 1/4 in. Pyrex rod. The parameter $\sqrt{\rho ck/\alpha}$ was 27 in cgs units where ρ, c, k and α are the density, specific heat, thermal conductivity and thermal resistivity respectively. Some measurements of the response of the heat transfer gauge to film detonations are shown in Fig. 4. 4; the heat transfer gauge is located at station 10a opposite station 10 while the other traces are from pressure transducers. For purposes of comparison the response of the heat transfer gauge to a 1 atm. stoichiometric hydrogen-oxygen gaseous detonation is shown in Fig. 4. 5. The heat transfer rate at a particular instant, t, is computed by a numerical integration of the voltage output according to the equation:

$$q(t) = \frac{\sqrt{\pi}}{2I_o R_o} \sqrt{\frac{\rho ck}{\alpha}} \left[\frac{2\Delta E(t)}{\sqrt{t}} + \int_0^t \frac{\Delta E(t) - \Delta E(\lambda)}{(t-\lambda)^{3/2}} \, d\lambda \right]$$

This equation was used to interpret Fig. 4. 4b and 4. 5, and the results are shown in Table V. From the slope of the heat transfer traces in Fig. 4. 4b and 4. 5 and the results of Table V it is evident that the maximum heat transfer rate is not as high for the film detonation compared to a hydrogen-oxygen gaseous detonation; however, the high heat transfer condition persists for a

Station 2 Trigger

Station 7

Station 9

Station 10a

Station 10

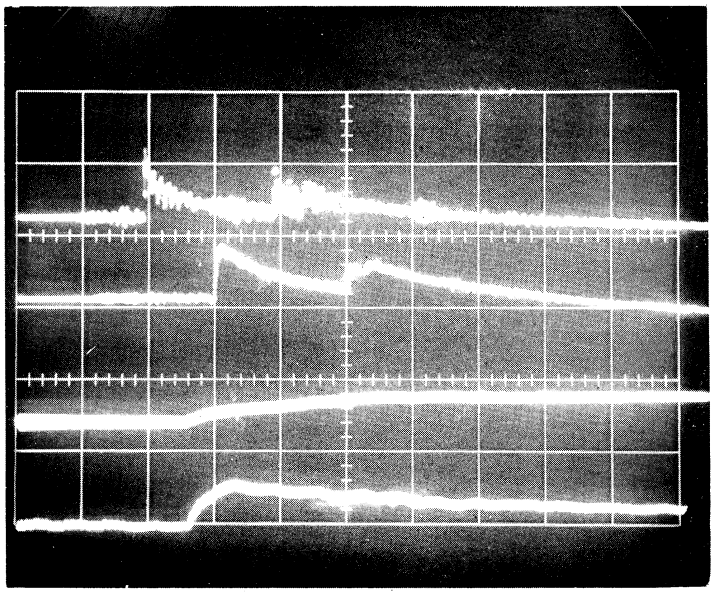

Station 7: Kistler 603, 143 psig/div., 500 μsec/div.

Station 9: Kistler 601A (27 KΩ Input filter), 80 psig/div., 500 μsec/div.

Station 10: Kistler 601A (27 KΩ Input filter), 80 psig/div., delayed 1500 μsec then 100 μsec/div.

Station 10a: Heat Transfer Gauge, 0.02 v/div., 33Ω, 10.0 ma delayed 1500 μsec then 100 μsec/div.

Fig. 4.4. Traces from Thin Film Heat Transfer Gauge and Pressure Transducers Using Driver Loaded With 30 in. Hg. $2H_2 + O_2$ for

(a) Shock Transmitted into 1 Atmosphere Air.

Station 2 Trigger

Station 7

Station 9

Station 10a

Station 10

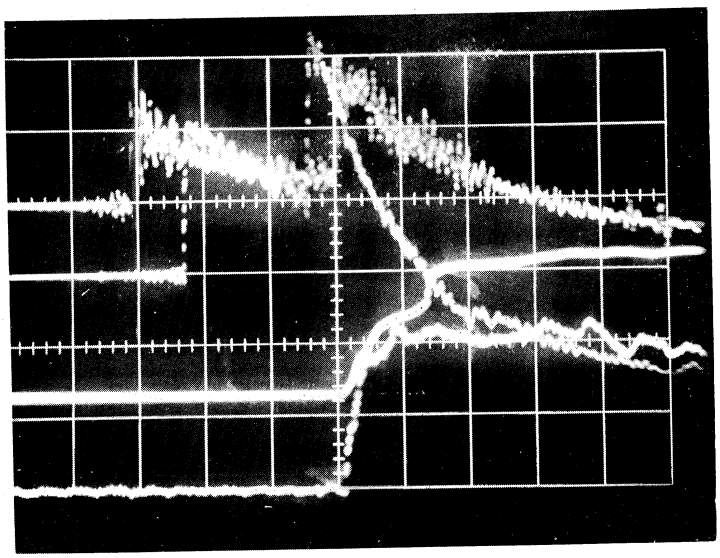

Station 7: Kistler 603, 143 psig/div., 500 μsec/div.

Station 9: Kistler 601A (27 KΩ Input filter), 80 psig/div., 500 μsec/div.

Station 10: Kistler 601A (27 KΩ Input filter), 80 psig/div., delayed 1000 μsec then 100 μsec/div.

Station 10a: Heat Transfer Gauge, 0.02 v/div., 33 Ω, 10.0 ma, delayed 1000 μsec then 100 μsec/cm.

Fig. 4.4.(b). Film Detonation from DECH Layer on Two Walls with 1 Atmosphere O_2.

Station 2 Trigger

Station 7

Station 9

Station 10a

Station 10

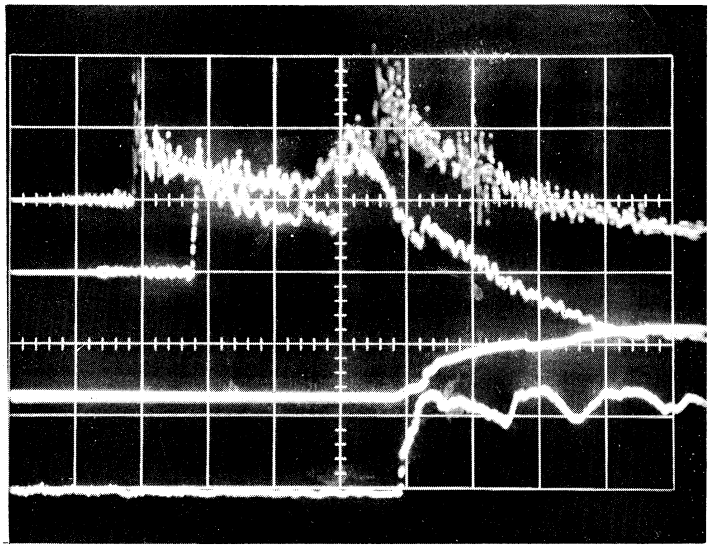

Station 7: Kistler 603, 143 psig/div., 500 μsec/div.

Station 9: Kistler 601A (27 KΩ Input filter), 80 psig/div., 500 μsec/div.

Station 10: Kistler 601A (27 KΩ Input filter), 80 psig/div., delayed 1000 μsec then 100 μsec/div.

Station 10a: Heat Transfer Gauge, 0.02 v/div., 21 Ω, 10.0 ma, delayed 1000 μsec/div. then 100 μsec/div.

Fig. 4.4.(c). Film Detonation from DECH Layer on One Wall with 1 Atmosphere O_2.

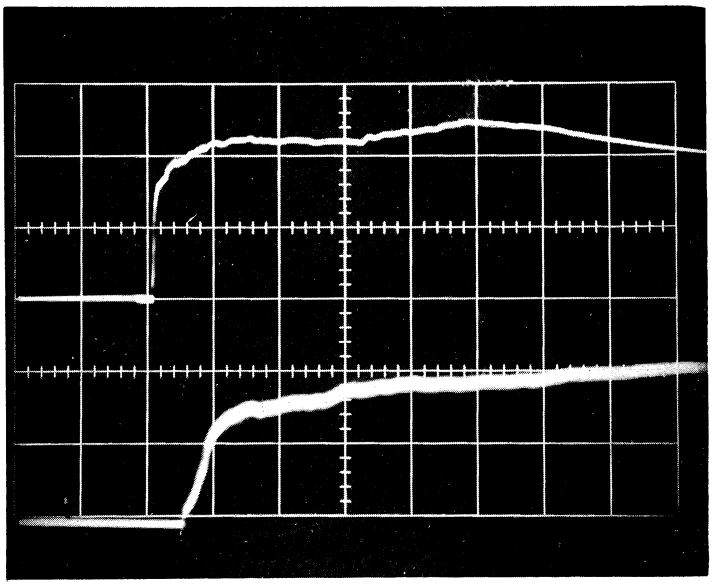

Upper beam: .02 v/div., 50 μsec/div.

Lower beam: .02 v/div., 5 μsec/div. (delayed)
27Ω, 10.0 ma.

Fig. 4.5. Thin Film Heat Transfer Gauge Trace of a Stoichiometric Hydrogen-Oxygen Detonation at 1 Atmosphere Initial Pressure.

TABLE V. SUMMARY OF HEAT TRANSFER RESULTS

Case	t (μsec)	q $\left(\frac{\text{BTU}}{\text{ft}^2\text{-sec}}\right)$
Film Detonation - 2 walls coated (Fig. 4. 4b)	120	225
$2H_2 + O_2$ Detonation (Fig. 4. 5)	10	1090
	35	436
$2H_2 + O_2$ Detonation (Theory of Ref. 21)	10	3600
	35	2790

longer time. The theoretical values shown in the table which were obtained by the method of Sichel and David[21] are much higher, but this might be expected since this method does not allow for the rarefaction wave behind the detonation front.

B. Other Observations of Film Detonations

To our knowledge this type of phenomena was first reported by Loison[22] in 1952 and additional experiments were reported in 1965 by Gordeev, Komov and Troshin[23, 24]. In Loison's experiment a steady state detonation of a thin film of lubricating oil propagating at 1200 m/sec was observed in a tube 80 m long by 250 mm diameter. Combustion of the film was initiated by a pulse of hot gas of acoustic strength. In the experiments of Gordeev ignition of a thin film of lubricating oil or grease on the walls of a tube 1. 6 m long by 22 mm diameter was accomplished by a methane-oxygen detonation, an exploding wire, or a charge of lead azide. For all of these ignition sources Gordeev reports that an accelerating combustion develops and turns into a detonation with velocities as high as 1700 m/sec depending on the particular fuel and thickness used. The minimum thickness of fuel necessary to establish detonation was determined. In fact two limits were established—development of detonation from one of these above ignition sources required at least $\sim$ 32 μ, while development of detonation from a previously formed detonation wave in an analogous heterogeneous system required at least $\sim$ 2. 2 μ,

for example (stoichiometric value was 2.5 μ). Several elucidating streak photographs of film detonations are presented by Komov and Troshin.

C. Physical Explanation of Film Detonations

The experimental evidence suggests the following mechanism for the propagation of a film detonation. (The mechanism of initiation and transition to detonation has not been considered explicitly.) As the detonation wave moves down the tube the leading shock front raises the pressure and temperature of the gaseous oxidizer and sets the oxidizer into motion. Heat is transferred from the oxidizer to the fuel layer by convection which initiates vaporization of the fuel surface. Heat conduction through the fuel film is minimal because of the low thermal diffusivity of the fuel and the relatively short times involved. The fuel vapor diffuses inward and a short time after passage of the shock-front (on the order of 10 μsec) enough fuel has mixed with the oxidizer to initiate combustion which in turn reinforces the heat and mass exchange. At a later time (on the order of 100 μsec) mechanical stripping of the fuel layer enhances chemical reaction. Heat release behind the shock and near the wall continues until all of the fuel and/or oxygen is consumed.

The above explanation implies that, at least initially, combustion takes place within the boundary layer which is formed behind the shock-front. The boundary layer is undoubtedly turbulent quite early because the low transition

Reynolds number observed in shock tubes is further reduced by the combustion. The combustion layer "sends out" pressure pulses which eventually collide with and thus reinforce the main shock-front. Spark schlieren photographs indicate that there are several rather strong secondary shocks emitted from the combustion zone, i. e., localized explosions due to large scale turbulent fluctuation. The main shock front is thus driven to an "equilibrium" position ahead of the combustion zone. The streak photographs of Komov and Troshin clearly show the nature of the secondary shocks. For their system secondary shocks are generated one behind the other with a frequency of approximately 18 kc and they cause the velocity of the main shock-front to vary about an average value, D, from 2D to 0. 5D.

D. Theoretical Analysis of Film Detonations

The existence of film detonations suggests, in terms of rocket motor design, that the walls and baffles of the combustion chamber should not be wetted by the fuel. To make a quantitative statement it is desirable to predict the rate of vaporization and combustion of the fuel on the wall as a function of free-stream properties, fuel properties and shock strength, and then to consider how the combustion drives the shock. To this end, the equations for a laminar boundary layer behind a shock with heat and mass addition are presented and the solutions indicated for various initial conditions. It is then planned to use the boundary layer solution to predict

the detonation velocity, and pressure and temperature behind the detonation front in a tube. The analysis will undoubtedly need to be extended to include turbulent flow. For the boundary-layer problem the approach of Emmons[25] and Mirels[26] has been utilized.

Consider a semi-infinite flat plate of fuel exposed to a stationary oxidizing gas which is swept over by a normal shock of constant strength. Choose a coordinate system as shown in Fig. 4. 6 which is fixed with respect to the shock. The following assumptions are made:

1. The flow is laminar, steady, at constant pressure and the usual boundary layer approximations hold.
2. The Prandtl number is unity, the Schmidt number based on binary diffusion coefficients for each pair of species is unity; body forces, radiative energy transport, and thermal diffusion are neglected.
3. $\rho\mu/\rho_e\mu_e = 1$
4. There is a one step chemical reaction of the form

$$\sum_{i=1}^{N} \nu_i' M_i \rightarrow \sum_{i=1}^{N} \nu_i'' M_i$$

5. The temperature of the vaporizing fuel is constant and equal to the equilibrium boiling point temperature.
6. The properties of the external stream are constant.

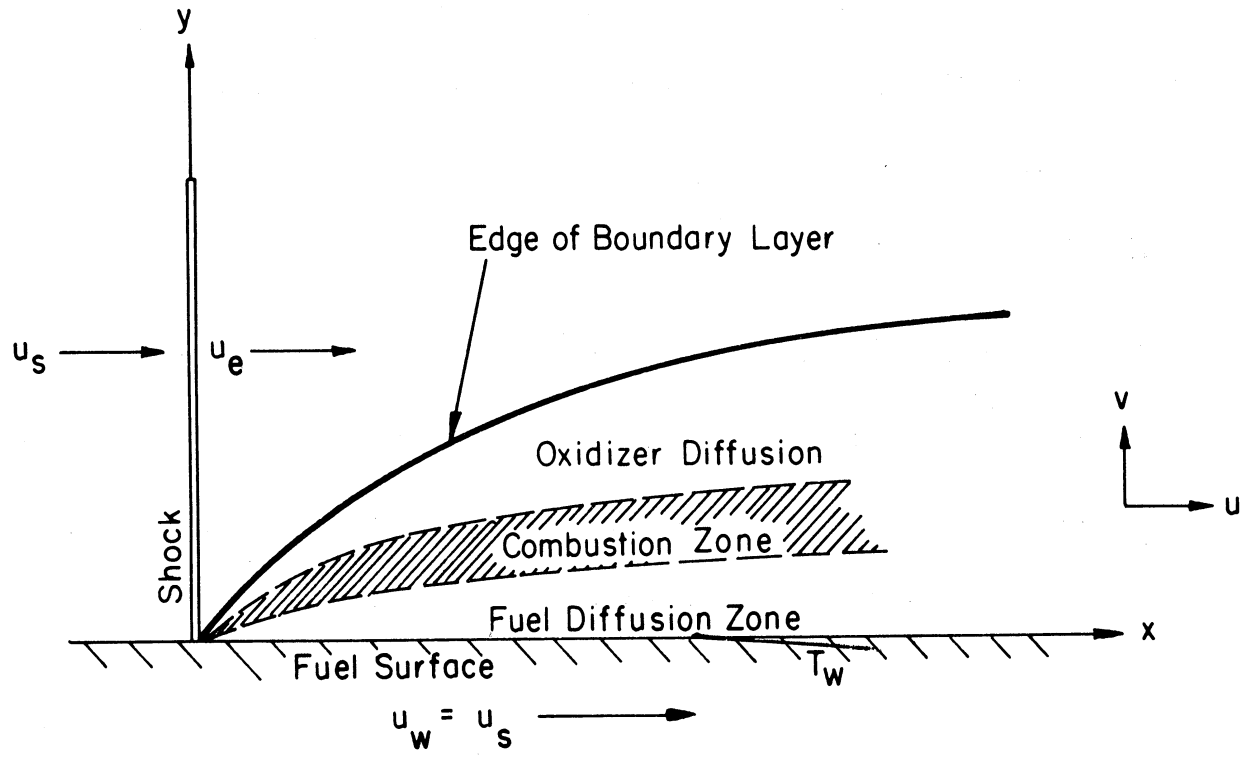

Fig. 4. 6. Normal Shock Moving Across a Flat Plate with Boundary Layer Combustion

Under the above assumptions the boundary layer equations in the form given by Williams[27] are:

Overall continuity,
$$\frac{\partial \rho u}{\partial x} + \frac{\partial \rho v}{\partial y} = 0 \tag{4.1}$$

Momentum,
$$\rho u \frac{\partial u}{\partial x} + \rho v \frac{\partial u}{\partial y} = \frac{\partial}{\partial y}\left(A \frac{\partial u}{\partial y}\right) \tag{4.2}$$

Energy,
$$\rho u \frac{\partial \beta_T}{\partial x} + \rho v \frac{\partial \beta_T}{\partial y} = \frac{\partial}{\partial y}\left(A \frac{\partial \beta_T}{\partial y}\right) \tag{4.3}$$

Continuity of species,
$$\rho u \frac{\partial \beta_i}{\partial x} + \rho v \frac{\partial \beta_i}{\partial y} = \frac{\partial}{\partial y}\left(A \frac{\partial \beta_i}{\partial y}\right) \tag{4.4}$$

where

$$\beta_T \equiv \frac{\int_{T^o}^{T} C_p \, dT + \frac{u^2}{2}}{\sum_{i=1}^{N} h_i^o W_i (\nu_i'' - \nu_i')} - \frac{Y_1}{W_1 (\nu_1'' - \nu_1')} \tag{4.5}$$

$$\beta_i \equiv \frac{Y_i}{W_i (\nu_i'' - \nu_i')} - \frac{Y_1}{W_1 (\nu_1'' - \nu_1')} \tag{4.6}$$

$$A \equiv \rho D_i = \mu = \frac{\lambda}{C_p} \tag{4.7}$$

and index 1 represents any particular species. However, it is convenient to have it represent the oxidizer.

In this formulation the reaction rate terms have been eliminated at the expense of obtaining a complete solution for the temperature and composition profiles. However, the velocity profile and the evaporation rate of the fuel layer may be obtained without further loss of generality. This formulation will be sufficient for our present purpose.

The boundary conditions for the energy equation are given by an energy balance at the liquid layer as shown below.

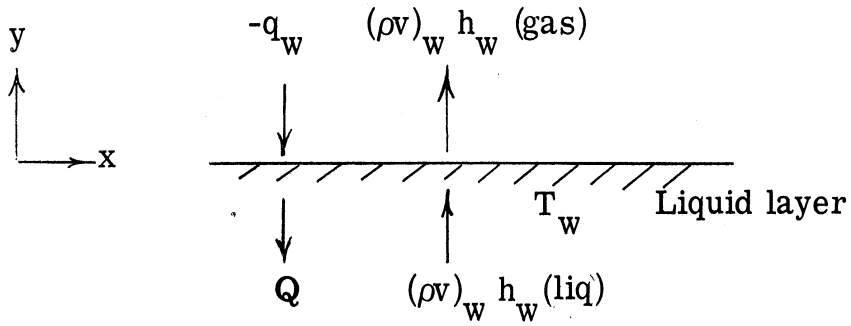

Since the thermal conductivity of liquids is comparatively low, the heat flux through the liquid, Q, is neglected. The heat transfer to the liquid, q_w, is given by:

$$q_w = \left[- k \frac{\partial T}{\partial y} + \rho \sum_{i=1}^{N} D_i h_i \frac{\partial Y_i}{\partial y} \right]_w$$

The second term on the right is much less than the first and may be neglected because at the wall the concentration gradients will approach zero due to the vaporization. The boundary conditions for the energy equation are then at $y = 0$, $T = T_W$, which is the equilibrium boiling temperature

of the fuel; and at y = 0,

$$k_w \left(\frac{\partial T}{\partial y}\right)_w = (\rho v)_w h_L$$

since $h_L = h_w(g) - h_w(\ell)$. At $y = \infty$, $T = T_e$, which is given by the normal shock relations.

In terms of β the boundary conditions for the energy equation are

at y = 0, $$\beta_T = \beta_{Tw} \tag{4.8}$$

at y = 0,

$$\sum_{i=1}^{N} h_i^o W_i (\nu_i' - \nu_i'') \left(\frac{\partial \beta_T}{\partial y}\right)_w - u_s \left(\frac{\partial u}{\partial y}\right)_w = \frac{C_{p_w} (\rho v)_w h_L}{k_w} \tag{4.9}$$

at $y = \infty$, $$\beta_T = \beta_{Te} \tag{4.10}$$

Boundary conditions on the velocity are at $y = \infty$, $u = u_e$, which is given by the normal shock relations; and at y = 0, $u = u_s$, which is the shock velocity. Also at y = 0, v must be determined by the vaporization and moving wall conditions as follows. Since the energy equation and the momentum equation have the same form, a particular solution for the energy in terms of the velocity is given by the "Crocco relation,"

$$\beta_T = \left(\frac{\beta_{Te} - \beta_{Tw}}{u_e - u_s}\right) u + \frac{\beta_{Tw} u_e - \beta_{Te} u_s}{u_e - u_s} \tag{4.11}$$

and differentiating,

$$\frac{\partial \beta_T}{\partial y} = \left(\frac{\beta_{Te} - \beta_{Tw}}{u_e - u_s} \right) \frac{\partial u}{\partial y} \tag{4.12}$$

Substituting Eq. (4.12) into Eq. (4.9) it is seen that at y = 0, v must satisfy the equation

$$\sum_{i=1}^{N} \frac{h_i^o \, w_i \, (\nu_i' - \nu_i'') \, (\beta_{Te} - \beta_{Tw}) - u_e \, u_s + u_s^2}{u_e - u_s} \left(\frac{\partial u}{\partial y} \right)_w = \frac{(\rho v)_w \, h_L \, C_{p_w}}{k_w} \tag{4.13}$$

In order to solve the momentum equation the first step is to transform the equation to incompressible form by applying the Howarth transformation,

$$z = \int_0^y \rho \, dy \tag{4.14}$$

$$w = \rho v + u \int_0^y \left(\frac{\partial \rho}{\partial x} \right) dy \tag{4.15}$$

The continuity and momentum equations become,

$$\frac{\partial u}{\partial x} + \frac{\partial w}{\partial z} = 0 \tag{4.16}$$

$$u \frac{\partial u}{\partial x} + w \frac{\partial u}{\partial z} = \rho_e \, u_e \frac{\partial^2 u}{\partial z^2} \tag{4.17}$$

Next introduce a stream function ψ and a similarity parameter η,

$$\psi = \sqrt{u_e \rho_e \mu_e x}\, f(\eta) \tag{4.18}$$

$$\eta = \frac{z}{2}\sqrt{\frac{u_e}{\rho_e \mu_e x}} \tag{4.19}$$

Then,

$$u = \frac{1}{2} u_e \frac{df}{d\eta} \tag{4.20}$$

$$\rho v = \frac{1}{2}\sqrt{\frac{u_e \rho_e \mu_e}{x}}\left(\eta \frac{df}{d\eta} - f\right) - \frac{1}{2} u_e \frac{df}{d\eta}\int_0^y \frac{\partial \rho}{\partial x}\, dy \tag{4.21}$$

and we obtain the Blasius equation,

$$\frac{d^3 f}{d\eta^3} + f\frac{d^2 f}{d\eta^2} = 0 \tag{4.22}$$

with the boundary conditions

$$\left(\frac{df}{d\eta}\right)_w = \frac{2 u_s}{u_e} \tag{4.23}$$

$$\left(\frac{df}{d\eta}\right)_\infty = 2 \tag{4.24}$$

$$\frac{fw}{\left(\frac{d^2 f}{d\eta}\right)_w} = -\frac{B'}{2\left(1 - \frac{u_s}{u_e}\right)} \tag{4.25}$$

where

$$B' = \frac{\sum h_i^o w_i (\nu_i' - \nu_i'') (\beta_{Te} - \beta_{Tw}) - u_e u_s + u_s^2}{h_L} \tag{4.26}$$

or substituting the definition of β_T from Eq. (4.5),

$$h_L B' = \int_{T^o}^{T_e} C_p \, dT - \int_{T^o}^{T_w} C_p \, dT + \frac{u_e^2}{2} + \frac{u_s^2}{2} - u_e u_s$$

$$+ \frac{Y_{o_e} \sum_{i=1}^{N} h_i^o w_i (\nu_i' - \nu_i'')}{w_o (\nu_o' - \nu_o'')} \tag{4.27}$$

The last term of Eq. (4.27) may be rewritten as,

$$Y_{o_e} \left[\frac{w_F (\nu_F' - \nu_F'')}{w_o (\nu_o' - \nu_o'')}\right] \left[\frac{\sum_{i=1}^{N} h_i^o w_i (\nu_i' - \nu_i'')}{w_F (\nu_F' - \nu_F'')}\right]$$

The first bracket is the fuel to oxidizer ratio, ϕ, while the second bracket is the heat of reaction, which for expediency will be set equal to the heat of combustion, ΔH. Finally, assuming constant specific heats the expression for B' reduces to

$$h_L B' = C_{p_e} T - C_{p_w} T_w + Y_{o_e} \phi \Delta H + \frac{1}{2}(u_e^2 + u_s^2) - u_e u_s \qquad (4.28)$$

For convenience redefine B' to contain only thermodynamic terms such that

$$h_L B = C_{p_e} T_e - C_{p_w} T_w + Y_{o_e} \phi \Delta H \qquad (4.29)$$

With the use of Eq. (4.28) and (4.29) the final form of the boundary value problem is:

$$\frac{d^3 f}{d\eta^3} + f \frac{d^2 f}{d\eta^2} = 0 \qquad (4.22)$$

$$\left(\frac{df}{d\eta}\right)_w = \frac{2 u_s}{u_e} \qquad (4.23)$$

$$\left(\frac{df}{d\eta}\right)_\infty = 2 \qquad (4.24)$$

$$\frac{f_w}{\left(\frac{d^2 f}{d\eta^2}\right)_w} = -\frac{B}{2\left(1 - \frac{u_s}{u_e}\right)} - \frac{u_e^2}{4h_L}\left(1 - \frac{u_s}{u_e}\right) \qquad (4.30)$$

The last term of Eq. (4.30) is generally negligible. For our experiments with DECH the value of B is approximately 37.

Solutions of Eq. (4. 22) are available for the cases B = 0 and $u_s/u_e = 0$ (Ref. 28), B = 0 (Ref. 8), and $u_s/u_e = 0$ (Ref. 29). Solutions of the Blasius equation for the complete set of boundary conditions are not known to the authors. Once the solution has been obtained the vaporization rate may be calculated by evaluating Eq. (4. 21) at the wall according to

$$(\rho v)_w = -\frac{f_w}{2}\sqrt{\frac{u_e \rho_e \mu_e}{x}} \tag{4. 31}$$

It should be mentioned that the temperature and species profiles can be obtained once the solution to the momentum equation is available, by making further restrictive assumptions. For the problem of combustion of a stationary fuel plate, Toong[30] obtained the temperature profile, composition profiles, position of the flame surface and burning rate of fuel at the flame surface by making the following additional assumptions:

1. The entire heat release takes place at a flame surface according to the one-step chemical reaction

$$\nu_F F + \nu_O O \rightarrow \nu_P P$$

in which F is fuel, O is oxidizer and P the average reaction products (inerts are assumed to have the same properties as P).

2. The position of the flame surface is such that the reaction takes place at a stoichiometric ratio.

3. The flame surface divides the boundary layer into two regions which are binary mixtures of perfect gases in which $C_{P_I} = C_{P_{II}}$ = constant, $D_I = D_{II}$ = constant, W_I = constant, W_{II} = constant. For the burning of hydrocarbon plates in air Toong found that the combustion rate was less than the evaporation rate since some of the vaporized fuel is swept downstream instead of entering the flame surface. For large values of B the ratio of fuel burned to fuel vaporized approaches 0. 15.

The solution of Eq. (4. 22) with the boundary conditions (4. 23), (4. 24), and (4. 30) is being carried out on the University of Michigan 90 amplifier hybrid analog computer. An analog computer was chosen rather than a digital computer because of the difficulty in choosing the correct values of f_w and $d^2f/d\eta^2$ to satisfy Eq. (4. 24) and (4. 30). The network used to solve Eq. (4. 22) is shown in Fig. 4. 7. The computer was programmed to solve this equation repetitively so that the effect of varying the initial condition pots in order to satisfy the solution at "infinity" was immediately apparent. Preliminary results of the initial conditions obtained in this manner are presented in Table VI. Also shown in the last column of Table VI is the vaporization rate behind the shock (Eq. 4. 31) in oxygen. A typical analog computer solution is shown in Fig. 4. 8. Some of the characteristic features of the solution are the great reduction in the shear stress (which is proportional to the second derivative of f) caused by mass addition, the inflection of the velocity profile, and a vaporization rate which is inversely proportional to the square root of the distance from the

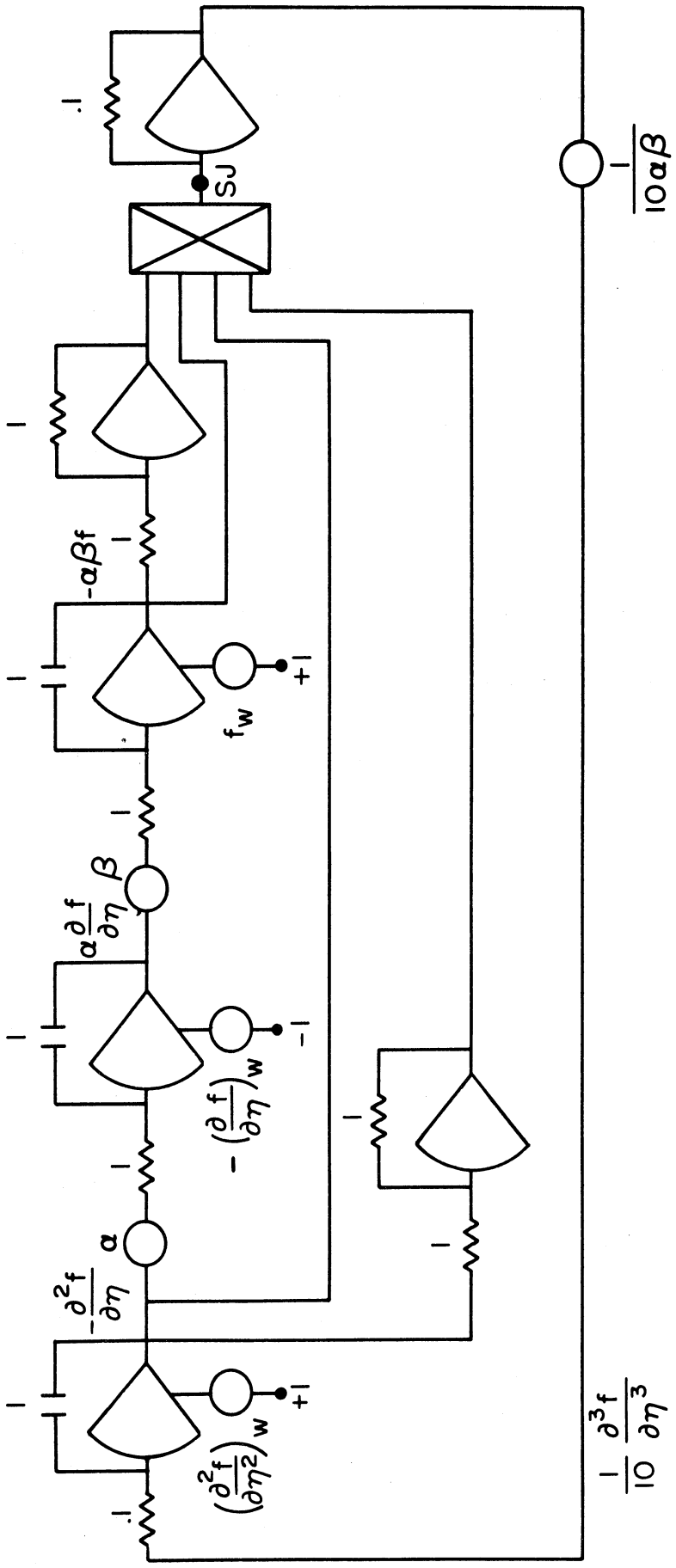

Fig. 4.7. Network for Analog Computer used to Solve the General Blasius Equation

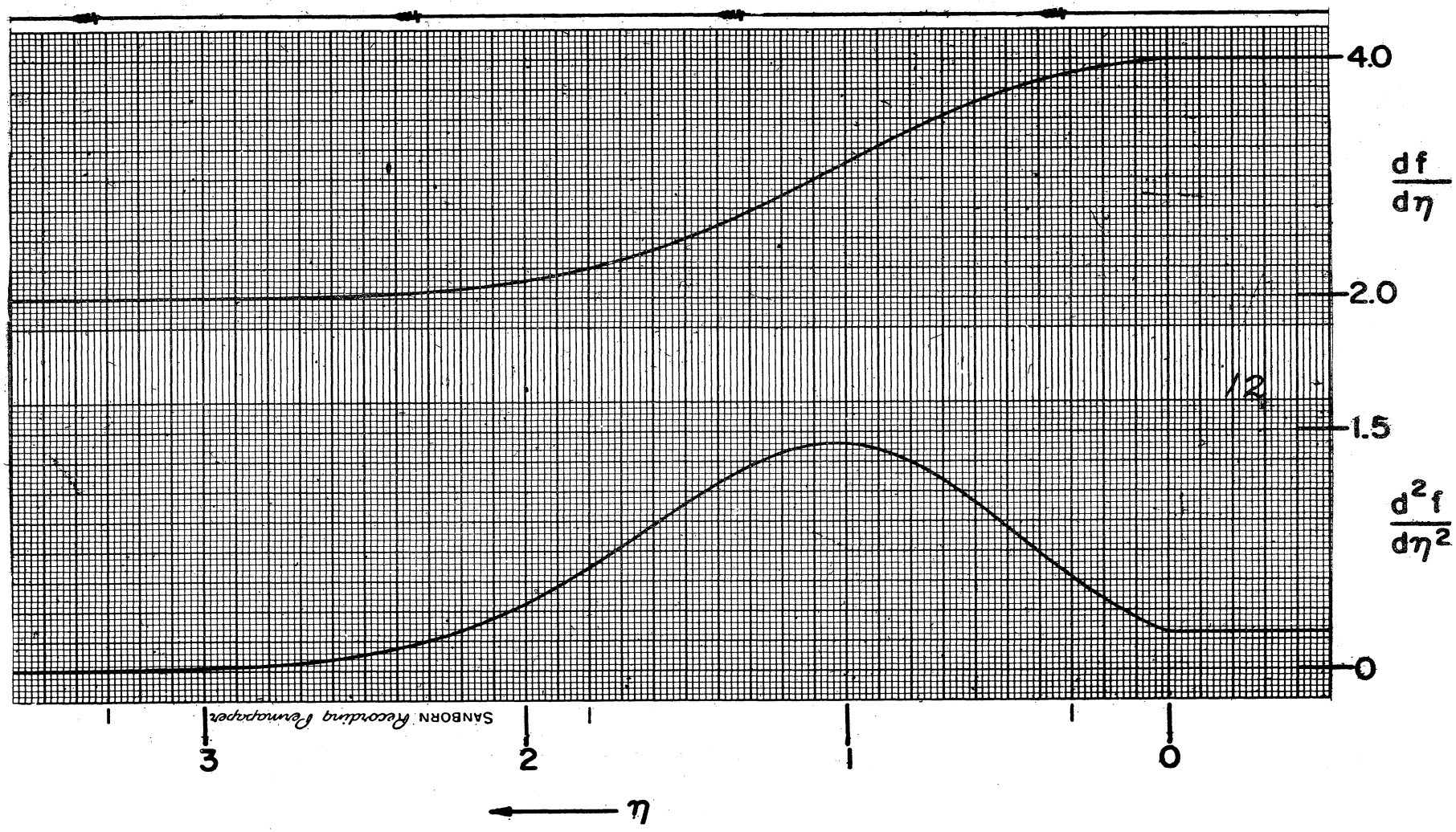

Fig. 4. 8. Analog Computer Solution of the Blasius Equation for M_s = 1. 57 and B = 31. 1

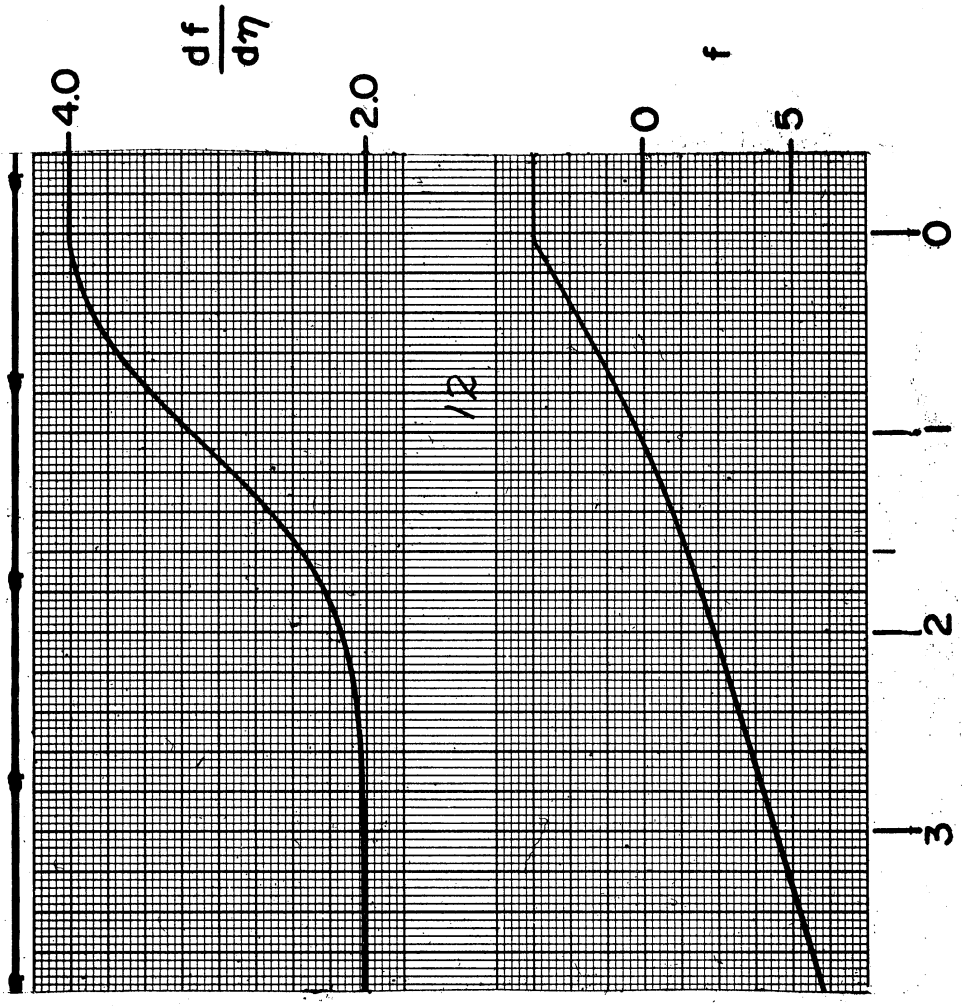

Fig. 4.8. Continued

TABLE VI. SUMMARY OF INITIAL CONDITIONS SATISFYING THE BLASIUS EQUATION FOR VARIOUS VALUES OF M_s AND B

Case	$\frac{df}{d\eta}_w$	M_s for $\gamma = 1.4$	$-f_w$	$-\frac{d^2f}{d\eta^2}_w$	B	$(\rho v)_w \sqrt{x}$ *
1	0	--	0	1.328	0	0
2	0	--	1.000	0.1421	14.08	--
3	4	1.57	0	2.882	0	0
4	4	1.57	1.000	1.776	1.13	.0243
7	4	1.57	2.000	0.9627	4.15	.0487
9	4	1.57	3.000	0.4513	13.29	.0730
10	4	1.57	3.500	0.2865	24.44	.0852
12	4	1.57	3.700	0.2385	31.10	.0901
11	4	1.57	3.750	0.2233	33.58	.0913
13	4	1.57	4.000	0.1746	59.82	.0974
14	4	1.57	4.729	0.0771	122.7	.115
26	6	2.23	0	6.792	0	0
27	6	2.23	3.600	1.077	13.38	.116
28	6	2.23	4.800	0.4290	44.76	.155
29	6	2.23	5.100	0.3309	61.64	.165
30	6	2.23	5.400	0.2514	85.92	.290
15	8	3.15	0	11.49	0	0
21	8	3.15	4.800	1.195	24.09	.212
25	8	3.15	5.600	0.681	49.35	.247
22	8	3.15	6.400	0.3648	105.2	.282
23	8	3.15	6.800	0.2574	158.5	.300
31	10	5.00	0	16.89	0	0
36	10	5.00	6.000	1.175	40.84	.418
35	10	5.00	7.000	0.5937	94.32	.488
34	10	5.00	7.500	0.4089	146.7	.522
33	10	5.00	8.000	0.2758	232.0	.557
32	10	5.00	8.500	0.1811	375.4	.592

* $lb/sec\ ft^{3/2}$

shock. As pointed out by Emmons there is a finite limit to the amount of heat which can be added to the boundary layer at which point the boundary layer will be "blown away." The effect of the moving wall is to extend this limit to suppress the inflection of the velocity profile, and to increase the vaporization rate. These computations will be completed over a full range of the parameter B, at the chosen shock speeds and the results will be applied to the problem of film detonations.

V. DROP SHATTERING STUDIES

The importance of droplet shattering to the development and propagation of detonation waves in two phase mixtures has been mentioned in the introduction. In view of this it is essential to know the rate of droplet breakup and breakup times as influenced by the drop characteristics and the flow field conditions. This problem has been studied in the past but never in the range of conditions characteristic of two phase detonation. The purpose of this work, then, is to supplement and extend earlier experimental and theoretical investigations by studying the interaction between a shock wave and a liquid drop for a range of conditions generated by two phase detonations. Conditions of interest involve shock waves moving over liquid drops of diameter 500-2000μ at Mach numbers of 1.5-8. These shocks lead to subsonic as well as supersonic convective flow over the drops with velocities up to many thousands of feet per second. As a result, breakup times of microseconds are expected.

The earlier work on the shattering problem has indicated that drop diameter and flow velocity are the major variables with the liquid properties being not as important. Consequently, the emphasis of this work is to do a detailed experimental and theoretical study on water drops and elucidate the mechanism at the higher Mach numbers before extending the work to other liquids.

A. Review of Drop Break-Up Studies

1. Review of Experimental Studies. The first experimental study of the interaction between a liquid drop and a shock wave was reported by Lane[31] in 1951. In a series of experiments, which utilized a so-called blast gun to form a shock wave and a burette to produce the drops, Lane was able to photograph the various stages of the shattering phenomenon and to obtain a sample of the mist into which a drop is shattered. Lane's photographs showed that a drop, which was spherical before the shock wave collided with it, was deformed into a lenticular body which then broke-up into a conglomeration of finer droplets. Unfortunately the times at which the various pictures were taken are not indicated in the paper and therefore the time required for the break-up to occur, which is the time elapsed between the collision of the shock wave with the drop and the complete disintegration of the drop, cannot be determined. However the photographs did provide the means for a comparison of the final shape and diameter, which the drop assumes just prior to its disintegration, with those predicted by Taylor's[32] incompressible analysis of the problem. The agreement found between the experimental results and Taylor's theory, which is subsequently discussed in this section, is remarkably good.

Samples of the mist into which the drop was shattered were collected on glass slides and evaluated to obtain droplet size and distribution data. An analysis of the data revealed that the atomization of the original drop, which

became progressively finer as the compression chamber pressure was increased, was such that for compression chamber pressures of 10 atmospheres or more and a test section pressure of 1 atmosphere, one half of the mass of the resulting spray was in the form of droplets of diameter greater than 15 microns. Unfortunately it was not possible to quantitatively correlate the atomization data with any of the properties characterizing the shock wave and the convective flow behind it because the strength of the shock and the character of the flow field produced by the gun were not precisely determined as a function of the compression chamber pressure.

Also contained in the photographs was sufficient evidence to support at least two possible mechanisms for the shattering phenomenon. Since during the process of break-up the liquid appears to be stripped away from the edge of the lenticular drop by the action of viscous shearing stresses, a boundary layer stripping model is a conceivable explanation for what was observed. However the evidence which supports the proposed stripping explan tion could likewise be interpreted to support a mechanism of unstable surface wave development. That is to say that, what looks like a stripping away of the drop material may in fact be a blowing away of the crests of large amplitude waves which develop on the surface of the drop. The waves which are observed on the windward face of the drop are generated by the action of the convective flow of air on the surface of the liquid and their stability depends, among other things, on the magnitude of the relative velocity between the air and the liquid

drop surface. Taylor's[32, 33] analyses for both the boundary layer stripping mechanism and the development and rate of growth of the surface waves are discussed further on in this section.

In 1955 Hanson, Domich, and Adams[34] investigated the shattering of liquid drops in a conventional shock tube facility. The radiation pressure generated by an ultrasonic sound field was used to support water and methyl alcohol drops, ranging in diameter from 100-700μ, in the test section of a shock tube. The shock wave was sensed by a pressure transducer which, after being fed through a time delay generator, produced a triggering signal to fire the spark source in the camera system. In this manner a large number of individual tests were made and the interactions were photographed to determine the so-called critical Weber number for breakup.

The Weber number is a dimensionless grouping given by $We = \rho_g V^2 D/\sigma$. Physically, the We No. represents the relative importance of the dynamic pressure of the airstream and the surface tension force of the liquid. The critical value of the dimensionless grouping is defined as that value of the Weber number which corresponds to the on-set of breakup. That is to say, that in a shock wave-drop interaction test conducted at less than the critical Weber number, no breakup of the drop occurs. Under these circumstances, the applied aerodynamic forces simply cause the drop to translate in the direction of flow.

The calculations made from the experimental results gave critical Weber numbers ranging in value from $(We)_{critical} = 3.6 - 8.41$ and the type of disintegration was observed to be the bag mode. The photographs show that the breakup results from the deformation of a drop into a bag of fluid that eventually collapses into a large number of fine droplets. It was also observed that when the strength of the shock was increased to produce a Weber number considerably in excess of 10, a stripping mode, like that reported by Lane[31], was observed. Hanson felt that the mere collision between a normal shock wave and a drop did not of itself cause the shattering phenomenon to occur but rather it was the relative velocity between the drop and the surrounding air which, if sustained for a sufficient length of time, produced the fragmentation.

Since the experiments of Hanson et al.[34] were inconclusive as to the effect of viscosity on the shattering phenomenon, in 1956 Hanson and Domich[35] conducted another investigation whose primary objective was to specifically determine the effect of viscosity on the interaction process. The experimental techniques employed were generally the same as those previously described in the preceding paragraphs with the exception that three Dow Corning Silicone fluids, having essentially the same densities and surface tensions but with viscosities of 10, 50, and 100 centistokes respectively, were used for the drops.

The experimental curves of droplet diameter versus critical velocity revealed a significant effect of viscosity. It was observed that increasing the viscosity increases the critical velocity required to shatter a drop of a given diameter and the trend becomes more pronounced as the drop diameter decreases. As a result of the effect of viscosity, the critical Weber numbers for breakup increased in magnitude, ranging in value from $(We)_{critical} = 6\text{-}24$. However a correlation of the results for the silicone fluids with those for water and methyl alcohol indicate that below 10 centistokes the effect of viscosity is very small. Photographs of the breakup process showed that a bag structure precedes the final breakup of viscous liquids just as was found in earlier tests with methyl alcohol and water.

In 1958, Engel[36] reported the results of a study made of the fragmentation of waterdrops resulting from an interaction with shock waves. The drops, which were formed at the tip of a hypodermic needle mounted above the test section of a shock tube, were allowed to fall through holes in the shock tube walls into a reservoir located beneath the underside of the tube. The freely falling waterdrops were photographed at various time intervals after they were intercepted by a shock wave. Although every picture that was taken was of a different drop, it was possible, by maintaining a constant Mach number and drop diameter and varying only the time delay from run to run, to maintain a

high degree of test similarity and to construct from the pictures a complete time history of the disintegration process and the drift of the waterdrops in the convective flow region behind the shock wave.

The photographs showed that the fragmentation process could be considered to take place in two rather distinct stages. The first stage was characterized by the deformation of the spherical drop into a plano-convex shaped body corresponding to the observations of Lane[31]. After assuming the lenticular shape, mist was observed to emanate from the leeward face of the waterdrop while the remaining portion of the drop itself remained intact. The Weber number for all of the experiments ranged in value from We = 800-10,000 and the type of breakup observed was, in all cases, the stripping mode. As the mass of the drop was stripped away, surface waves were observed to develop on the windward face of the drop and their amplitude progressively increased with time so as to give the surface a corrugated appearance.

Since Engel photographed the entire sequence of events, from the moment the shockwave first intercepted a drop until the time of complete disintegration, it was possible, for the first time, to correlate the observed breakup time with the original diameter of the spherical waterdrop and the convective flow properties behind the shock wave. No attempts were made in the experiments to vary the physical properties of surface tension, viscosity, and density of the liquid in the drop and therefore no correlations between the breakup time

and these variables were possible. However the correlations which were made indicate that, for the range of conditions covered in the experiments, the breakup time is roughly proportional to the original waterdrop diameter and inversely proportional to the velocity of the convective flow field established by the shock wave. The shortest breakup time observed, $t_b = 580\mu$sec, corresponded to the interaction of a shock wave having a Mach number $M_s = 1.7$ with a drop whose original diameter was $D = 1400\mu$.

From a consideration of the evidence contained in the photographs, Engel felt that the most likely mechanisms for shattering were those which took into account the effect of the rapid airstream on the waterdrop. The mist which was observed was thought to be made up of contributions from the whipping-off or from the breaking of the crests of waves, from the spill-off at the equatorial belt of the moving boundary layers on the windward face, and from the stripping of water from the leeward face by the vortices that form in the dead water region behind the drop. According to Engel, it seemed unlikely that any one of these mechanisms operated to the complete exclusion of the others.

In a discussion of the limitations of the observations, Engel pointed out that the results which were obtained and the conclusions that were drawn in the study applied only to drops of water that have a diameter in the range of 1.4 to 2.7 mm and that disintegrate in airstreams having velocities in the range of 500 to 1070 ft/sec. Engel cautioned that to extrapolate the

conclusions to conditions outside of these ranges could result in spurious inferences because it appeared that not only the rate of fragmentation but also the very mechanism by which it occurs was strongly dependent on these variables.

In an attempt to determine the effect of shock waves on the shattering and on the drag of burning and non-burning liquid fuel drops, Rabin, Schallenmuller, and Lawhead[37] in 1960 conducted a series of shock tube experiments to investigate the interaction problem. A fuel drop was suspended in the test section of the shock tube on a fine wire which was attached to a solenoid and retracted just before the shock wave collided with the drop. The retraction of the support wire was synchronized with the firing of the shock tube so as to leave the drop free of the wire and motionless in the test section. For the burning drop study, ignition was accomplished by using a high voltage spark of short duration. The time history of the shattering phenomenon was photographically recorded by taking high speed motion pictures of the interaction process with a Fastax camera. The experiments were designed specifically to obtain further information on the effects of convective flow velocity, surface tension, and chamber pressure on the breakup characteristics for both burning and non-burning drops of propellant.

The two distinct modes of breakup, the bag type and the stripping type, were observed because the experiments covered a range of Weber number

from We = 1.1-294. The photographs revealed that the general features of the bag and stripping disintegration processes for both burning and non-burning fuel drops were in every way identical to those observed by Hanson[34] and Engel[36]. It appeared that the actual collision between the shock wave and the drop had a negligible effect on the breakup process which seemed to be completely governed by the properties of the convective flow behind the shock front. Since the study utilized rather weak shock waves, $M_{s_{max}} \cong 1.2$, and drops with diameters, $D \cong 1000\mu$, the recorded breakup times were in the range of t_b = 2330-3200 μsec.

The experimental data also showed that the separate effects of burning and of increased test section pressure both lowered the observed critical velocity for breakup. The major effect of burning was to lower the surface tension of the drop to less than 50% of its non-burning value and the isothermal increase in the test section pressure created a proportional increase in the density level which influenced the magnitude of the dynamic pressure. An analysis of the experimental data for both the burning and non-burning fuel drops produced a correlation between the critical Weber number and the critical Reynolds number of $We_{(crit)} Re_{(crit)}^{-1/2} \cong .5$. The analytical form of the correlation was shown to agree with what one might expect from a boundary layer analysis of the stripping type of breakup.

In 1963, Rojec[38] published the results of an experimental study which was designed to obtain high resolution photographs of the events that take

place immediately following the collision between a shock wave and a liquid fuel drop. A shock tube was used to generate the shock waves and fuel drops of RP-1 were hung on a fine wire from the upper wall of the test section of the shock tube. The interaction between the drop and the convective flow field was photographed at various time intervals after the shock had passed the test drop position by delaying the triggering signal to the spark light source in the camera system, and in this manner, one picture was taken of each drop.

Using this technique Rojec was able to obtain photographs of fuel drops, which were undergoing a stripping mode of breakup, that contained an amazing amount of detail. For example, the enlarged pictures clearly showed the development and the rate of propagation of capillary surface waves from the front to the rear stagnation points. With the progression of time, the capillary waves were observed to grow rapidly in amplitude to give the windward surface an extremely corrugated appearance. When the convective flow velocity was V = 1250 ft/sec, a wake of very fine mist began to develop at about 25 μsec after the passage of the shock front. For V = 320 ft/sec, appreciable amounts of liquid began to leave the drop at about 110 μsec after the wave had passed. The fluid particles were observed shedding from the surface at the region of maximum shear, at the boundary layer separation point, and at the crests of the surface waves.

In an attempt to supplement the breakup time data obtained by Engel[36] and Rabin et al.[37], Wolfe and Andersen[18] in 1964 undertook to study the shattering of liquid drops, having various sizes and physical properties, with high speed motion picture equipment. Drops ranging in size from D = 500-3000μ and having physical properties of surface tension, σ = 18-487 dynes/cm; density, ρ_ℓ = 0.75-14 gm/cm^3; and viscosity, μ_ℓ = .5-170 centipoise, were introduced into the test section of a shock tube and subjected to shock waves that produced convective flow velocities in the range of V = 50-450 ft/sec. The interaction process was photographed by using a Dynafax camera and samples of the shattered drop residue were taken to determine the distribution and the size of the micro-droplets into which the drop was broken. Photomicrographs of the sampled material showed that, as the convective flow velocity was increased from V = 80-400 ft/sec, the mass-median diameter of the micro-droplets decreased from about 120 μ-15μ.

The range of conditions covered in the experiments was such that both the bag and the stripping modes of shattering were observed. In addition, the motion pictures provided some knowledge about the breakup time. The experimental breakup times indicated in their report correspond to the time for the dynamic stage of fragmentation to reach a certain state and not to the time required for the complete disintegration of the drop. The data presented showed that in general the breakup time was directly proportional to the original diameter of the drop and to the square root of the density of the liquid

in the drop and inversely proportional to the convective flow velocity behind the shock wave. The main effect of an increase in viscosity was to retard the rate of deformation of the drop but it was almost negligible at the higher convective flow velocities.

In addition to their experimental study, Wolfe and Andersen developed analytical expressions predicting the dependence of the breakup time and the dependence of the mass mean diameter of the micro-droplet residue on the variables in the problem. The derivation of the expression for the breakup time is presented later in this section. A correlation of the breakup times obtained from the experiments with those calculated from the analysis showed some general agreement.

The most recent study of the shock wave-drop interaction problem was conducted by Nicholson and Hill[39] who in 1965 reported on the results of a dimensional analysis of the drop shattering problem and on an experimental study that was conducted in an effort to produce empirical confirmation of a postulated scaling law for the drop breakup time in a high speed airstream. A dimensional analysis similar to that of Nicholson and Hill is presented in Appendix A.

The interaction between 1.5 mm water drops and shock waves ranging in strength from M_s = 1.8 - 2.85 was photographed by using a high speed Fastax camera. A correlation between the observed breakup time with the

local dynamic pressure resulted in an expression for the breakup time; $t_b = 23.9\ D/q^{1/2}$. From a differentiation of the drop displacement versus time data taken from the movies of the breakup, a curve of drop velocity versus time was obtained. The velocity versus time curve for every run was found to have a sharp change in slope that was interpreted as corresponding to the moment at which the remaining core of the original drop shatters into a number of finer droplets and this moment was defined as the breakup time.

In addition to the experimental work which has been cited in the preceding paragraphs, Morrell[40] and Clark[41] have investigated the disintegration of liquid jets which is a phenomenon physically similar to that of drop shattering. Using streak and high-speed framing photographic techniques, Morrell studied the interaction of liquid jets 0.052, 0.0785, and 0.157 in. in diameter with shock waves in a shock tube having a Mach number range $M_s = 1.11 - 1.73$. An analysis of the experimental data revealed that the breakup time of the jets increased regularly with an increase in the ratio of jet radius to the convective flow velocity behind the shock wave.

In another series of experiments on jet breakup, Clark photographed the shattering of water jets 0.065, 0.089, and 0.120 in. in diameter by a transverse flow of nitrogen whose velocity was varied over the range from $V = 65 - 430$ ft/sec. The corresponding Weber number range for the experiments was $We = 31 - 11,000$. Shock waves were not employed to establish the convective flow of nitrogen gas around the jets and therefore any possible

effect that the shock wave interaction might have had on the fragmentation of the jets was completely eliminated from the tests. The experimental results showed that the degree of jet breakup increased with increasing convective flow velocity and density and with decreasing liquid jet diameter.

Table VII is presented as a convenient summary of the shock wave-drop interaction studies which have been reviewed in the preceding paragraphs. The interesting feature of the table is that it shows at a glance that very little experimental work has been done on the shattering problem for the conditions which are pertinent to detonation in two-phase media.

2. Review of Theoretical Studies.

a. Unstable Surface Wave Development. Taylor[33] considered the instability of liquid surfaces when accelerated in a direction perpendicular to their planes and found that when the direction of acceleration is from the lighter to the heavier fluid the amplitude of an initial disturbance will grow exponentially with time. He treated analytically the situation shown

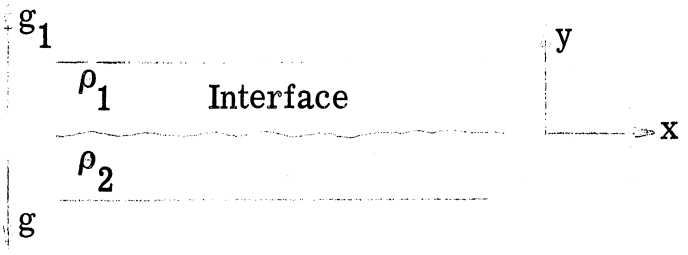

where ρ_1 and ρ_2 are the densities of the upper and the lower fluid respectively with $\rho_2 > \rho_1$. The acceleration due to gravity is g and g_1 is a vertically upwards acceleration applied to the fluids whose depths are large compared to

TABLE VII. SUMMARY OF SHOCK WAVE — DROP INTERACTION STUDIES

Year	Investigator(s)	Liquid(s)	Drop Diameter D, μ	Shock Mach No. M_s	Convective Mach No. M	Convective Flow Velocity V, ft/sec	Breakup Time t_b, μsec	Type of Breakup	Weber No. We	Reynolds No. Re
1951	Lane	Water Dibutyl Phthalate	50-4000	→2.1	→1.0	→875	Not Available	Stripping	2.56×10^3	28.7×10^3
1955	Hanson Domich Adams	Water Methol Alcohol	100-700	1.02-1.13	.05-.21	60-238	Not Available	Bag	3-9	$.5 \times 10^3$ - 1.5×10^3
1956	Hanson Domich	Dow Corning Silicone Fluids	100-600	1.03-1.16	.065-.25	74-282	Not Available	Bag	6-24	1×10^3 - 4×10^3
1958	Engel	Water	1400 2700	1.3, 1.5, 1.7	.4 .6 .75	500 777 1070	600-900	Stripping	800- 10,000	35×10^3 - 89×10^3
1960	Rabin Schallenmuller Lawhead	RP-1 DECH	50-1600	1-1.07	.003-.124	3.4-140	2330-3200	Bag and Stripping	1.1-294	60- 10,000
1963	Rojec	RP-1	1800	1.16, 1.18, 2.1	.24 .28 .835	275, 320 1250	Not Available	Stripping	595- 17,700	30- 100,000
1964	Wolfe Andersen	Water Mercury Bis Silicones	500-3000	1.02-1.28	.044-.39	50-450	Not Available	Bag and Stripping	.8- 1400	178- 25,600
1965	Nicholson Hill	Water	1500	1.8, 2.1 ›2.85	.839 1.06 1.32	1175 1590 2370	295-900	Stripping	7×10^3 - 30×10^3	56×10^3 - 120×10^3

the wavelength of the disturbance of the interface. If $g_1 > g$ and if the initial displacement of the interface from the plane y = 0 is

$$\eta_0 = C \cos KX \tag{5.1}$$

and the initial velocity is zero, then

$$\eta = C \cosh nt \cos KX \tag{5.2}$$

where n is taken to be the positive value of

$$\sqrt{-K(g + g_1)\frac{(\rho_2 - \rho_1)}{(\rho_2 + \rho_1)}}$$

where $(g + g_1)$ is negative. If one defines the amplification factor of an unstable fluid surface as the ratio of the amplitude of the disturbance at any time to its initial value, we obtain for a vertical downward acceleration g_1

$$\frac{\eta}{\eta_0} = \cosh nt = \cosh \left[-K(g_1 - g)\frac{(\rho_2 - \rho_1)}{(\rho_2 + \rho_1)} \right]^{\frac{1}{2}} t \tag{5.3}$$

Since for the case of an accelerating water drop the acceleration g_1 due to the imposed aerodynamic forces is from the lighter fluid air to the heavier fluid water and of the order of $g_1 = .5 \times 10^6$ g's and the density of water $\rho_2 \cong 10^3 \times \rho_1$ where ρ_1 is the density of the surrounding air, Eq. (5.3) can be written as

$$\frac{\eta}{\eta_0} = \cosh \left(.5\, gK \times 10^6\right) t \tag{5.4}$$

Substituting in Eq. (5. 4) the values,

$$g = 32.2 \text{ ft/sec}^2$$

$$K = \frac{2\pi}{\lambda} = \frac{2\pi}{10\mu}$$

where $\lambda = 10\mu$ has been chosen as a characteristic capillary wavelength and

$$t = 2 \ \mu\text{sec}$$

as a representative time, results in an amplification factor of

$$\frac{\eta}{\eta_0} = \cosh 3.48 = 16.6$$

Thus under conditions fairly representative of those of interest in this report, small disturbances can be amplified considerably in a very short time.

Mayer[42] developed a theory of liquid atomization in high velocity gas streams by considering the gas-liquid interface behavior in the regime of capillary wave propagation. From the analysis it was found that all wavelengths λ exceeding a minimum value λ_{min} grow at an exponential rate characterized by a time modulus τ dependent on λ and the density and the relative velocity of the convective flow of gas and the density, surface tension, and viscosity of the liquid in the drop.

From an approximate energy balance for the surface wave of amplitude α Mayer wrote that

$$\frac{d\alpha}{dt} = \frac{\alpha}{\tau} \qquad (5.5)$$

where the reciprocal time modulus $1/\tau$ was expressed in terms of the wavelength λ as

$$\frac{1}{\tau} = \frac{f}{\lambda^{1/2}} - \frac{\nu}{\lambda^2} \tag{5.6}$$

where

$$f = \sqrt{\pi/2}\,\frac{\beta\,\rho_g\,V_g^{\,2}}{\sqrt{\sigma\,\rho_\ell}}$$

is the forcing parameter, in which $\beta \leq 1$ is called the sheltering parameter, and $\nu = 8\pi^2\mu_\ell/\rho_\ell$ the viscous damping parameter. In view of the character of Eq. (5.5) the capillary waves will grow or diminish exponentially with time according to whether τ is positive or negative. Thus the wind maintained wavelengths are greater than a minimum value obtained from Eq. (5.6) by setting the forcing parameter equal to the viscous damping parameter and solving to obtain

$$\lambda \geq \lambda_{min} = \left(\frac{\nu}{f}\right)^{\frac{2}{3}} = 2\pi\sqrt[3]{16}\left(\frac{\mu_\ell\sqrt{\sigma/\rho_\ell}}{\beta\,\rho_g\,V_g^{\,2}}\right)^{\frac{2}{3}}$$

It was postulated that when the convective flow induced wave of length λ has grown to an amplitude comparable to λ, the rest of the wave is shed as a ligament from which micro-droplets of diameter D are formed. From a consideration of the steady state droplet formation rate on a large liquid surface,

an expression was derived for the micro-droplet size distribution function which yielded the formula

$$\overline{D} = 9\pi\sqrt[3]{16}\, B\left(\frac{\mu_\ell \sqrt{\sigma/\rho_\ell}}{\rho_g V_g^2}\right)^{\frac{2}{3}}$$

for the average droplet size obtained on primary atomization. The result for $\overline{D}$ was shown to agree well with empirical correlations proposed by Weiss and Worsham[43].

b. Theories Concerning the Drop Shape. Taylor[32] developed a theory for the shape which a liquid drop assumes when accelerated by an incompressible high-speed airstream from a theory of large air bubbles rising in water. Large air bubbles have been observed to assume a definite shape which is very closely spherical at the top and more or less flat below; the same plano-convex shape into which a liquid drop deforms. Taylor postulated that this shape results as the pressure due to the hydrodynamic flow around the bubble exactly neutralizes the variations in pressure due to gravity at all points on the upper surface. Furthermore, it was assumed that the surface tension plays no part in determining the air bubble shape and that the flat bottom of the bubble occupies the plane at which the pressure is equal to the pressure at the same level far from the bubble.

The distribution of pressure over three plano-convex lenticular-shaped bodies whose edges subtended angles of 60^{o}, 110^{o}, and 150^{o} was measured[44] and the results compared to the calculated pressure distribution for a complete sphere. The comparison showed that for some body intermediate between the 60^{o} and 110^{o} bodies it is probable that the pressure would be very close to the ideal one calculated for the sphere. Thus if the criterion for determining the position where the base of a bubble would be in relation to the top were that the pressure at the base is the same as that at the same level far from the bubble, the edge would be expected to subtend at the center of the sphere a double angle of 84^{o} which is that calculated as the region on a complete sphere over which the pressure is greater than that at infinity.

Assuming that the pressure over the spherical surface of a plano-convex lenticular body exposed to a stream velocity V is the same as the theoretical pressure over a complete sphere of the same radius

$$\frac{p - p_o}{1/2\, \rho_g V^2} = 1 - \frac{9}{4} \sin^2 \theta \qquad (5.7)$$

where θ is the angle of the radius from a point to the polar axis of the body as shown and p_o is the pressure in the undisturbed stream.

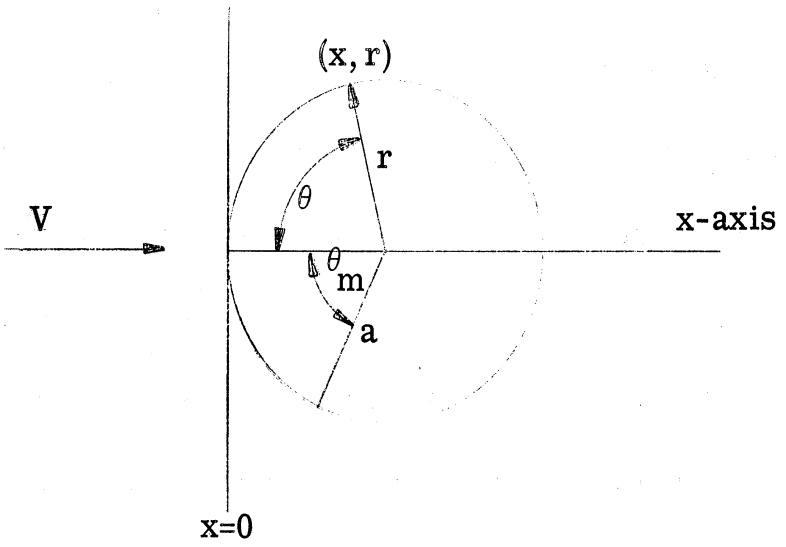

The equation to the spherical surface in the neighborhood of the stagnation point is

$$r^2 = 2ax$$

and $x/a = 1 - \cos\theta, \cong 1/2\,\theta^2$ when θ is small, while $\sin^2\theta$ can be taken as θ^2 to the same order of approximation. Equation (5. 7) thus becomes

$$p - p_o = \frac{1}{2}\rho_g V^2 \left(1 - \frac{9}{2}\frac{x}{a}\right) \tag{5. 8}$$

But in order that the fluid inside the lenticular shape may be accelerated uniformly through its volume the pressure within must be

$$p = p_o + \frac{1}{2}\rho_g V^2 + \rho_\ell fx$$

where f is the acceleration. Since the pressure inside the drop must be the same as that outside at all points on the surface

$$\rho_\ell f = \frac{9}{4}\rho_g \frac{V^2}{a} \tag{5. 9}$$

Assuming that the edge of the plano-convex lenticular body is defined by the condition that the pressure at the rear surface is the same as that far from the drop, the value of θ which defines the edge is found from Eq. (5. 8) and is $\theta_m = \sin^{-1}(2/3)$. The volume V of the plano-convex body is

$$V = \frac{1}{3}\pi a^3 \left[2(1 - \cos\theta_m) - \sin^2\theta_m \cos\theta_m\right]$$

If D is the diameter of the flattened drop

$$D = 2a \sin\theta_m = \frac{4}{3}a$$

and if R is the radius of the original drop

$$V = \frac{4}{3}\pi R^3$$

The requirement that the volumes be equal leads to

$$\frac{D}{R} = \left(\frac{32 \sin^3\theta_m}{2 - 2\cos\theta_m - \sin^2\theta_m \cos\theta_m}\right)^{\frac{1}{3}} = 3.76 \qquad (5.10)$$

and from Eq. (5. 9) the acceleration is given by

$$f = \frac{9}{4}\frac{\rho_g}{\rho_\ell}\frac{V^2}{a} = 3\frac{\rho_g}{\rho_\ell}\frac{V^2}{D} \qquad (5.11)$$

The prediction by Eq. (5. 10) that the deformed drop will have a diameter approximately twice as large as its initial value is in excellent agreement with a considerable amount of the experimental data that has been accumulated for shock Mach numbers of $M_s \leq 2$. However, if we make the following substitutions in Eq. (5. 11)

$$\frac{\rho_g}{\rho_\ell} \cong 10^{-3}$$

$$V = 777 \text{ ft/sec}$$

corresponding to $M_s = 1.5$ and

$$D = 1400\mu$$

then,

$$f = .013 \times 10^6 \text{ g's}$$

which is an order of magnitude larger than the acceleration observed by Engel[36] under identical experimental conditions.

A solution for the time dependence of the flattening of a water drop in an air flow was developed by Burgers[45]. It was assumed that a liquid is located at the origin of a rectangular coordinate system as shown and that the motion throughout the whole volume of the sphere as a result of the pressure distribution begins instantaneously.

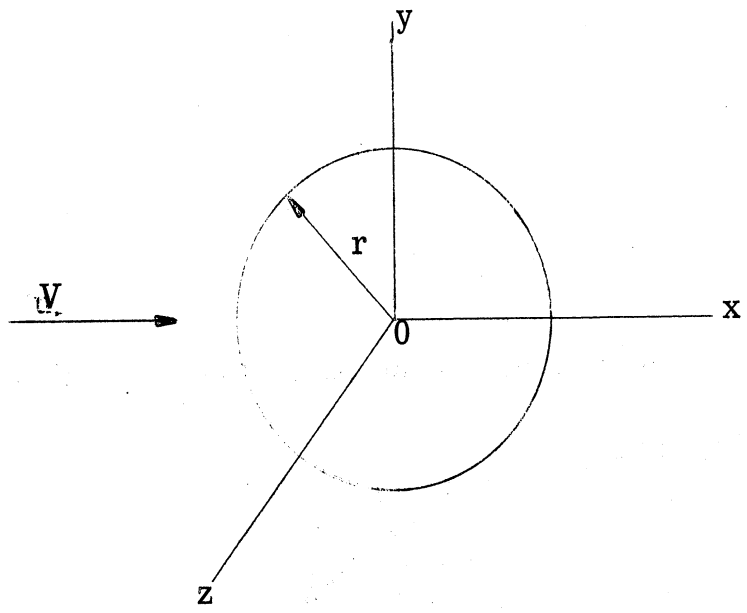

A solution of the continuity equation is given by

$$u = -2bx, \qquad v = by, \qquad w = bz \tag{5.12}$$

where u, v, w are the velocities along the x-, y-, and z-axis respectively and b is a function of time which must be determined. From Eq. (5.12) it follows that the velocity potential for the motion is given by

$$\phi = b\left(-x^2 + \frac{1}{2}y^2 + \frac{1}{2}z^2\right)$$

The equation of motion is

$$p = -\rho_\ell \frac{d\phi}{dt} + \text{constant} \tag{5.13}$$

where the term $1/2\,\rho_\ell\,(u^2 + v^2 + w^2)$ is neglected as small for short times after the shock-waterdrop collision. Application of Eq. (5.13) at the point $x = \pm r$ and at the points $y = \pm r$ and $z = \pm r$ on the surface of the sphere provides an evaluation of the pressures p_x and $p_{y,z}$ from which the pressure

difference Δp is found as

$$\Delta p = p_x - p_{y,z} = \frac{3}{2} \rho_\ell r^2 \frac{db}{dt} \tag{5.14}$$

If the pressure difference Δp is considered independent of time then Eq. (5.14) can be integrated to yield

$$b = \frac{2}{3} \frac{\Delta p}{\rho_\ell r^2} t$$

Since the velocity of the liquid at the equator of the sphere is given by $v = by$ and $w = bz$, the outward displacement D at the points $y = \pm r$ and $z = \pm r$ is found by integrating

$$V = br = \frac{dD}{dt}$$

to get that

$$D = \frac{1}{3} \frac{\Delta p}{\rho_\ell r} t^2 \tag{5.15}$$

The lateral growth rate of a drop predicted by Eq. (5.15) agrees extremely well with experimental observations made by Engel[36].

c. Boundary Layer Stripping Analysis. Taylor[32] developed a theoretical model for the stripping away of the surface of a drop through the action of the viscous forces imposed at the air-liquid interface by the convective flow around the drop. The boundary layer normalized velocity distributions

were expressed as

$$u_g = \frac{u}{V} = 1 - A \exp\left(- y/\alpha_g \sqrt{x}\right) \qquad \text{in the air} \qquad (5.16)$$

and,

$$u_\ell = \frac{u}{V} = (1 - A) \exp\left(- y/\alpha_\ell \sqrt{x}\right) \qquad \text{in the water} \qquad (5.17)$$

where A, α_g, α_ℓ are quantities that must be determined, and the x-axis lies in the air-water interface and the y-axis is perpendicular to it as shown.

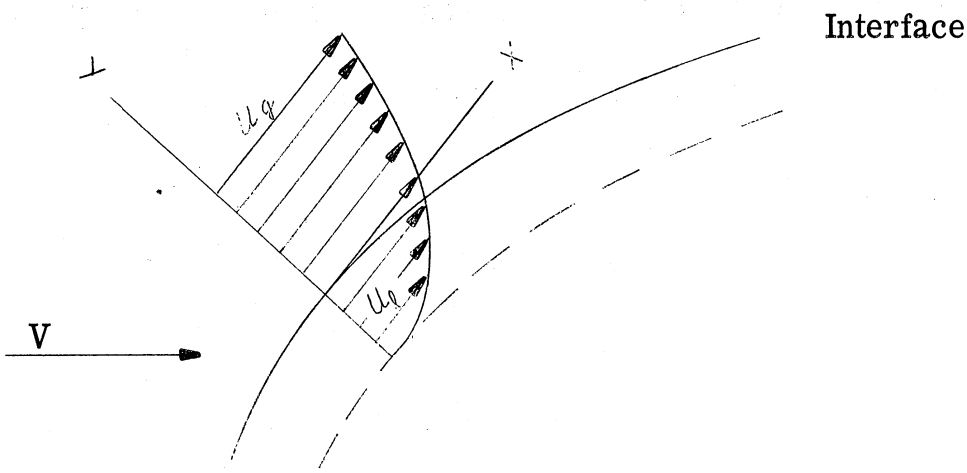

The choice of Eq. (5.16) and (5.17) satisfies the boundary conditions that as $y \to \infty$, $u_g \to 1$, and $u_\ell \to 0$, and that for $y = 0$, $u_g = u_\ell$. This choice also satisfies the Karman boundary layer integral equations from which it is found that

$$\alpha_g^2 = \frac{2\nu_g}{V\left(1 - \frac{A}{2}\right)}$$

and,

$$\alpha_\ell^2 = \frac{4}{V}\frac{\nu_\ell}{(1 - A)}$$

where ν_g and ν_ℓ are the kinematic viscosities for air and water respectively. From the condition that the tangential stress at the interface must be continuous and using the condition that when $\nu_\ell/(\alpha_\ell^2 V)$ is small, $\nu_g/(\alpha_g^2 V) \simeq 1/4$ it was shown that

$$\frac{\nu_\ell}{\alpha_\ell^2 V} \simeq \frac{1}{4}\left(\frac{\rho_g}{\rho_\ell}\right)^{\frac{2}{3}}\left(\frac{\nu_g}{\nu_\ell}\right)^{\frac{1}{3}}$$

The efflux of water out of the boundary layer per unit length of periphery when the mass of water itself has velocity W is

$$\int_0^\infty (V - W)(1 - A)\exp(-y/\alpha_\ell \sqrt{x})\, dy = (V - W)(1 - A)\,\alpha_\ell \sqrt{x}$$

and therefore the total loss of volume per unit time is

$$\frac{dV}{dt} = 4\pi r\left(\frac{\rho_g}{\rho_\ell}\right)^{\frac{1}{3}}\left(\frac{\nu_g}{\nu_\ell}\right)^{\frac{1}{6}}\sqrt{V - W}\,\sqrt{\nu_\ell}\,\sqrt{x}$$

d. Breakup Time Analyses. Morrell[40] found an expression for the breakup time of a liquid jet by considering the volumetric removal rate of fluid from the surface of the jet. The volumetric removal rate was written as

$$-\frac{dV}{dt} = (2\,\delta_\ell\,u_{\ell,avg})\Big|_{x=L} \tag{5.18}$$

where the assumed breakup model is shown in the sketch below.

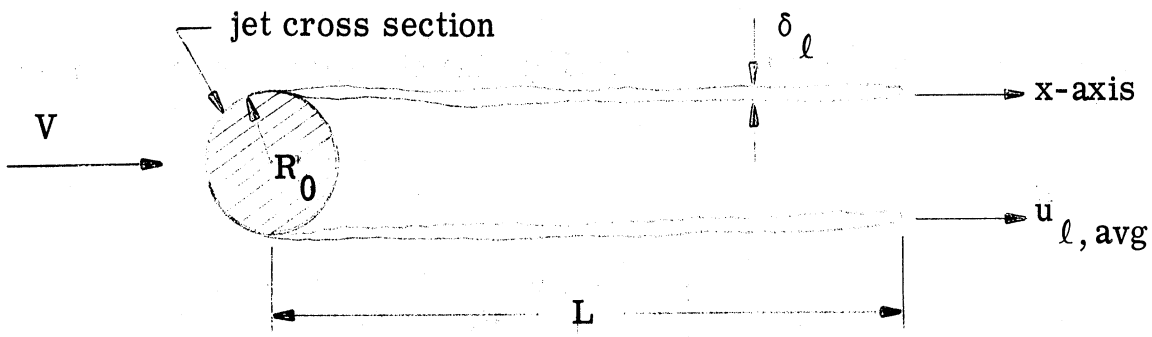

Equation (5.18) was integrated under the assumption that, with L and V the free stream gas velocity held constant, $(\delta_\ell\,u_{\ell,avg})\Big|_{x=L}$ is constant and therefore

$$t_b = \frac{\pi R_0^2}{(2\,\delta_\ell\,u_{\ell,avg})\Big|_{x=L}} \tag{5.19}$$

where R_0 is the initial jet radius and t_b is the breakup time that corresponds to the moment at which the volume of the fluid in the jet has been reduced to zero.

The length of the liquid sheet was found by equating the frictional drag according to Blasius with the surface tension force

$$\tau_0 L = \sigma$$

indicating that,

$$L \sim R_0 \frac{We_0}{\sqrt{Re_0}}$$

where the Weber number We_0 and the Reynolds number Re_0 are based on R_0. From the experimental data of jet breakup, the sheet length was well represented by

$$L = 2R_0 \left(1 - 2\frac{We_0}{\sqrt{Re_0}}\right) \tag{5.20}$$

The boundary layer thickness and velocity were estimated by assuming a flat plate model with velocity profiles

$$\frac{u_g}{V} = 1 - (1 - A)\left[1 - \left(\frac{y}{\delta_g}\right)\right]^2 \qquad \text{for the gas} \tag{5.21}$$

and,

$$\frac{u_\ell}{V} = A\left[1 - \left(\frac{y}{\delta_\ell}\right)\right]^2 \qquad \text{for the liquid} \tag{5.22}$$

The use of Eq. (5.21) and (5.22) together with the Karman boundary layer integral equations led to the solution

$$\delta_\ell = \sqrt{\frac{\nu_\ell x}{\lambda V}} \tag{5.23}$$

for the boundary layer thickness and

$$u_{\ell,\,avg} = 10\,\lambda V \qquad \text{for the average velocity} \qquad (5.24)$$

for the average velocity where

$$\lambda = 0.043\,(\rho_g/\rho_\ell)^{2/3}\,(\nu_g/\nu_\ell)^{1/3}$$

Substitution of Eq. (5.20), (5.23), and (5.24) into Eq. (5.19) yielded

$$t_b = 0.536\left(\frac{\rho_\ell}{\rho_g}\right)^{\frac{2}{3}}\left(\frac{\mu}{\mu_\ell}\right)^{\frac{1}{3}}\frac{R_0}{V}\sqrt{\frac{Re_0}{1+2\dfrac{We_0}{\sqrt{Re_0}}}}$$

from which it was observed that when $We_0/\sqrt{Re_0} \gg 1$ the dependence of t_b on R_0 and V was

$$t_b \simeq \left(\frac{R_0}{V}\right)^{1.25} \qquad (5.25)$$

In a study similar to that of Morrell, Clarke[41] developed an expression for the breakup time of a liquid jet of fluid by working with the equation for the transverse motion of a deforming jet. The equation of motion is

$$\bar{a} = \frac{d\bar{W}}{dt} = \frac{1}{\rho_\ell}\nabla p - \frac{\mu_\ell}{\rho_\ell}\nabla^2\bar{W} + \bar{g} \qquad (5.26)$$

with

$$|\nabla p| \simeq \frac{\Delta p}{\Delta s} \simeq \frac{2\left(\frac{1}{2}\rho_g V^2\right)}{\frac{1}{2}D_0} = 2\rho_g \frac{V^2}{D_0} \qquad (5.27)$$

where $\overline{W}$ is the non-axial velocity and D_0 is the original diameter of the undistorted jet as shown in the sketch below. The term $2\left[(1/2)\rho_g V^2\right]$ in Eq. (5.27) represents the pressure difference Δp between the stagnation and the separation points and the average distance Δs between these points is $1/2\, D_0$

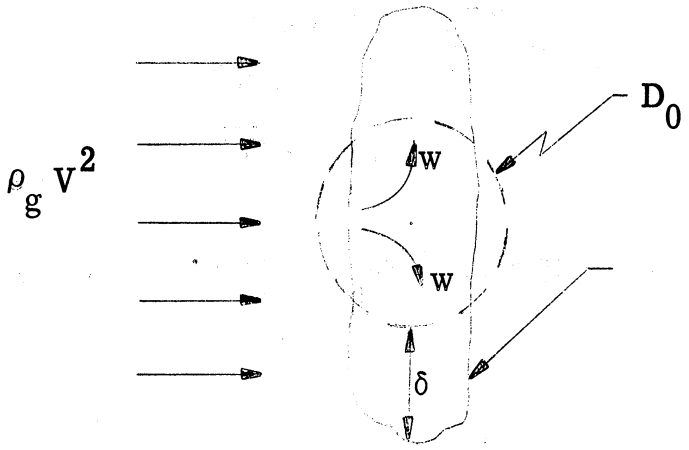

Based on an order of magnitude analysis of the individual terms the gravitational and viscous effects in Eq. (5.26) were neglected to yield

$$a = 2\frac{\rho_g}{\rho_\ell}\frac{V^2}{D_0} \qquad (5.28)$$

an expression giving the acceleration of the liquid in a direction transverse to the convective flow. Integration of Eq. (5.28) gives the velocity of the motion

$$W = 2\frac{\rho_g}{\rho_\ell}\frac{V^2}{D_0}t$$

and the lateral displacement

$$\delta = \frac{\rho_g}{\rho_\ell} \frac{V^2}{D_0} t^2 \tag{5.29}$$

If ϵ is defined as

$$\epsilon \equiv \frac{\delta}{D_0} = \frac{\rho_g}{\rho_\ell} \left(\frac{Vt}{D_0} \right)^2$$

then Eq. (5.29) can be written as

$$t_b = \frac{D_0}{V} \sqrt{\epsilon_b \frac{\rho_\ell}{\rho_g}} \tag{5.30}$$

where ϵ_b corresponds to that value of ϵ for breakup. A comparison of Eq. (5.30) with Clarke's empirical data showed that breakup began at an $\epsilon_b = 1 - 2$ and was essentially complete for $\epsilon_b = 10 - 15$. If one attempts a physical interpretation of the value of ϵ_b corresponding to complete breakup one finds that the ratio of the final diameter to the original diameter

$$\frac{D}{D_0} = \frac{D_0 + 2\delta}{D_0} = 1 + 2\epsilon_b$$

which, for $\epsilon_b = 10$, has the rather astounding value of

$$\frac{D}{D_0} = 21$$

which is an order of magnitude larger than all previous observations.

Wolfe and Andersen[18] worked out a general theory for the breakup time which is applicable to both the bag and the stripping modes of disintegration by considering a model like the one shown below.

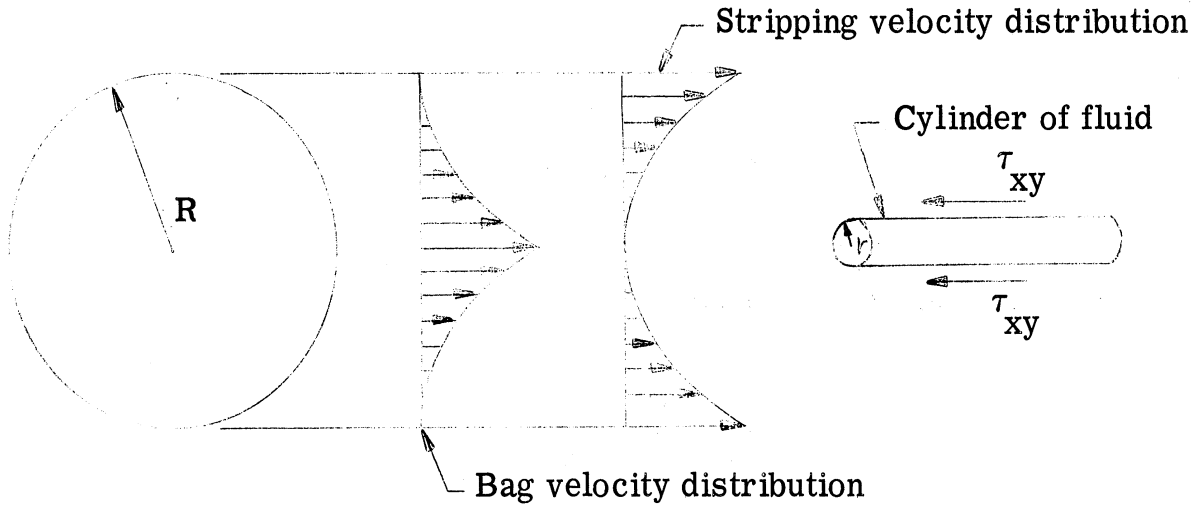

The rate of shear of the fluid due to the aerodynamic pressure forces applied at the surface of the drop was written as

$$\frac{dV}{dr} = \frac{\tau_{xy}}{\mu_\ell} \tag{5.31}$$

where V is the velocity and τ_{xy} is the shear stress acting to restrain the relative motion of adjacent fluid elements within the drop. Equating the pressure and viscous forces for a cylinder of fluid as shown

$$\pi r^2 p_h = 2\pi rD\, \tau_{xy}$$

which when substituted into Eq. (5.31) and integrated for the conditions that

$V = 0$ at $r = R$ $\Rightarrow$ Bag (-) dV/dr

$V = 0$ at $r = 0$ $\Rightarrow$ Stripping (+) dV/dr

gives respectively,

$$V = p_h \frac{(R^2 - r^2)}{4 \mu_\ell D}$$

$$V = p_h \frac{r^2}{4 \mu_\ell D}$$

from which,

$$V_{max} = p_h \frac{R^2}{4 \mu_\ell D} \tag{5.32}$$

for r = 0 and r = R. The pressure head p_h is the difference between the aerodynamic stagnation pressure and the pressure required to provide the kinetic energy of the liquid flow[46]; i. e. ,

$$p_h = p - \frac{1}{2} \rho_\ell V^2 \tag{5.33}$$

Substitution of Eq. (5.33) into Eq. (5.32) and solving the resulting quadratic expression for V yields

$$V = \frac{dx}{dt} = - \frac{16 \mu_\ell}{\rho_\ell D} + \sqrt{\left(\frac{16 \mu_\ell}{\rho_\ell D}\right)^2 + \frac{2}{\rho_\ell} p} \tag{5.34}$$

from which an expression for the breakup time is found by integrating Eq. (5.34) and assuming that the length x of the cylinder of fluid is at the moment of breakup twice as long as the original diameter D of the drop. The breakup time is then found to be

$$t_b = \frac{D}{(A^2 + BP)^{1/2} - A} \tag{5.35}$$

where

$$A = \frac{16\,\mu_\ell}{\rho_\ell\, D} \quad , \quad B = \frac{2}{\rho_\ell}$$

The pressure P in Eq. (5.35) was assumed to be of the form

$$P = \frac{1}{2}\rho_g V^2 C_D - K\frac{\sigma}{D}$$

where K is the curvature constant for the drop. If μ_ℓ and σ are considered negligible and $C_D = 1$ then,

$$A = \frac{16\,\mu_\ell}{\rho_\ell\, D} = 0$$

$$P = \frac{1}{2}\rho_g V^2 C_D - K\frac{\sigma}{D} = \frac{1}{2}\rho_g V^2$$

and,

$$t_b = \frac{D}{V}\sqrt{\frac{\rho_\ell}{\rho_g}} \tag{5.36}$$

which has a striking functional resemblance to the breakup time as derived by Morrell and Clark.

Using a dimensional analysis similar to that given in Appendix A, Nicholson and Hill[39] developed an expression for the breakup time by neglecting the effects due to air and liquid viscosity and due to the surface tension of the liquid in the drop and the Mach number of the convective flow. Their result was that

$$t_b = \frac{D}{V} \phi_3 (\beta)$$

where,

$$\beta = \frac{\rho_\ell}{\rho_g}$$

The relative distortion ϵ as defined by Clark,

$$\epsilon \equiv \frac{\delta}{D} = \frac{\rho_g}{\rho_\ell} \left(\frac{Vt}{D} \right)^2 \qquad (5.37)$$

was used to define a scaling law for high speed breakup

$$\frac{t_b}{D} = \left(\frac{\epsilon_b \rho_\ell}{2} \right)^{\frac{1}{2}} q^{-\frac{1}{2}} = K q^{-\frac{1}{2}} \qquad (5.38)$$

where q = dynamic pressure and where breakup is assumed to occur when ϵ_b reaches a critical value which was determined from the experiment. If q is measured in lbs/in.^{2}, t_b in milliseconds, and D in in., then $K = 6.85\sqrt{\epsilon_b}$. A plot of the breakup time versus the dynamic pressure data from the experiments gave

$$\frac{t_b}{D} = 23.9\, q^{-\frac{1}{2}} \qquad (5.38)$$

and the corresponding value of ϵ_b was calculated to be $\epsilon_b = 12$ which agrees well with the value of ϵ_b reported by Clark.

The striking feature of these breakup analyses is that, although each formulated model for the fragmentation is in itself unique, the derived functional dependence of the breakup time on the variables in the problem, Eq. (5.25, 5.30, 5.36, 5.38), is in each instance essentially the same. In other words, each analysis has shown that the breakup time is directly proportional to the product of the original drop diameter and the square root of the density ratio of liquid to gas, and inversely proportional to the convective flow velocity. However, although correlations of the experimental data accumulated to date exhibit reasonable agreement with the aforementioned functional dependence of the breakup time, it is not at all clear that this will necessarily be the case for shock wave-drop interactions at shock Mach numbers considerably in excess of $M_s = 2$.

B. Experimental Arrangement and Procedure

1. Design Considerations and Performance Calibration. A schematic diagram of the shock tube which is designed purposely for the drop shattering experiments is shown in Fig. 5.1. The length of the tube is chosen to provide

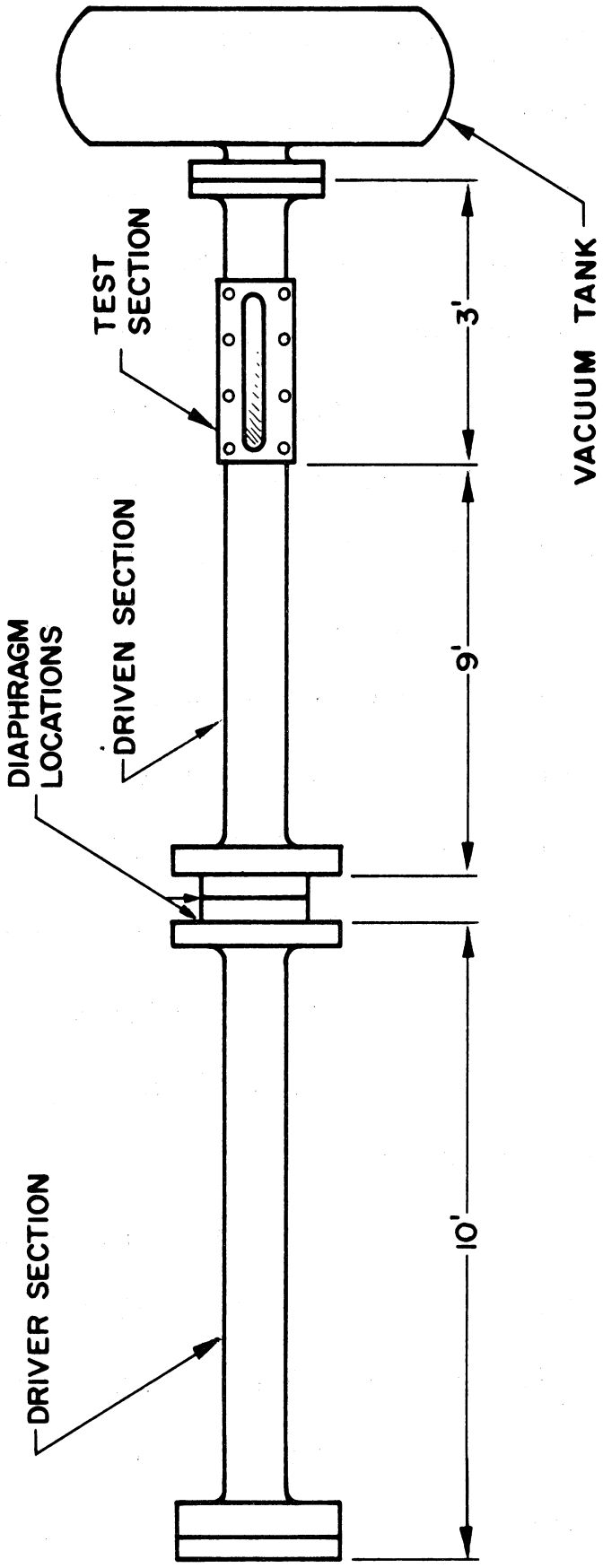

Fig. 5.1 Schematic Diagram of Shock Tube

a testing time of approximately 2 millisec for a shock Mach number $M_s = 1.5$ and 200 μsec for a shock Mach number $M_s = 5$. The actual testing time, which is the time elapsed between the passage of the shock front and the arrival of the interface or the reflected rarefaction in the test section, whichever comes first, is determined from experiment and is plotted as a function of the shock Mach number M_s in Fig. 5.2. The testing time information is obtained by simultaneously displaying and sweeping on an oscilloscope the output of a thin film heat transfer gauge with that of a Kistler 601-A quartz pressure transducer both of which are flush mounted in the wall of the test section. A sample trace is shown in Fig. 5.3 where the sharp change in slope of the heat transfer trace corresponds to the passage of the interface. As is usually the case, the interface for this particular run has arrived in the test section well ahead of the reflected rarefaction which is not seen on the static pressure trace.

The desired shock strength is obtained by charging the driver section with either N_2, He, or H_2 to the pressure required for producing the test Mach number of interest. Since the driven section pressure is 1 atmosphere, the pressure ratio across the diaphragm is controlled exclusively by the pressure established in the driver and a plot of shock Mach number versus driver pressure for N_2, He, and H_2 is shown in Fig. 5.4. The experimentally determined performance of the shock tube, which is also shown in Fig. 5.4, is found by calculating the Mach number of propagation corresponding to a given driver pressure and driver gas from a measurement of the time required for the shock

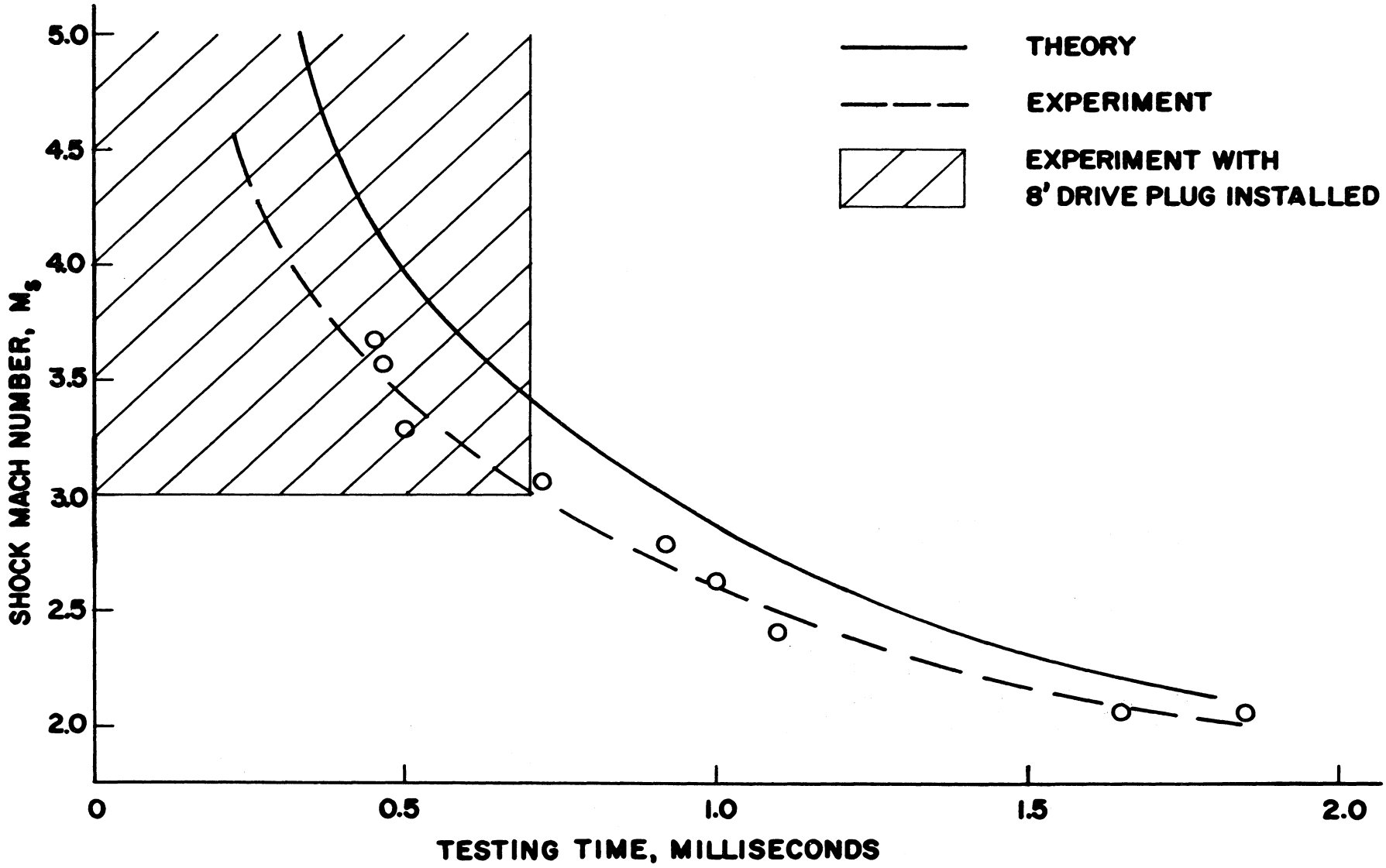

Fig. 5.2 Shock Mach Number vs. Testing Time

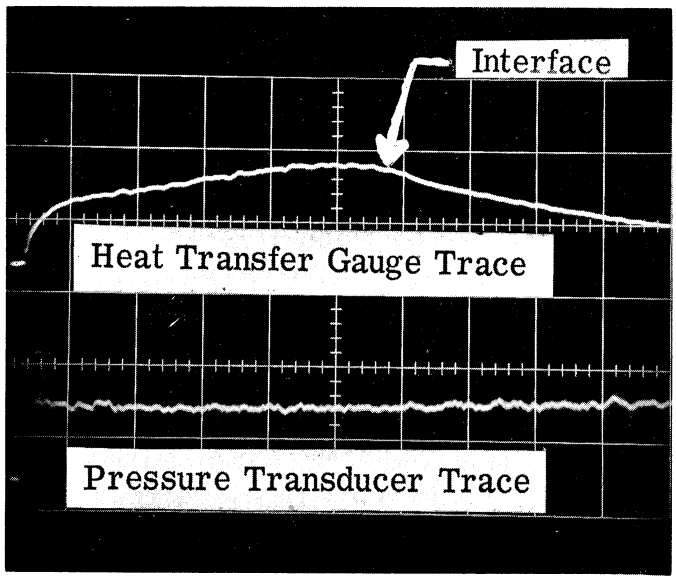

$M_s = 1.78$

$P_1 = 1$ atm.

Heat Transfer Gauge Sensitivity = 2 mv/cm
Kistler 601A Pressure Transducer Sensitivity = 50 psi/cm
Scope Sweeping Rate = 0.5 millisec/cm
No Plug In Driver Section

Fig. 5.3. Output Trace of Pressure Transducer and Heat Transfer Gauge.

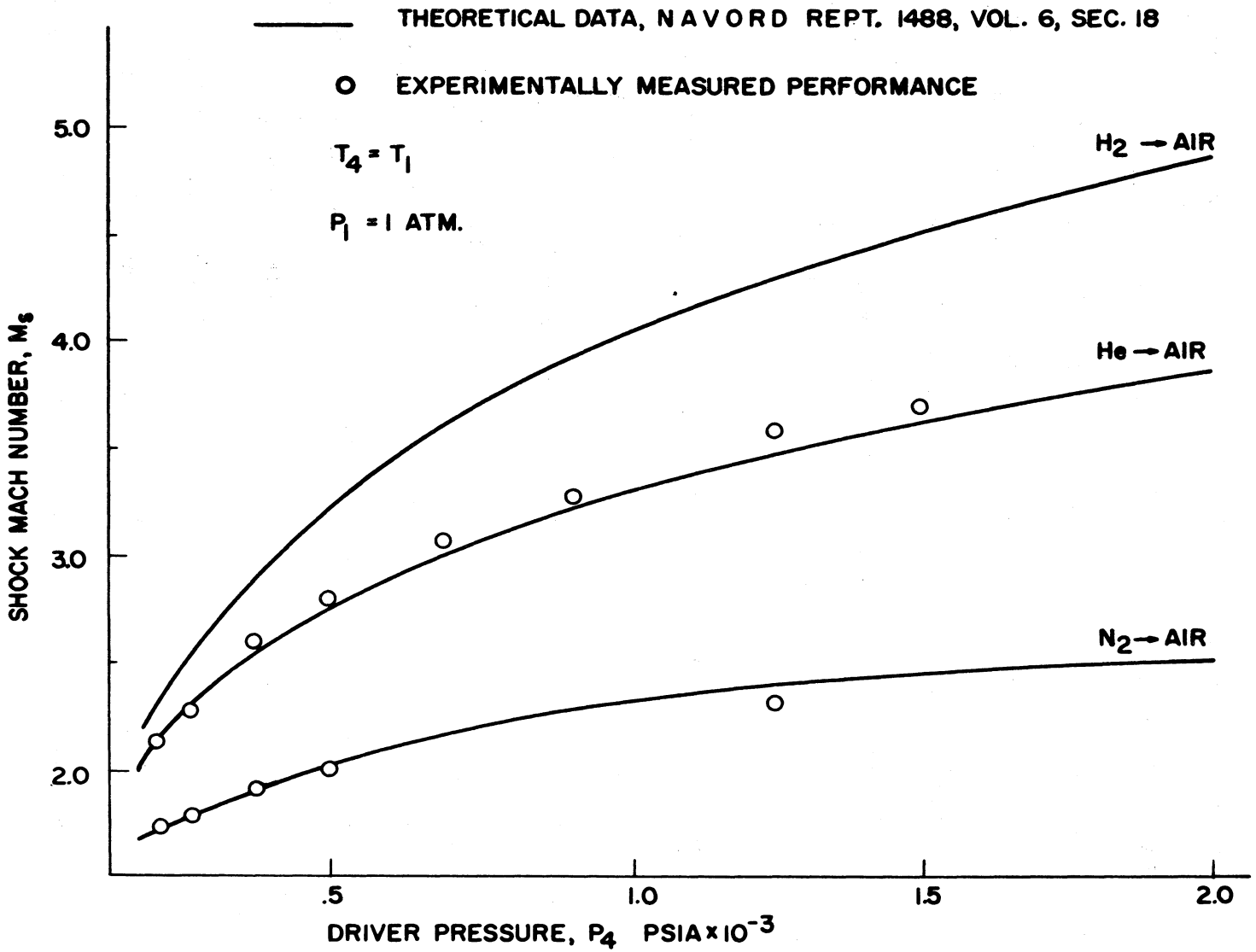

Fig. 5.4 Shock Mach Number vs. Driver Pressure

wave to travel a known distance in the shock tube. Two pressure switches of design similar to that shown in Fig. 3. 16, are actuated by the passage of the shock wave, one mounted in the wall of the shock tube just upstream of the test section and the other at a point 1 1/2 ft further downstream, are utilized in conjunction with a thyratron unit to start and stop a CMC 757B micro-second counter for the purpose of measuring the elapsed time. Figure 5. 5 shows the convective flow Mach number M, the Weber number We, and the Reynolds number Re simulation capability of the shock tube as a function of the shock Mach number M_s in equilibrium air.

2. Design of Shock Tube System Components. The driver section of the shock tube is fabricated from a 3 in. I. D. schedule 80 seamless stainless steel pipe 10 ft long. It is designed for a maximum allowable working pressure of 3000 psi. This length is chosen to provide approximately 2 millisec of testing time at M_s = 1. 5, but for the higher Mach number experiments a testing period considerably less than 2 millisec is adequate because the drop breakup time is drastically reduced and therefore a driver 10 ft in length is not required. For this reason the driver section is designed to accommodate end plugs which effectively reduce both its length and its volume. Aside from reducing the amount of driver gas required for a particular run the use of plugs also minimizes the final pressure in the entire shock tube.

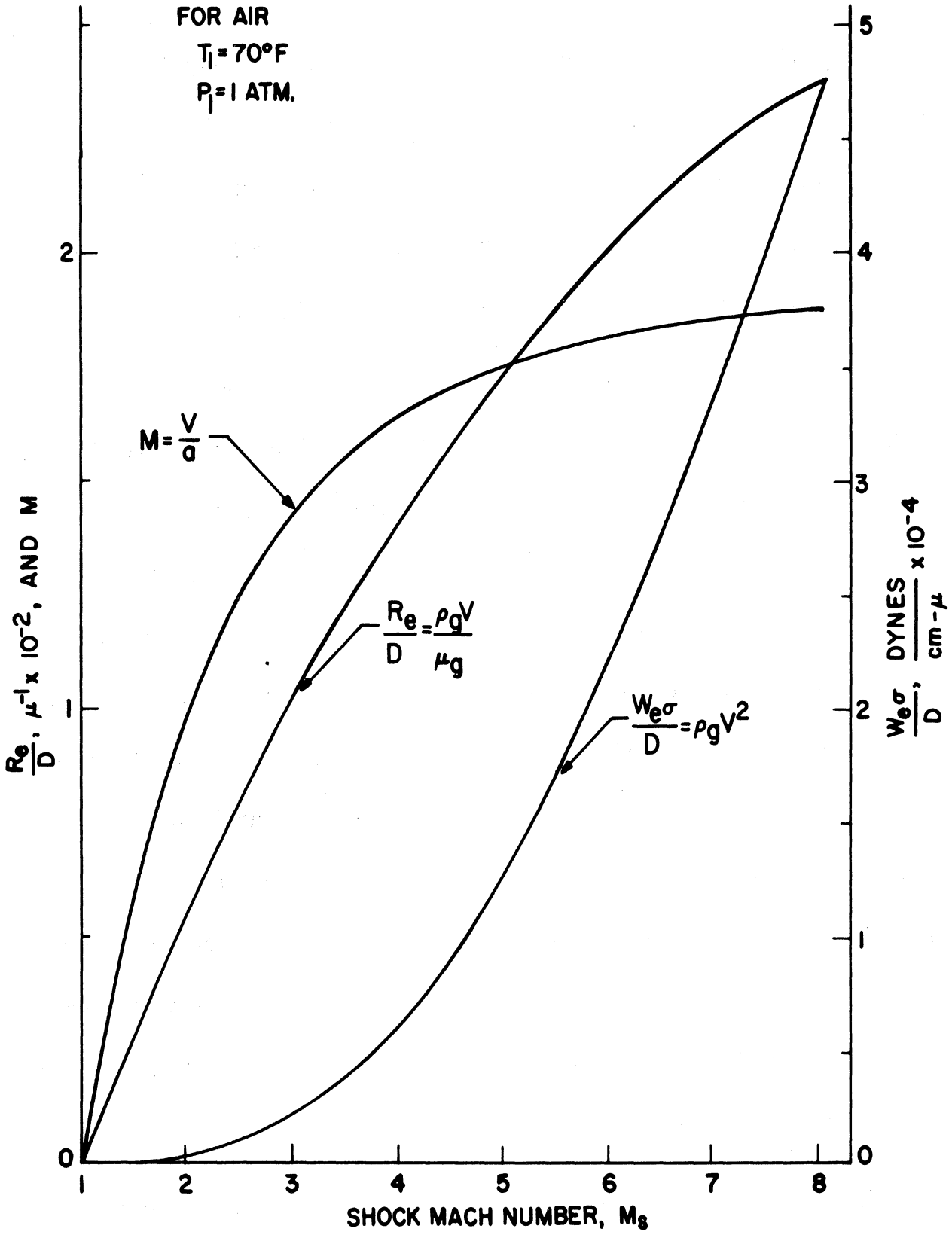

Fig. 5.5 Convective Mach Number, Reynolds Number, and Weber Number vs. Shock Mach Number

The end plugs are made of kiln dried birch approximately 2.9 in. in diameter. They are held in place in the driver section by sliding them onto a 1 in. diameter steel pipe with jam nuts at each end. The pipe is then threaded into the blind flange at the end of the driver section to restrain the plug assembly from moving like a free piston when the shock tube is fired.

The diaphragm section, which separates the driver section from the driven section, is a double diaphragm design. The choice of this design provides the operator with a simple means of controlling both the time at which firing of the shock tube is desired and the pressure ratio at the instant of diaphragm burst. The diaphragm section consists of two diaphragm holders placed between the flanges of the driver and the driven sections. To operate the shock tube, two scored metal diaphragms are placed between the diaphragm holders and then the pressure in the driver p_4 and the pressure between the diaphragms p_D are established simultaneously such that $p_D \simeq 1/2\, p_4$. Since the diaphragms are designed to rupture at a pressure differential slightly in excess of $1/2\, p_4$, the opening of the diaphragm section solenoid reduces p_D causing the diaphragms to burst. A picture of one of the ruptured steel diaphragms is shown in Fig. 5.6.

The driven section of the shock tube is a rectangular seamless stainless steel tube with internal dimensions of 1.5 x 2.5 in. and a wall thickness of 3/8 in. This section, which is 12 ft long, is flanged at the downstream end

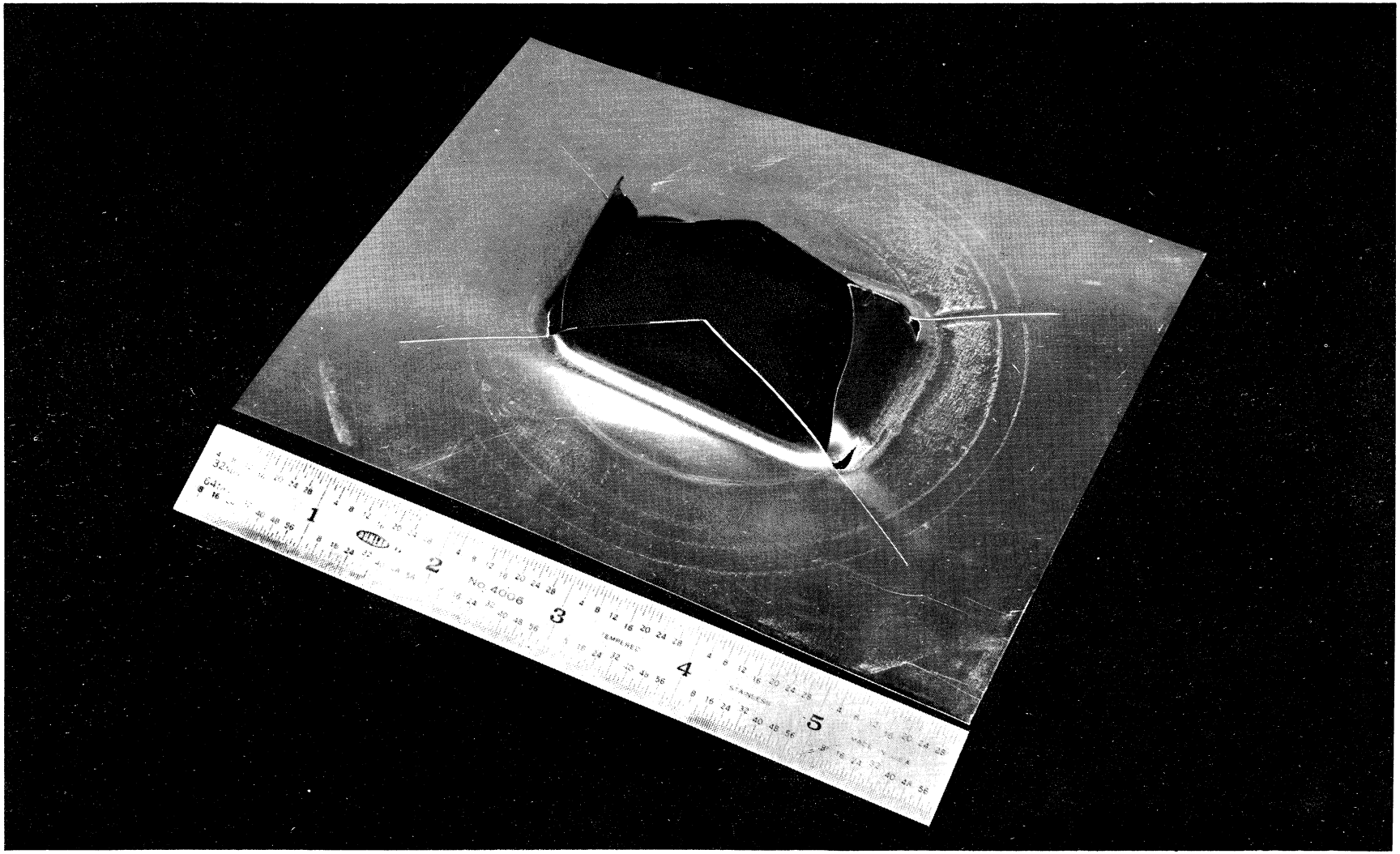

Fig. 5. 6. Ruptured Steel Diaphragm.

to a dump tank which is shown in Fig. 5.7. A mylar diaphragm is used between the driven section and the dump tank so that the tank can be evacuated and used as both a sound suppressor and a volume for the expansion of the high pressure gas.

The test section, which is also shown in Fig. 5.7, was made by cutting a slot in each side of the rectangular driven tube 9 ft downstream from the diaphragm section. Schlieren quality plate glass windows 11 3/4 in. long, 1 in. wide, and 1 3/16 in. thick are held in flanges which fit into the slots on either side of the tube. The windows are flush with the inside wall of the shock tube so that no flow disturbance is created in the test section. Holes in the top and in the bottom of the test section are provided for the stream of drops to fall through.

The drop generating system is depicted schematically in Fig. 5.8 and various parts of the system are visible in Fig. 5.7. This system is extremely well suited to the production of stable streams of waterdrops. Since a complete discussion of the formation and stabilization of drops using this technique can be found in Ref. 1 and elsewhere in this report, the details of the generating system are not repeated here.

Photographs of the disintegrating drops are taken by using a Beckman and Whitley type 501A image converter camera. The drops are back-lighted with a collimated high intensity light beam produced by the discharge of a

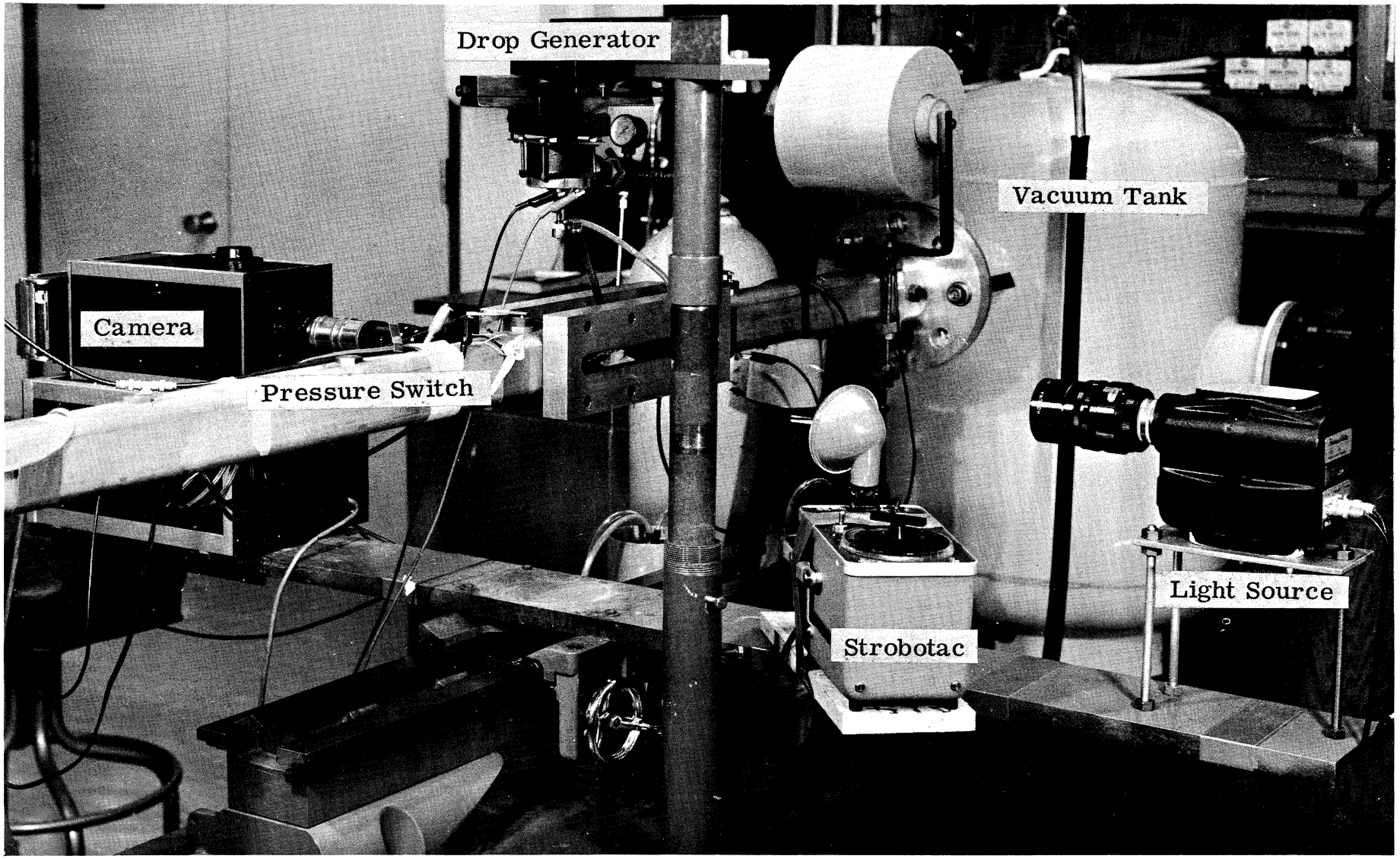

Fig. 5.7. Photograph of Shock Tube Test Section.

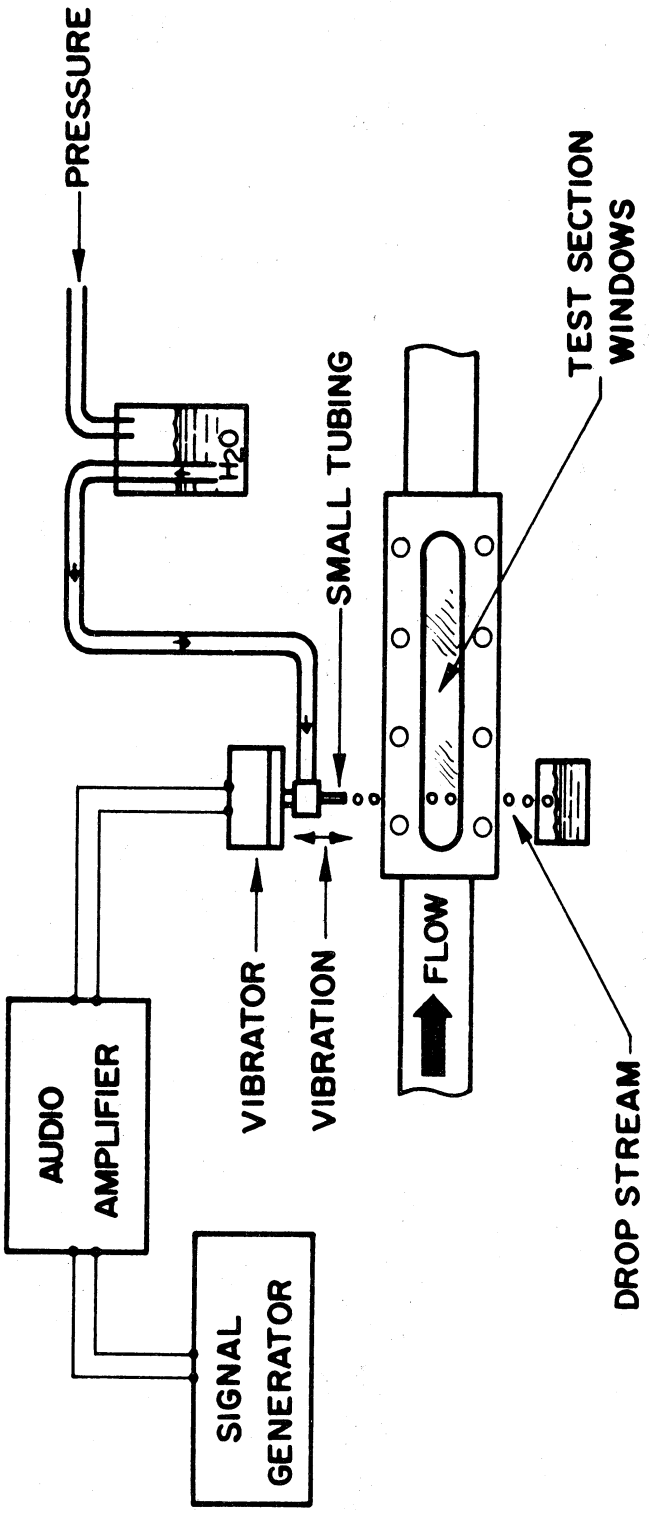

Fig. 5.8 Schematic of Drop Generating System

Beckman and Whitley 5401 spark light source which is synchronized internally with the operation of the image tube. This system has an exposure speed capability of 5-1000 nanoseconds and the optics can be adjusted to produce magnification ratios as large as 10/1. The image converter camera and light source are mounted on a piece of channel iron which is bolted across the saddle of a 48 in. lathe bed as shown in Fig. 5.7. The lathe bed is supported on a table under the test section and the lathe saddle can be translated along the bed to move the optical path back and forth along the test section as required. The camera is triggered by a thyratron circuit which is fired by a signal produced from a pressure switch located in the wall of the shock tube just upstream of the test section. This switch can be seen in Fig. 5.7 which also shows the strobotac used to check the stability of the drop stream before the shock tube is fired.

Because only one photograph is made each time the shock tube is fired a time history of the shattering phenomenon is obtained through a series of pictures made in successive experiments. The wave speed and the drop diameter and trajectory are controlled within extremely small limits so that the only variable is the time delay in the photographic system. The method of controlling and measuring this delay is shown schematically in Fig. 5.9.

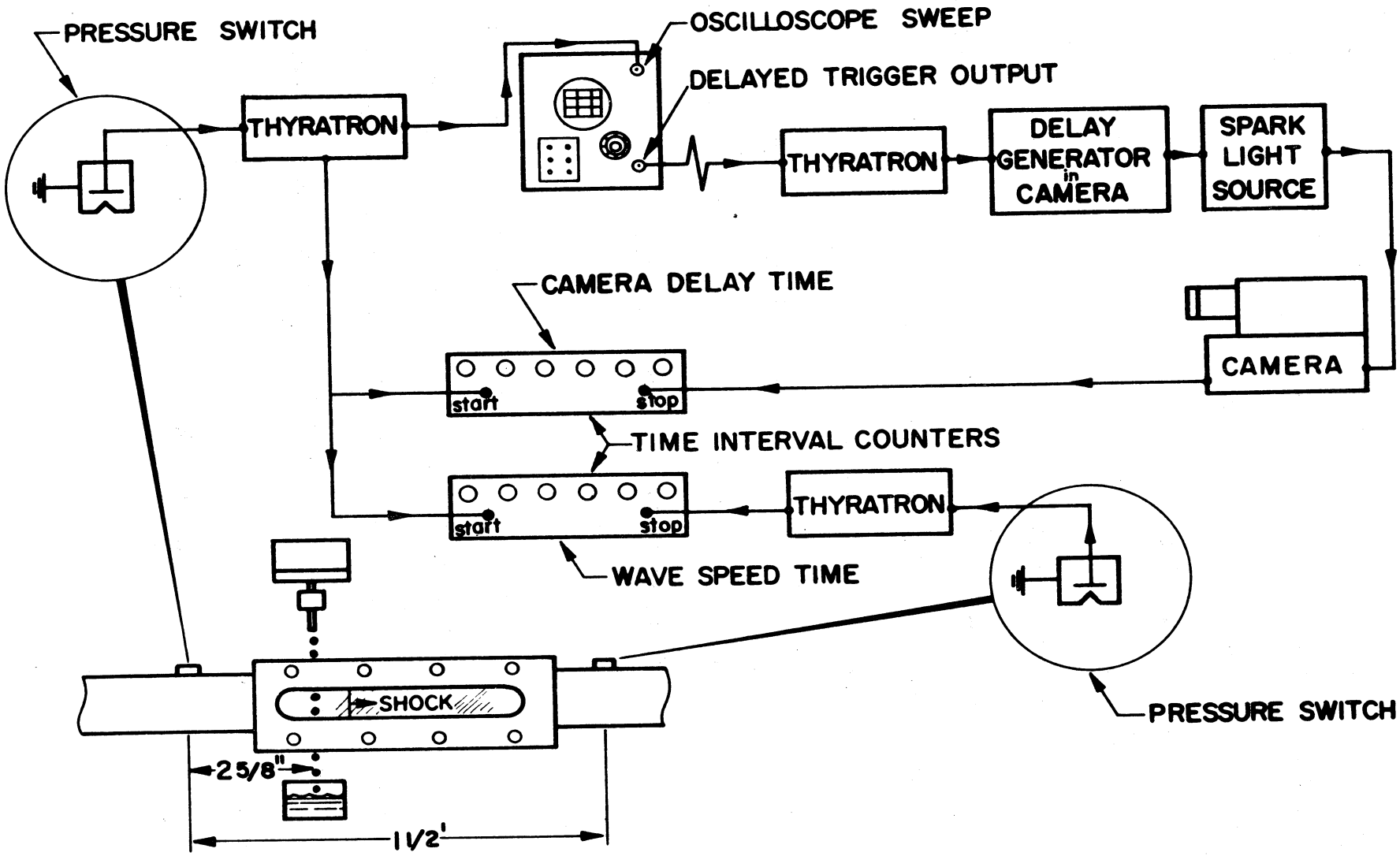

Fig. 5.9 Trigger and Time Delay Circuit

3. Experimental Procedure. The experimental procedure consists of obtaining a time history of the disintegration and the drift of a water drop by taking a series of photographs, one at a time, at different time intervals after the shock wave intercepts the drop. The time that elapses between the instant that the air shock intercepts the water drop and the instant that the picture is taken is found by subtracting from the camera delay time the time required for the shock wave to move from the start pressure switch to the water drop. A calculation of the time it takes the air shock to move from the start pressure switch to the water drop is made by dividing the distance separating the two, as shown in Fig. 5.9, by the measured velocity of propagation of the shock wave. The velocity at which the air shock moves down the shock tube is calculated from the time required for it to traverse a known distance as shown in Fig. 5.9. The reading on the wave speed time interval counter is the time in microseconds required for the shock wave to move the 1.5 ft between the two pressure switches.

The drift of a shattering drop is measured directly from the photographs by measuring the distance between the position of the forward stagnation point at the moment the shock intercepts the drop and the position it has at some subsequent moment in time. In this manner it is possible to obtain the time history of the motion of the drop from which both the velocity and acceleration can be calculated.

C. Discussion of Results

The drop shattering experiments to date have covered the shock Mach number range from M_s = 1.54 - 3.25 with water drops having diameters in the range D = 750 - 1090μ. Photographs of the shock wave-drop interactions are shown for shock Mach number M_s = 1.54, M_s = 2.7, and M_s = 3.25 in Fig. 5.10, 5.11, and 5.12, and Fig. 5.13, 5.14, and 5.15 show respectively the drop flattening, the drop displacement, and a comparison of drop breakup time results.

Figure 5.10 shows the sequence of events leading to the disintegration of a 780μ waterdrop by an air shock whose Mach number is M_s = 1.54. As noted previously, the breakup is divided into two very distinct stages; a dynamic stage during which the drop is flattened-out followed by the stripping process which eventually reduces the drop to a cloud of mist. The plot of drop flattening versus time after collision with the shock shows that for a given drop size the rate of change of drop diameter with time increases very rapidly with increasing shock Mach number and the maximum drop diameter attained appears to be a function of both the mass of the original drop and the strength of the colliding shock wave. The comparison of Burgers[45] theory with the drop flattening curves indicates that the parabolic dependence of the diameter on the time after collision with the shock agrees very well with the experimental data, however the observed maximum diameter was in almost all cases larger than the prediction of the Taylor[32] theory. Figure 5.10 also

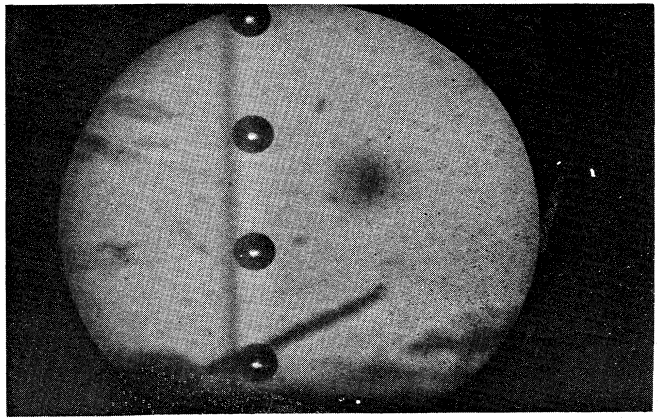

Shadow Photograph of Undisturbed 780μ Waterdrops

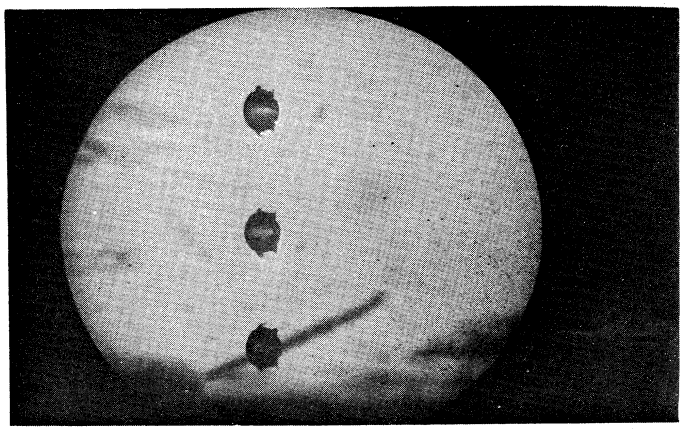

Shadow Photograph of 780μ Waterdrops
M_s = 1.54
T = 20.9 μ-sec After Shock Passage

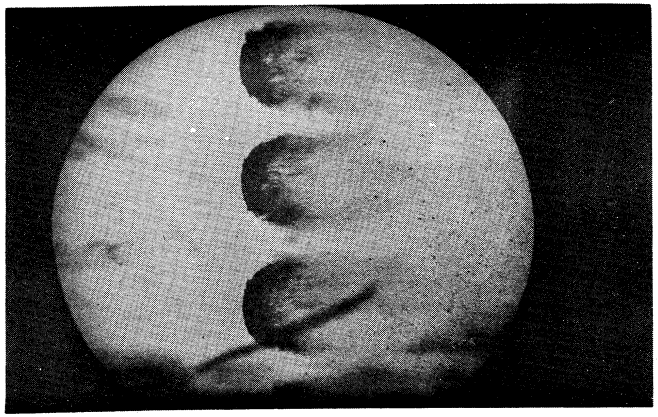

Shadow Photograph of 780μ Waterdrops
M_s = 1.54
T = 45 μ-sec After Shock Passage

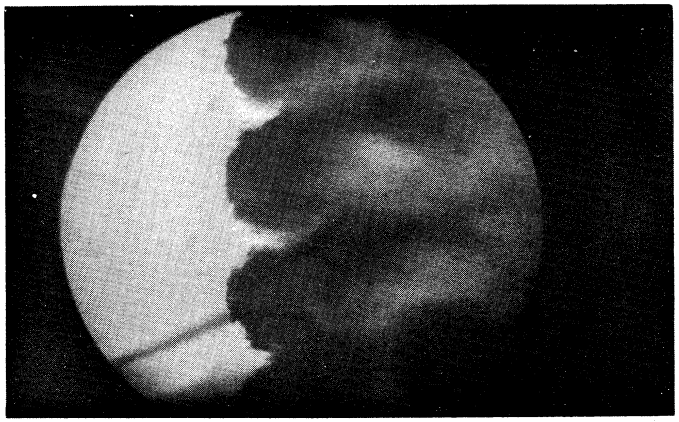

Shadow Photograph of 780μ Waterdrops
M_s = 1.54
T = 102 μ-sec After Shock Passage

Fig. 5.10. Photographing Sequence of the Shattering of 780μ Drops by M_s = 1.54 Shock.

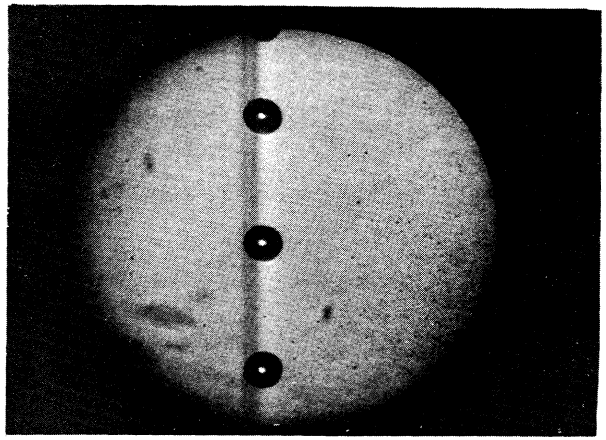

Shadow Photograph of Undisturbed 750 μ Waterdrops

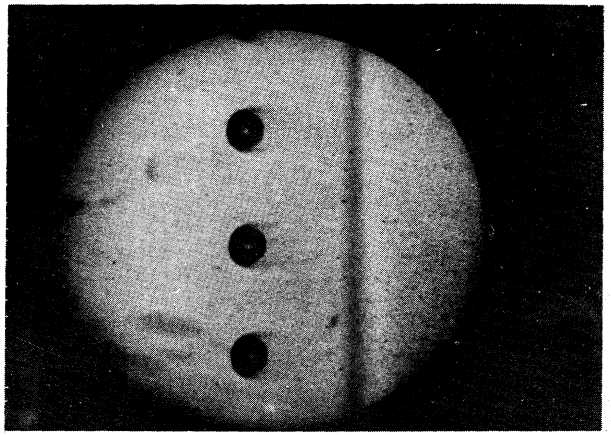

Shadow Photograph of 750μ Waterdrops

M = 2. 7
T = 2. 6 μ-sec After Shock Passage

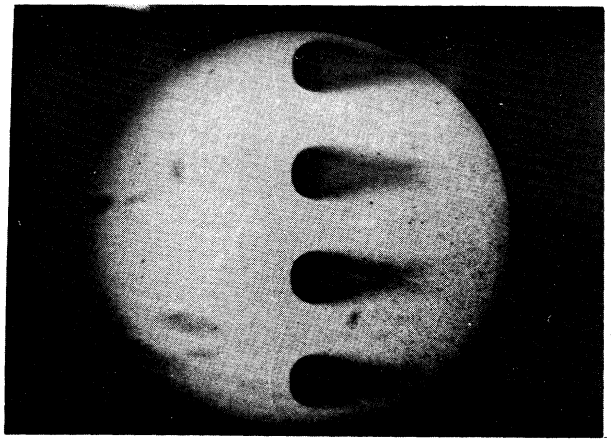

Shadow Photograph of 750μ Waterdrops

M = 2. 7
T = 4. 4 μ-sec After Shock Passage

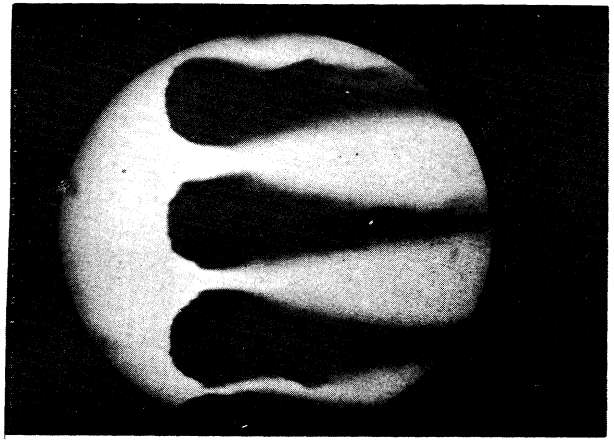

Shadow Photograph of 750μ Waterdrops

M = 2. 7
T = 14. 4 μ-sec After Shock Passage

Fig. 5. 11. Photographing Sequence of the Shattering of 750μ Drops by M_S = 2. 7 Shock.

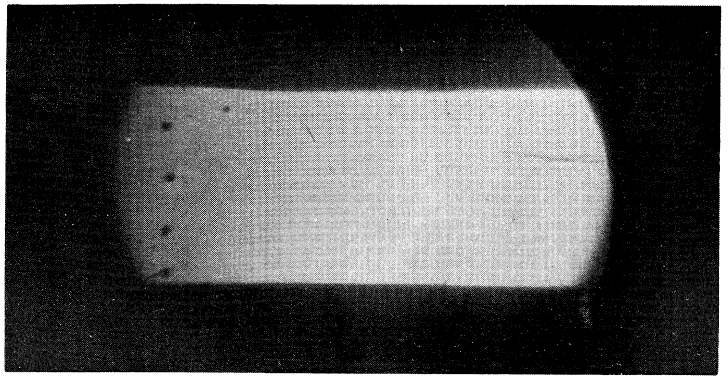

Shadow Photograph of Undisturbed 1090μ Waterdrops

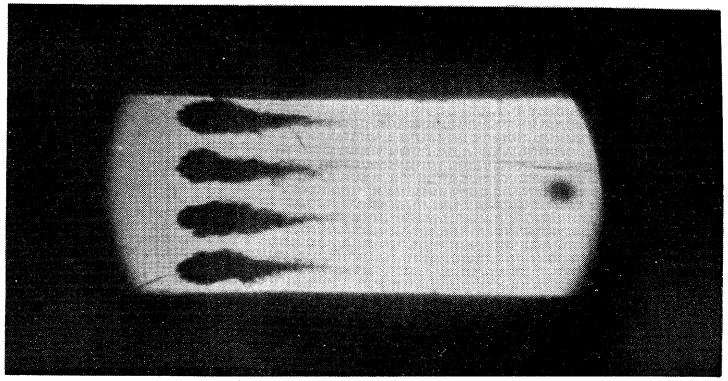

Shadow Photograph of 1090μ Waterdrops
M_s = 3. 25
T = 38. 8 μ-sec After Shock Passage

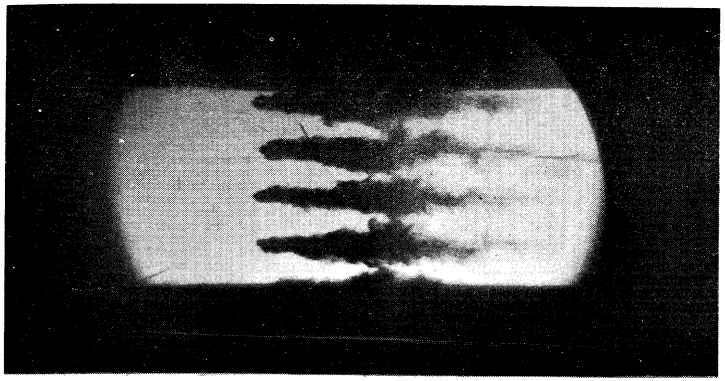

Shadow Photograph of 1090μ Waterdrops
M_s = 3. 25
T = 69. 8 μ-sec After Shock Passage

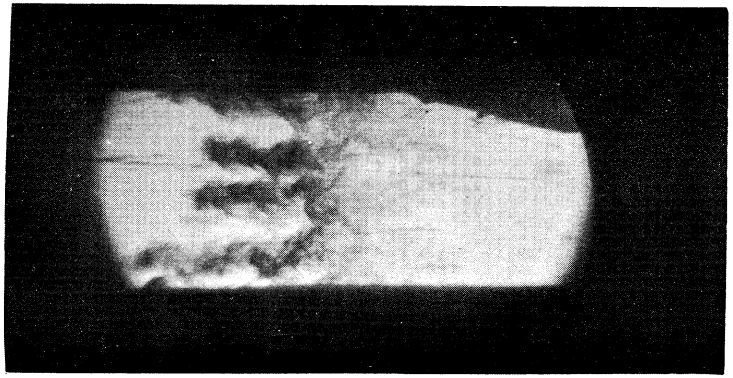

Shadow Photograph of 1090μ Waterdrops
M_s = 3. 25
T = 134. 7 μ-sec After Shock Passage

Fig. 5. 12. Photographing Sequence of the Shattering of 1090μ Drops by M_s = 3. 25 Shock.

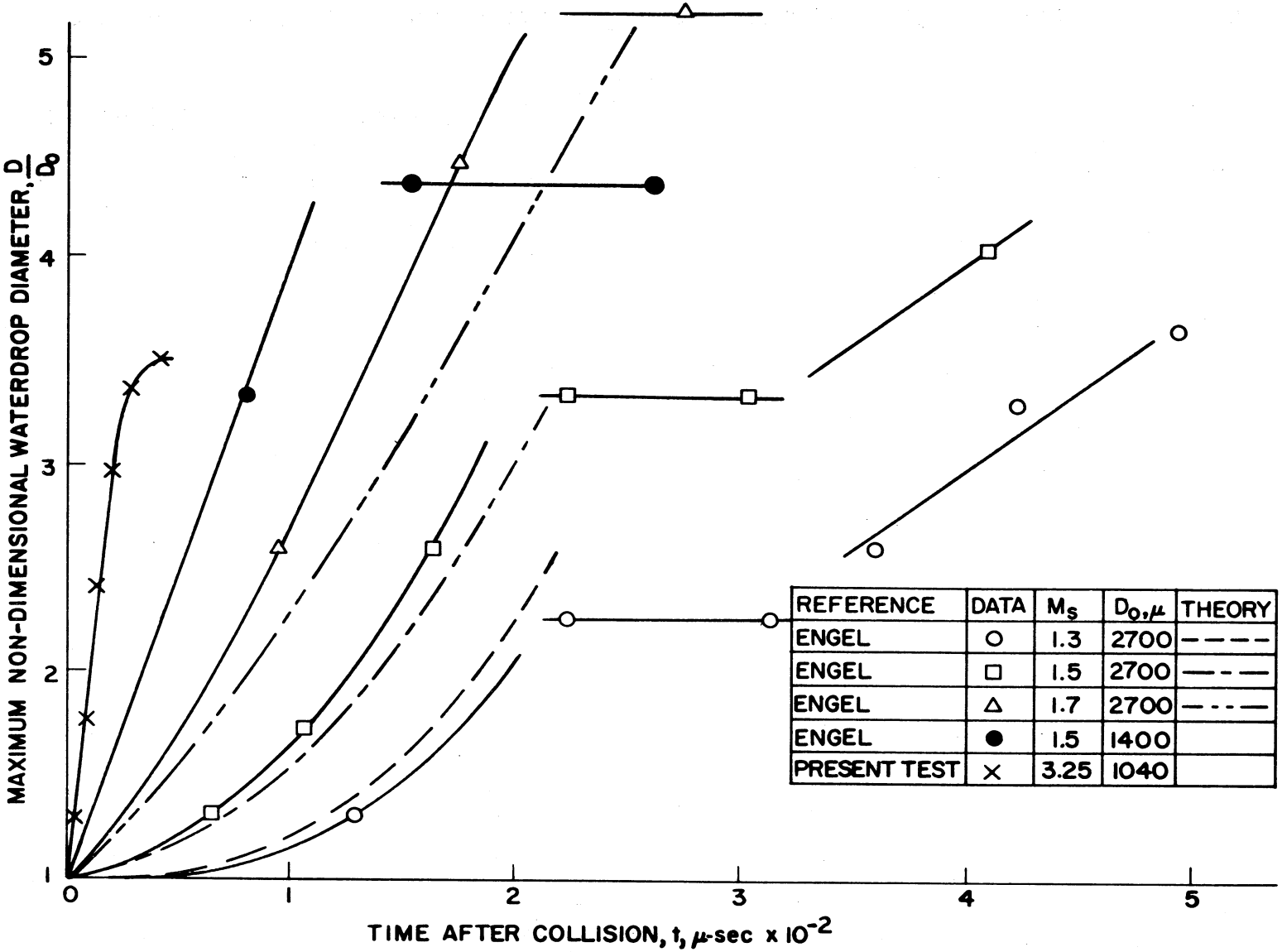

Fig. 5.13 Waterdrop Flattening vs. Time After Collision

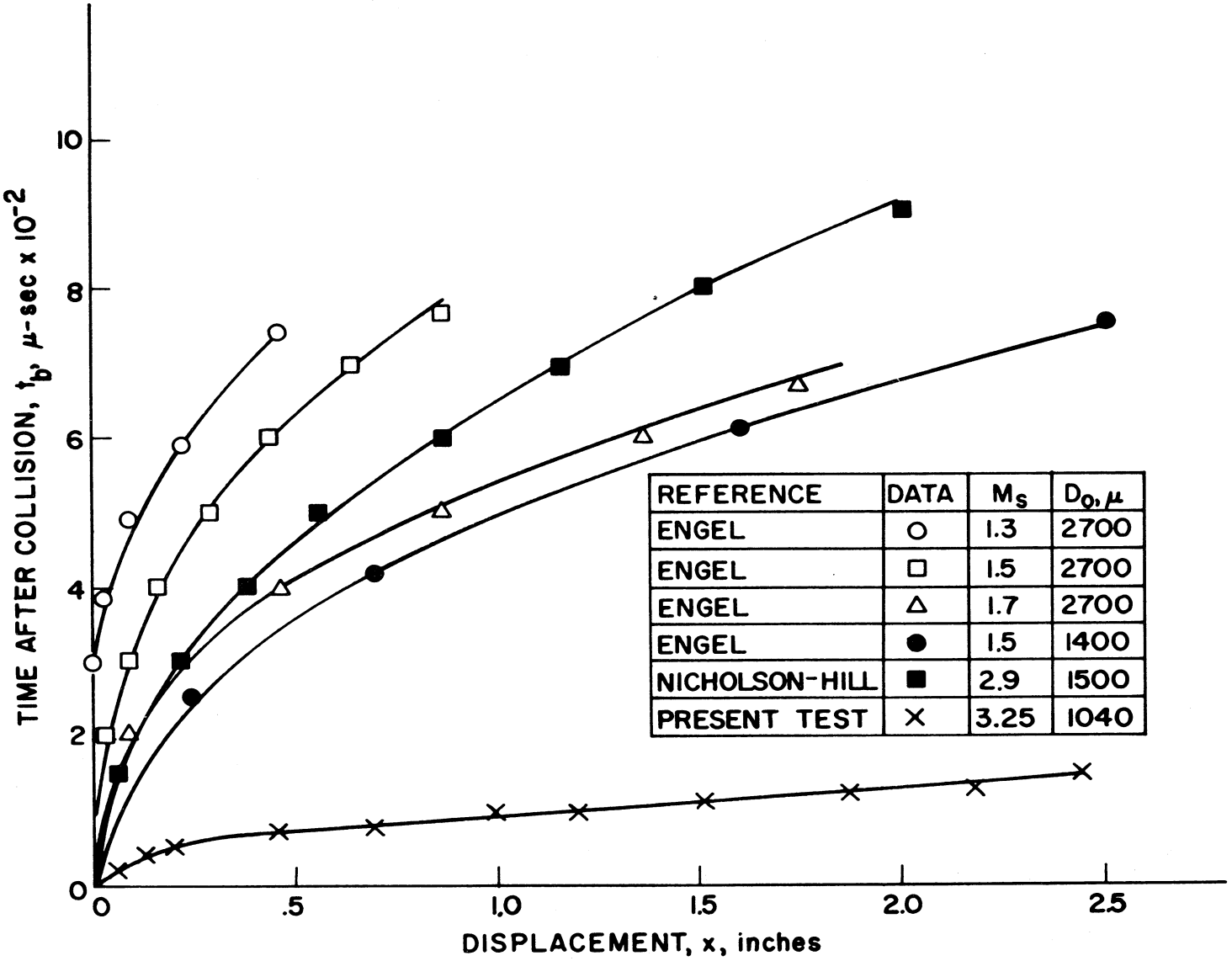

Fig. 5.14 Waterdrop Displacement vs. Time After Collision

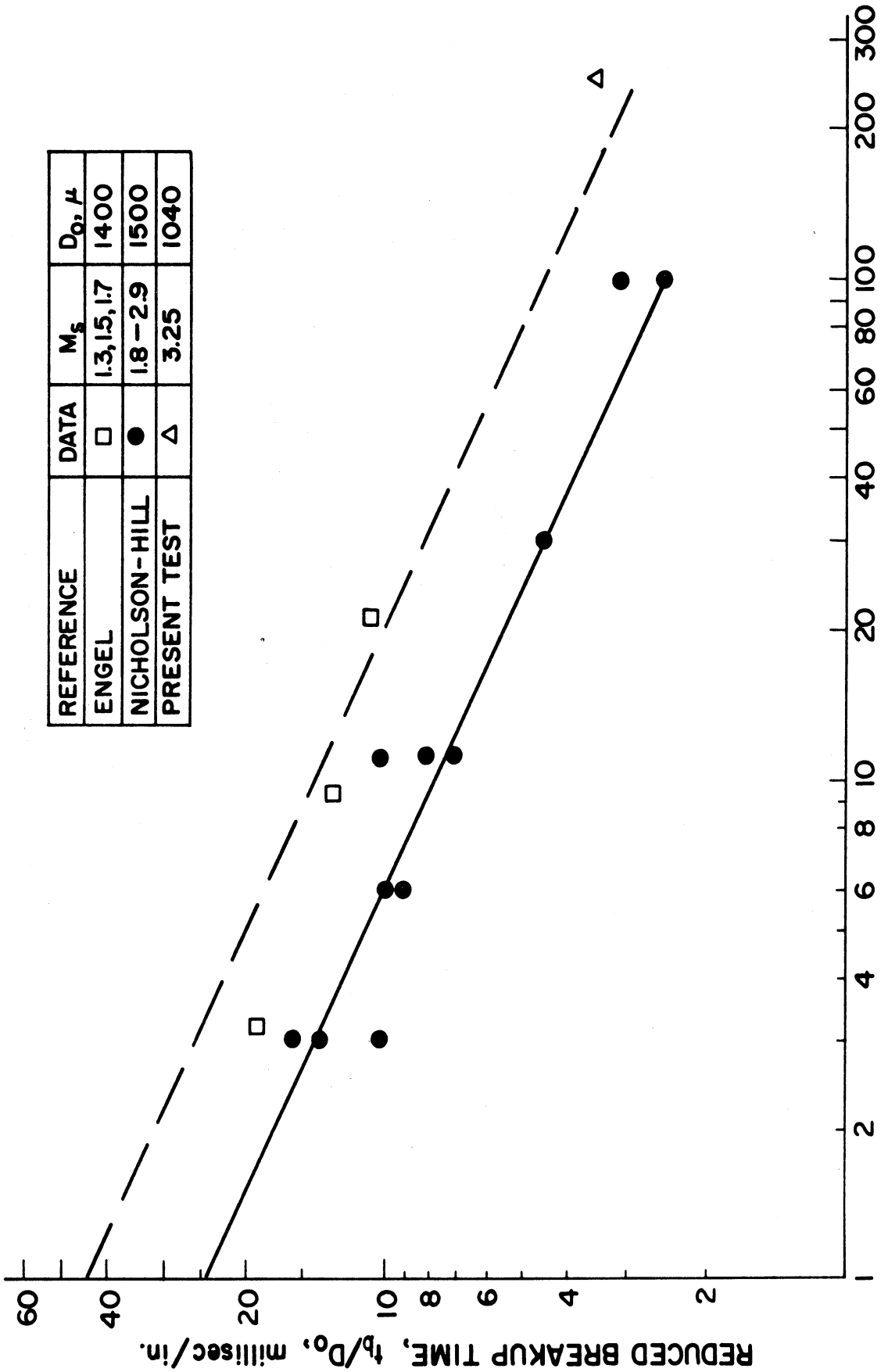

Fig. 5.15 Comparison of Experimental Breakup Time Results

shows that at T = 20.9 μsec after the passage of the shock the drop is still dynamically deforming with the windward face remaining spherical in shape while the leeward surface becomes planar. After T = 45 μsec the drop has been flattened considerably to a diameter approximately twice that of the original drop and it has entered the second stage of breakup characterized by the stripping process. The amplitude of the surface waves increased until at T = 102 μsec the windward surface is seen to have a very rough appearance. Subsequent photographs showed that the time required to reduce a 780 μ waterdrop to a trace of mist was t_b = 250 μsec; approximately one-half the time reported by Engel to breakup a 1400 μ drop under similar conditions. The collision that takes place when the shock wave intercepts the drop does not appear to be a significant factor influencing the interaction process. However it is possible that for very strong shock waves, where the drop internal pressures become very large, a different breakup mechanism might be experienced.

The photographs in Fig. 5.11 for M_s = 2.7 and 750 μ waterdrops show some significant changes in the interaction process as compared to the case where M_s = 1.54. The so-called dynamic stage of the breakup is no longer a distinct time during which the drops deform into lenticular plano-convex shapes but rather the deformation occurs simultaneously with the stripping process which is observed to begin at only T = 2.6 μsec after the passage

of the shock. At T = 4.4 μsec a substantial wake, similar in shape to that found behind a hypersonic blunt body, of very fine micro-droplets has developed. Since the convective flow relative to the drops is supersonic with a Mach number of M = 1.3, stand-off bow shocks are clearly visible.

The photographs in Fig. 5.12 show the breakup of 1090μ waterdrops when the shock Mach number was M_s = 3.25. From the picture taken at T = 38.8 μsec it can be seen that the tip of the wake of micro-droplets is convecting at about 15 μsec behind the propagating shock front. Other pictures taken under the same conditions as those indicated in Fig. 5.12 show that at T = 7.8 μsec the tip of the wake is only 4 μsec behind the shock wave. The photographs taken at T = 69.8 μsec and at T = 134.7 μsec show that the shattering process consists of a continuous stripping away of the drop material by the action of the convective flow. A rather long wake of what appears to be very fine micro-droplets develops and breakup is considered to be complete when the wake has the appearance of that shown at T = 134.7 μsec. The parabolic representation given by

$$x = 1.11 \times 10^{-4} T^2$$

where x has the units of inches, T in μsec and 1.11×10^{-4} in./(μsec)^2 is an excellent curve fit to the displacement data obtained from the experiments conducted at M_s = 3.25 and D = 1090μ. This expression was used to calculate both the velocity, which is a linear function of the time after

impact with the shock wave, and the acceleration of the disintegrating water drop. The calculations revealed that the shattered drop attained a velocity equal to 90% of the convective flow value by the time T = 134.7 μsec and the acceleration was constant throughout the interaction and equal to $a = .5 \times 10^6$ g's.

A comparison of the experimental breakup time results of Engel, Nicholson and Hill, and the present test shows that there is good correlation between the reduced breakup time and the dynamic pressure of the convective flow field. Both the solid and the dashed lines drawn in Fig. 5.15 have a slope of (-1/2) and they are analytically represented respectively by $t_b/D_0 = 23.9\, q^{-1/2}$ and $t_b/D_0 = 44\, q^{-1/2}$. The former expression agrees well with the experimental data of Nicholson and Hill but the latter is a better fit to the results of Engel and the present test. This difference could result from the definition of the breakup time adopted by Nicholson and Hill.

VI. CONCLUSIONS

1. A dilute spray can be treated as a pseudo-ideal gas thereby simplifying the calculation of the properties of spray detonations.

2. Spray detonations can be easily initiated by a transmitted shock in a shock tube setup with either He or H_2-O_2 detonation products as the driver. In the latter case it appears that the minimum Mach number of the transmitted shock necessary to initiate detonation is smaller than that of the He case.

3. In general, the detonation velocity is smaller than the theoretically calculated velocity and the pressure ratio is compatible with a shock travelling at the detonation speed. For a monodisperse spray with 940 μ drop size a steady velocity within 15% of the theoretical was attained when the equivalence ratio was .50.

4. From combined shadow and direct light photographs, the delay between the passage of the shock and the appearance of luminosity is comparable to the drop shattering time, indicating that spray detonations are controlled by the mechanical breakup of the liquid drops.

5. Experiments on film detonations, indicate that the phenomenon is controlled by evaporation and mechanical stripping of the film. The stripped liquid film remains within the boundary layer and hence combustion is initiated in this region.

6. An analytical study of film detonation is started with the formulation of boundary layer flow with mass and heat addition under conditions compatible with the physical situation.

7. The breakup of a liquid drop by a shock wave occurs as a result of the interaction between the drop and the convective flow field established by the shock wave. Two stages can be distinguished at low Mach numbers: deformation and stripping. At the higher Mach numbers however the stripping away of the surface appears to take place simultaneously with the dynamic deformation of the drop.

8. The drop fragmentation process is a continuous one and an absolute criterion for identifying the moment of complete fragmentation is not feasible. Identification of complete breakup is largely a qualitative judgement based on the photographs of the phenomenon.

9. The reduced breakup time is proportional to the drop diameter and inversely proportional to the square root of the local dynamic pressure.

VII. FUTURE PLANS

1. Spray detonation experiments will be continued with the aim of assessing the effects of drop sizes and mixture ratios. The threshold strength of the initiating shock as a function of drop sizes and mixture ratios will be determined.

2. Detonation in polydisperse sprays with particular emphasis on bimodal spray distributions will also be investigated.

3. Fuels different than DECH will also be tried.

4. Theoretical treatment of the reaction zone structure which will take into consideration the breakup, evaporation and eventual combustion of the liquid drops will be conducted.

5. Further experiments on film detonation will be made to investigate the effects of film thickness and the type of fuels. Threshold initiating shock strengths will be determined.

6. The theoretical treatment on film detonations started in this report will be continued.

7. The experimental and theoretical investigations on drop shattering will concentrate on extending the present work to cover all the conditions pertinent to detonation phenomena in two-phase media. These conditions are for a Mach number range of 3-8, a drop diameter range of 200-2000 μ, and for a few different liquids.

Appendix A

DIMENSIONAL ANALYSIS OF DROP SHATTERING PROBLEM

The drop shattering problem is characterized by two sets of variables one of which is associated with the convective flow field that interacts with the drop and the other with the physical properties of the liquid in the drop. The most important variables characterizing the convective flow are the convective flow velocity V, the speed of sound a_g, the density ρ_g, and the viscosity μ_g. Those characterizing the drop are the original diameter D, the surface tension σ, the viscosity of the liquid μ_ℓ, the density of the liquid ρ_ℓ, and the breakup time t_b.

Breakup time	t_b	$L^0M^0T^1$
Drop diameter	D	$L^1M^0T^0$
Surface tension	σ	$L^0M^1T^{-2}$
Liquid viscosity	μ_ℓ	$L^{-1}MT^{-1}$
Liquid density	ρ_ℓ	$L^{-3}M^1T^0$
Flow velocity	V	$L^1M^0T^{-1}$
Speed of sound	a_g	$L^1M^0T^{-1}$
Flow density	ρ_g	$L^{-3}M^1T^0$
Flow viscosity	μ_g	$L^{-1}MT^{-1}$

Since there are nine variables and three fundamental units in the problem Buckingham's π-theorem states that a physical equation involving these variables can be expressed in the form

$$\phi_1 (\pi_1, \pi_2, \pi_3, \pi_4, \pi_5, \pi_6) = 0 \qquad \text{(A. 1)}$$

where the π's are dimensionless parameters formed of the products of powers of the variables. The number of such independent π terms will be in this case the number of variables (9) minus the number of fundamental units (3) or 6. If we let

$$\nu_1 = D$$

$$\nu_2 = \rho_g$$

$$\nu_3 = V$$

$$\nu_4 = \sigma$$

$$\nu_5 = t_b$$

$$\nu_6 = \mu_g$$

$$\nu_7 = \mu_\ell$$

$$\nu_8 = a_g$$

$$\nu_9 = \rho_\ell$$

then it can be shown that

$$\pi_1 = \nu_4\, \nu_2^{-1}\, \nu_3^{-2}\, \nu_1^{-1} = \sigma/\rho_g\, V^2\, D$$

$$\pi_2 = \nu_5\, \nu_3\, \nu_1^{-1} = t_b\, V/D$$

$$\pi_3 = \nu_6\, \nu_2^{-1}\, \nu_3^{-1}\, \nu_1^{-1} = \mu_g/\rho_g\, V\, D$$

$$\pi_4 = \nu_7\, \nu_2^{-1}\, \nu_3^{-1}\, \nu_1^{-1} = \mu_\ell/\rho_g\, V\, D$$

$$\pi_5 = \nu_8\, \nu_3^{-1} = a_g/V$$

$$\pi_6 = \nu_9\, \nu_2^{-1} = \rho_\ell/\rho_g$$

where π_1 = Weber number

π_2 = Non-dimensional breakup time = $\bar{t}$

π_3 = Gas phase Reynolds number

π_4 = Liquid phase Reynolds number

π_5 = Mach number

π_6 = Density ratio = β

and Eq. (A. 1) can be written as,

$$\phi_1\,(We,\ \bar{t},\ Re_g,\ Re_\ell,\ M_g,\ \beta) = 0$$

from which,

$$\bar{t} = \phi_2\,(We,\ Re_g,\ Re_\ell,\ M_g,\ \beta)$$

or

$$t_b = \frac{D}{V}\,\phi_2\,(We,\ Re_g,\ Re_\ell,\ M_g,\ \beta)$$

REFERENCES

1. Nicholls, J. A., Dabora, E. K., and Ragland, K. W., "A Study of Two Phase Detonation as it Relates to Rocket Motor Combustion Instability," NASA CR 272, August 1965.

2. Busch, C. W., Laderman, A. J., and Oppenheim, A. K., "Parametric Study of the Generation of Pressure Waves by Particle-Fueled Combustion," AIAA Second Annual Meeting and Technical Demonstration, San Francisco, Paper 65-357, July 1965.

3. Nicholls, J A., Cullen, R. E., and Ragland, K. W., "Feasibility Studies of a Rotating Detonation Wave Rocket Motor," AIAA J. of Spacecraft and Rockets (to be published).

4. Harrje, D. T. and Sirignano, W. A., "Nonlinear Aspects of Combustion—Instability in Liquid Propellant Rocket Motor," Report No. 553-ëÿ Princeton Univ., 1965.

5. Cherepanov, G. P., "The Theory of Detonation in Heterogeneous Systems," PMTF, No. 4, April 1965, p. 163 (in Russian).

6. Williams, F. A., "Detonations in Dilute Sprays," Progress in Astronautics and Rocketry, Academic Press, New York, Vol. 6, 1962, pp. 99-114.

7. Dabora, E. K., Ragland, K. W., and Nicholls, J. A., "A Study of Heterogeneous Detonations," AIAA Paper No. 66-109, 1966 (to be published in Astronautica Acta).

8. Rudinger, G., "Some Effects of Finite Particle Volume on the Dynamics of Gas-Particle Mixtures," AIAA J., Vol. 3, No. 7, 1965, pp. 1217-1222.

9. Adamson, T. C., Jr., Unpublished notes.

10. Zeleznik, F. J. and Gordon, S., "A General IBM 704 and 7090 Computer Program for Computation of Chemical Equilibrium Compositions, Rocket Performance, and Chapman-Jouguet Detonations," NASA TN D 1454, October 1962. See also NASA TN D 1737, October 1963 and ARS J., Vol. 32, No. 4, pp. 607-15.

11. Anonym., Diethylcyclohexane, Technical Data Sheet, Monsanto Chemical Company, January 12, 1959.

12. Anonym., Evaluation of Hydrocarbons for High Temperature Jet Fuels, Part II. Fuel Evaluation and Property Correlation, Volume II. Hydrocarbon Properties, WADC TR 59-327.

13. Rayleigh, J.W.S., "Instability of Jets," Proc. London Math Soc., 1878, Vol. 10, pp. 4-13.

14. Lindblad, N.R. and Schneider, J.M., "Production of Uniform-Sized Liquid Droplets," J. Sc. Inst., Vol. 42, August 1965, pp. 635-638.

15. Ragland, K.W., Dabora, E.K., and Nicholls, J.A., "Shock Induced Heterogeneous Detonations," Paper WSCI 65-22 presented at the Western Section of the Combustion Institute, October 1965.

16. Willmarth, W.W., Univ. of Michigan, private communication.

17. Knight, H.T. and Duff, R.E., "Precision Measurement of Detonation and Strong Shock Velocity in Gases," Rev. of Sci. Inst., Vol. 26, March 1955, p. 257.

18. Wolfe, H. and Andersen, W., "Aerodynamic Break-up of Liquid Drops," American Physical Society Paper SP70, April 1965.

19. Rabinowicz, J., "Aerodynamic Studies in the Shock Tube," California Institute of Technology Hypersonic Research Project Memorandum No. 38, June 1957.

20. Taylor, B.W., "Development of a Thin Film Heat-Transfer Gauge for Shock-Tube Flows," Univ. of Toronto, UTIA TN 27, June 1959.

21. Sichel, M. and David, T.S., "Theoretical Estimate of Wall Heat Transfer Behind Chapman-Jouguet Detonations in H_2-O_2 Mixtures," Univ. of Michigan (to be published in AIAA J.).

22. Loison, R., "The Propagation of Deflagration in a Tube Covered with an Oil Film," Comptes Rendus, Vol. 234, No. 5, Paris, 1952.

23. Gordeev, V.E., Komov, V.F., and Troshin, Ya.K., "Concerning Detonation Combustion in Heterogeneous Systems," Proceedings of the Academy of Science, USSR, Vol. 160, No. 4 (Physical Chemisty), 1965.

24. Komov, V.F. and Troshin, Ya.K., "The Structure and Detonation Mechanism of Heterogeneous Systems," Proceedings of the Academy of Science, USSR, Vol. 162, No. 1 (Physical Chemistry), 1965.

25. Emmons, H.W., "The Film Combustion of Liquid Fuel," Z. Angew. Math. Mech., Vol. 36, No. 1/2, Jan/Feb 1956.

26. Mirels, H., "Laminar Boundary Layer Behind Shock Advancing into Stationary Fluid," NACA TN 3401, March 1955.

27. Williams, F. A., Combustion Theory, Addison-Wesley, 1965.

28. Rosenhead, L., Laminar Boundary Layers, Oxford, 1963, p. 224.

29. Emmons, H. W. and Leigh, D. C., "Tabulation of the Blasius Function with Blowing and Suction," Aeronautical Research Council Current Paper No. 157, London, 1954.

30. Toong, T. Y., "Interactions Among Burning Fuel Droplets (1) A Single Fuel Plate," AFOSR TN 60-516, May 1960.

31. Lane, W. R., "Shatter of Drops in Streams of Air," J. of Ind. and Eng. Chemistry, Vol. 43, No. 6, June 1951, pp. 1312-1317.

32. Taylor, G. I., "The Shape and Acceleration of a Drop in a High-Speed Air Stream," Collected works of G. I. Taylor.

33. Taylor, G. I., "The Instability of Liquid Surfaces when Accelerated in a Direction Perpendicular to their Planes," Proc. Roy. Soc. London, (A) 201, 192, 1950.

34. Hanson, A. R., Domich, E. G., and Adams, H. S., "An Experimental Investigation of Impact and Shock Wave Break-up of Liquid Drops," Res. Rept. 125, Rosemount Aero. Lab., Minneapolis, Minn., January 1956.

35. Hanson, A. R., Domich, E. G., "The Effect of Liquid Viscosity on the Break-up of Droplets by Air Blasts—A Shock Tube Study," Eng. Res. Rept. 130, Univ. of Minnesota Institute of Technology, June 1956.

36. Engel, O. G., "Fragmentation of Waterdrops in the Zone Behind an Air Shock," J. of Res. Nat'l. Bur. Standards, Vol. 60, No. 3, March 1958.

37. Rabin, E., Schallenmuller, A. R., and Lawhead, R. B., "Displacement and Shattering of Propellant Droplets," Final Summary Rept. AFOSR, Washington, D. C., TR 60-75, March 1960.

38. Rojec, E. A., "Photographic Investigation of Shear Type Droplet Breakup," Rocketdyne Res. Rept. 63-39, November 1963.

39. Nicholson, J. E. and Hill, A. F., "Rain Erosion on Spike Protected Supersonic Radomes," Mithras, Inc., Cambridge, Mass., MC-61-6-R3, April 1965.

40. Morrell, G. and Povinelli, F. P., "Break-up of Various Liquid Jets by Shock Waves and Applications to Resonant Combustion," NASA TN D-2423.

41. Clark, B. J., "Breakup of a Liquid Jet in a Transverse Flow of Gas," NASA TN D-2424.

42. Mayer, E., "Theory of Liquid Atomization in High-Velocity Gas Streams," ARS J., December 1961.

43. Weiss, M. A. and Worsham, C. H., "Atomization in High Velocity Airstreams," ARS J., April 1959.

44. Fage, A., Aeronautical Research Committee Reports and Memoranda, R and M No. 1766, ARC Tech. Rept. (1937).

45. Burgers, J. M., Ned. Akad. v. Wetensch. Afd. Natuurkunde, L II, No. 8 en 9 (1943).

46. Prandtl, L. and Tietjens, O. G., Applied Hydro- and Aeromechanics, Dover Publishing Inc., New York, 1937.